IMPROVED DIAGNOSIS OF HEPARIN-INDUCED THROMBOCYTOPENIA

EPITOPE-TARGETED STRATEGIES FOR INHIBITING PATHOGENIC IMMUNE COMPLEX FORMATION IN HEPARIN-INDUCED THROMBOCYTOPENIA

By: ANNA-LISE BISSOLA, B.A.S. (Hon.)

A Thesis

Submitted to the School of Graduate Studies in

Partial Fulfilment of the Requirements for the Degree

Master of Science

McMaster University

MASTER OF SCIENCE (2022) McMaster University

(Biochemistry and Biomedical Sciences) Hamilton, Ontario

TITLE: Epitope-Targeted Strategies for Inhibiting Immune Complex Formation in Heparin-Induced Thrombocytopenia

AUTHOR: Anna-Lise Bissola, B.A.S. (Hon.) (University of Guelph)

SUPERVISOR: Dr. Ishac Nazy

SUPERVISORY COMMITTEE: Dr. Colin Kretz, Dr. Donald M. Arnold, Dr. Sara Andres

NUMBER OF PAGES: xvii, 112

LAY ABSTRACT

Heparin-induced thrombocytopenia (HIT) is an immune-mediated adverse drug reaction that can occur following treatment with the anticoagulant medication heparin.[1,2] HIT is characterized by the production of pathogenic antibodies that bind to complexes of platelet factor 4 (PF4) and heparin, causing platelet activation and an increased risk of thrombosis.[1,3-6] Although most patients exposed to heparin produce anti-PF4/heparin antibodies, only a small percentage develop HIT. [2,6-10] This can complicate diagnosis due to the challenge of differentiating between antibodies that can (pathogenic) and cannot (non-pathogenic) cause HIT.[10-12] Previous work has demonstrated pathogenic antibodies bind to a localized region on PF4/heparin complexes that is distinct from non-pathogenic antibodies.[13] Therefore, this work aims to develop a high-affinity inhibitor that will exclusively block pathogenic antibodies from binding to PF4. This inhibitor will then be used to design a novel assay that can more accurately detect pathogenic antibodies to improve HIT diagnostic testing.

ABSTRACT

Heparin-induced thrombocytopenia (HIT) is an immune-mediated adverse drug reaction to the anticoagulant heparin.[1,2] HIT is characterized by pathogenic antibodies that form immune complexes with platelet factor 4 (PF4) and heparin, which can cause platelet activation and thrombosis.[1,3-6] Prompt diagnosis is crucial because HIT patients experience a 5-10% daily increased risk of thrombotic episodes, which are fatal in up to 30% of patients.[2,6-10] The immune response in HIT is polyspecific, resulting in the production of anti-PF4/heparin antibodies that either can (pathogenic) and/or cannot (non-pathogenic) activate platelets.[10-12] Differentiating between pathogenic and non-pathogenic antibodies remains a significant diagnostic challenge in HIT, exacerbated by the low specificity and limited availability of current laboratory assays.[10,14,15]

Previously it was shown that platelet-activating immune complexes form when pathogenic antibodies bind PF4 at a localized region that is distinct from non-pathogenic antibodies.[13] In this work, high affinity inhibitors of pathogenic anti-PF4/heparin antibodies were designed using a murine monoclonal antibody (named KKO) that binds to a region on PF4 overlapping with pathogenic antibodies.[16] These inhibitors were used to develop a novel diagnostic assay that can detect pathogenic antibodies with improved specificity compared to most standard tests for HIT (specificity ~50-70%).[2,15] Enzyme immunoassays (EIAs) are widely used for HIT diagnosis, but have high false-positive rates because they cannot differentiate between pathogenic and non-pathogenic antibodies.[10,14,15] This study found that incorporating inhibitors to block clinically significant antibody binding sites on PF4 improved the specificity (90%) of a diagnostic EIA for HIT without sacrificing sensitivity (90-100%). Unlike most high-sensitivity and -specificity diagnostic tests for HIT, such as platelet-activation assays, this EIA can also be performed with technical ease in non-specialized laboratories.

ACKNOWLEDGEMENTS

I would like to thank my supervisor Dr. Ishac Nazy for his support, guidance, and endless encouragement throughout the entirety of this degree, especially when I was a new graduate student struggling navigate public health uncertainties over these last few years. Thank you for always being a source of motivation and challenging me to be a better scientist. I want to also recognize Dr. Colin Kretz for welcoming me into his lab at TaARI and for his integral collaboration on my project. Thank you for your enthusiastic support and for always being as dedicated to my success as your own students'. I would also like to thank my additional committee members and supervisors: Dr. Donald Arnold, Dr. Sara Andres, and Dr. John Kelton, for providing valuable expertise that has helped improve my quality of research and allowed me to grow as a graduate student.

Thank you to my lab mates: Mercy Daka, Andrea Huick, Nikola Ivetic, John Vrbensky, Angela Huynh, and Taylor Elliott. The long days and even longer nights would have been unbearable without you guys. Thank you not only for your knowledge, but for always offering a much needed laugh to distract me from experiments gone awry. I also want to acknowledge Taylor Sparring, Kanwal Singh, Hasam Madarti, and Cherie Teney, for getting me through the COVID-19 lockdowns. Thank you for your mentorship and for being like a second lab to me. I will always value my time at TaARI and I'm so grateful that I had the chance to work alongside all of you.

Thank you to everyone past and present at the McMaster Platelet Immunology Lab, especially Jim Smith, Jane Moore, and Hina Bhakta, for all your assistance and expertise. I would also like to recognize Rumi Clare for always offering his support to the students, myself especially, whether it be through editing, help with experiments, or constant reassurance. I appreciate everything you have done and am thankful for all the guidance you have given me.

I want to thank my parents for providing me with support, love, and all other opportunities in life that allowed me to pursue higher education. Thank you to my sister, Sarah Bissola, for letting me temporarily hijack her room in Hamilton. I would also like to thank my friends for keeping me sane over the last few years, but more importantly for editing all my professional/academic emails. Lastly, thank you to Devon Miller, for all your unconditional love and encouragement. I wouldn't have been able to achieve any of this without your patience. Thank you for the innumerable tanks of gas, waiting for me to finish day-long experiments, and for motivating me when I couldn't do it myself.

TABLE OF CONTENTS

TITLE PAGE……………………………………………………………………………..i

DESCRIPTIVE NOTE……………………………………………………………......……ii

LAY ABSTRACT……………….………..…..…..………....…...…………………………...…iii

ABSTRACT……………………………………………………………………………...…iv

ACKNOWLEDGMENTS…………………………………………………………….……v

TABLE OF CONTENTS…………………………..……………………………..……….vii

LIST OF FIGURES……………………………………………………………….….….x

LIST OF TABLES……………………………………………………………………….…..xii

LIST OF SUPPLEMENTARY FIGURES………………………......………………..……xiii

LIST OF SUPPLEMENTARY TABLES……………………………..……………..…..xiv

LIST OF ABBREVIATIONS…………………………………………………………….xv

DECLARATION OF ACADEMIC ACHIEVEMENT…………………………......…..xvii

1.0. INTRODUCTION…………………………......………………………………....……….…….1
1.1. Platelets...…………………………………………………………………......…………..1
1.2. Anticoagulation and Heparin……………………………..…………………………………...2
1.3. Heparin-Induced Thrombocytopenia (HIT)…………………………..………….……… 3
1.3.1. Clinical Features of HIT……….…………………..……………………………… 3
1.3.2. HIT Pathophysiology……..…………………..……………………………………… 4
1.4. The Role of Platelet Factor 4 (PF4) and Heparin Complexes in HIT …………………………5
1.5. Clinical and Laboratory Diagnosis of HIT……………….…………..……………………….7
1.6. Diagnostic Limitations of Laboratory Assays………....…………….……………………..9
1.7. Reactivity of Polyspecific HIT Antibodies…………………………………………………..10
1.8. Pathogenic Epitopes on PF4……………...…………...…………………………….………… 11
1.9. Single Chain Variable Fragments (scFv)………………………….. …………………… 12

2.0. RESEARCH OUTLINE……………...…………...…………………………………….... 14
2.1. Overall Objective…………………...………..…………………………..……………… 14
2.2. Rationale……………..……..……...……..………..…………………..……………………….. 14
2.3. Hypothesis……………………….....……..…..…………………..…………………………....15
2.4. Specific Objectives………………………....……………………………...………………15

3.0. MATERIALS AND METHODS……………………………………………………………16
3.1. Phage Display Library Construction……………………………………………………16
3.2. Phage Library Preparation and Purification……………………………………………17
3.3. Fluid-Phase Phage Bio-Panning Using Streptavidin Coated Magnetic Beads………………18
3.4. Construction and Bacterial Expression of Wildtype and Mutant KKO-scFv………………19
3.5. Ni-NTA Affinity Purification of KKO-scFv……………………………………………20
3.6. Inhibitory PF4/heparin IgG-specific Streptavidin Enzyme Immunoassay (EIA)……………20
3.7. Biolayer Interferometry (BLI) using Wildtype and Mutant KKO-scFv……………………21
3.8. BLI Data Acquisition and Kinetic Analysis……………………………………………22
3.9. Epitope Mapping of KKO-scFv Binding to PF4…………………………………………23
3.10. Serotonin-Release Assay (SRA) using KKO-scFv………………………………………24
3.11. Statistical Analysis…………………………………………………………………25

4.0. RESULTS…………………………………………………………………………25
4.1. KKO-scFv Phage Library Construction…………………………………………………25
4.1.1. Wildtype KKO-scFv Cloning and Mutant Library Preparation……………………25
4.2. Phage Bio-Panning Optimization and Mutant Library Screening…………………………26
4.2.1. Characterizing Wildtype KKO-scFv Phage Binding………………………………26
4.2.2. Isolation of High Affinity KKO-scFv Clones from a Phage Display Library……..27
4.2.3. Expression and Purification of Wildtype and Mutant KKO-scFv…………………27
4.3. Characterizing Wildtype and Mutant KKO-scFv Binding……………………………….28
4.3.1. Binding Kinetics Using Biolayer Interferometry (BLI)……………………………28
4.3.2. Full-Length KKO Inhibition and Determining IC_{50} Values ………………………30
4.3.3. Epitope Mapping of the KKO-scFv Binding Site on PF4…………………………31
4.4. Inhibiting SRA-Positive and SRA-Negative Anti-PF4/Heparin Antibody Binding…………32
4.5. Assessing the Clinical Application of High-Affinity KKO-scFv Mutants…………………..35
4.5.1. Large-Scale Screening of HIT-Negative (EIA+/SRA-) and HIT-Positive (EIA+/SRA+) Patient Sera……………………………………………………………...35
4.5.2. Determining New Positivity Thresholds and Diagnostic Performance of a Novel HIT Diagnostic Assay………………………………………………………………...36
4.5.3. Inhibiting Immune Complex-Mediated Platelet Activation ………………………...37

5.0. DISCUSSION………………………………………………………………………… 38
5.1. Improving the Affinity of KKO-scFv Using Random Mutagenesis and Phage Display…....39
5.1.1. Preparation and Identification of KKO-scFv Mutant Constructs…………………39
5.1.2. Purification of Wildtype and Mutant KKO-scFv Constructs………………………41
5.2. Characterization Studies Using Wildtype and Mutant KKO-scFv …………………………42
5.2.1. Full-length KKO inhibition and BLI Binding Kinetics……………………………42
5.2.2. Identifying the KKO-scFv Epitope on PF4………………………………………...43
5.3. Evaluation of a Rapid and Accurate Diagnostic Assay for HIT Using KKO-scFv…………45
5.4. Limitations ……………………………………………………………………………..48

6.0. FUTURE DIRECTIONS……………………………………………………………......50

7.0. CONCLUSION……………………………………………………………………….53

8.0. FIGURES……..…….55

9.0. TABLES……..……..…….79

10.0. SUPPLEMENTARY FIGURES……87

11.0. SUPPLEMENTARY TABLES……101

12.0. BIBLIOGRAPHY…….102

LIST OF FIGURES

Figure 1. PF4 crystal structure with epitope mapping of antibody binding.

Figure 2. Mutant KKO-scFv phage library polymerase chain reaction colony screen.

Figure 3. Binding characterization of phage displaying wildtype (WT) KKO-scFv to PF4/heparin.

Figure 4. Purification of KKO-scFv from BL21 cells using Ni-NTA affinity chromatography.

Figure 5. BLI Binding response of KKO-scFv against PF4.

Figure 6. BLI Binding response of KKO-scFv against PF4/heparin.

Figure 7. KKO-scFv inhibition of full-length monoclonal antibody KKO binding in a modified streptavidin enzyme immunoassay (EIA).

Figure 8. Identification of amino acids that are critical for the binding of KKO-scFv to PF4.

Figure 9. KKO-scFv inhibition of pathogenic anti-PF4/heparin antibody binding in a modified streptavidin enzyme immunoassay (EIA).

Figure 10. KKO-scFv inhibition of non-pathogenic anti-PF4/heparin antibody binding in a modified streptavidin enzyme immunoassay (EIA).

Figure 11. Percent inhibition of anti-PF4/heparin antibody binding from HIT-positive and HIT-negative patients by KKO-scFv in a streptavidin enzyme immunoassay (EIA).

Figure 12. Large-scale screening of HIT-positive and HIT-negative patients in a streptavidin enzyme immunoassay (EIA) using wildtype KKO-scFv.

Figure 13. Large-scale screening of HIT-positive and HIT-negative patients in a streptavidin enzyme immunoassay (EIA) using KKO-scFv Mutant B.

Figure 14. Large-scale screening of HIT-positive and HIT-negative patients in a streptavidin enzyme immunoassay (EIA) using KKO-scFv Mutant F.

Figure 15. Distinguishing between pathogenic and non-pathogenic anti-PF4/heparin antibodies in a streptavidin enzyme immunoassay (EIA) using KKO-scFv.

Figure 16. The receiver operating characteristics (ROC) curves of an IgG-specific streptavidin anti-PF4/heparin EIA using KKO-scFv.

Figure 17. KKO-scFv inhibition of HIT antibody-mediated platelet activation in the ^{14}C-serotonin release assay.

Figure 18. Schematic diagram of the IgG-specific streptavidin PF4/heparin EIA with and without KKO-scFv.

LIST OF TABLES

Table 1: Current development and progress of therapeutic antibody fragments.

Table 2: Phage library selection and enrichment process.

Table 3: Frequency of identical mutant sequences.

Table 4: Summary of experimental IC_{50} values for wildtype and mutant KKO-scFv constructs against full-length KKO with 95% confidence intervals (CI) and R^2 values.

Table 5: Mean absorbance (optical density [OD] @ 405nm) of anti-PF4/heparin antibodies from HIT-Positive (n=10) and HIT-negative (n=10) patient sera.

Table 6: Wildtype and mutant KKO-scFv mean percent (%) inhibition of anti-PF4/heparin antibodies from HIT-Positive (n=10) and HIT-Negative (n=10) patient sera at 50 μg/mL.

Table 7: Area under the curve (AUC) and positivity threshold for the streptavidin IgG-specific anti-PF4/heparin inhibitory enzyme immunoassay with KKO-scFv (KKO-scFv PF4/hep-EIA).

Table 8: Performance characteristics of a streptavidin IgG-specific anti-PF4/heparin inhibitory enzyme immunoassay with KKO-scFv (KKO-scFv PF4/hep-EIA).

LIST OF SUPPLEMENTARY FIGURES

Supplementary Figure 1. Plasmid Map of pADL-22c Phagemid Vector.

Supplementary Figure 2. Wildtype (WT) KKO-scFv phage colony screen polymerase chain reaction.

Supplementary Figure 3. Binding Characterization of KKO-scFv Phage Using von Willebrand Factor (vWF) D' Domain Phage on Streptavidin-Coated Magnetic Beads.

Supplementary Figure 4. Aligned sequences of wildtype and mutant KKO-scFv.

Supplementary Figure 5. Purification of Wild-Type KKO-scFv from BL21 cells using affinity chromatography.

Supplementary Figure 6. Purification of Mutant B KKO-scFv from BL21 cells using affinity chromatography.

Supplementary Figure 7. Purification of Mutant C KKO-scFv from BL21 cells using affinity chromatography.

Supplementary Figure 8. Purification of Mutant D KKO-scFv from BL21 cells using affinity chromatography.

Supplementary Figure 9. Purification of Mutant E KKO-scFv from BL21 cells using affinity chromatography.

Supplementary Figure 10. Purification of Mutant F KKO-scFv from BL21 cells using affinity chromatography.

Supplementary Figure 11. Binding kinetics of wildtype KKO-scFv against biotinylated PF4 and heparin complexes immobilized on streptavidin sensors.

Supplementary Figure 12. Binding kinetics of wildtype KKO-scFv against biotinylated PF4 complexes immobilized on streptavidin sensors.

Supplementary Figure 13. Binding kinetics of full-length KKO against biotinylated PF4 and PF4/heparin complexes immobilized on streptavidin sensors.

Supplementary Figure 14. Heparin-dependent and -independent pathogenic antibody binding sites on PF4.

LIST OF SUPPLEMENTARY TABLES

Supplementary Table 1: Initial primer sets used for verifying correct wildtype and mutant KKO-scFv insertion into the pADL-22c phagemid vector that overlap with the ligation sites at both ends.

LIST OF ABBREVIATIONS

ACE2	Angiotensin-converting enzyme 2
aTTP	Acquired thrombotic thrombocytopenic purpura
Amp^R	Ampicillin resistance gene
AUC	Area under curve
BCA	Bicinchoninic acid
BLI	Biolayer interferometry
b-heparin	Biotinylated-heparin
bp	Base pair
BSA	Bovine serum albumin
CDR	Complementary determining region
CFU	Colony forming units
CI	Confidence interval
CLIA	Chemiluminescent immunoassay
CPB	Cardiopulmonary bypass
Da	Daltons
d_f	Dilution factor
DNA	Deoxyribonucleic acid
DOC	Deoxycholic acid
DVT	Deep vein thrombosis
E. coli	Escherichia coli
EDTA	Ethylenediaminetetraacetic acid
EIA	Enzyme immunoassay
Fab	Fragment antibody binding
Fc	Fragment crystallizable
FXa	Factor Xa
GAG	Glycosaminoglycan
GP	Glycoprotein
HA	Hemagglutinin
HCl	Hydrochloric Acid
HIPA	Heparin-induced platelet activation assay
HIT	Heparin-induced thrombocytopenia
His	Histidine
PaGIA	Particle gel immunoassay
Ig	Immunoglobulin
IPTG	Isopropyl-D-1-thiogalactopyranoside
k_{on}	Association rate
kDa	Kilodaltons
k_{off}	Dissociation rate
K_D	Equilibrium constant
LB	Luria-Bertani
LFA	Lateral flow assay
LMWH	Low molecular weight heparin
mAb	Monoclonal antibody
MI	Myocardial infarction

MW	Molecular weight
NaCl	Sodium chloride
Ni-NTA	Nickle-Nitrilotriacetic acid
NMR	Nuclear magnetic resonance
NPV	Negative predictive value
NP	Nucleocapsid protein
OD	Optical density
pIII	Filamentous phage protein III
PBS	Phosphate buffered saline
PCR	Polymerase chain reaction
PDB	Protein data bank
PE	Pulmonary embolism
PEA	P-selectin expression assay
PEG	Polyethylene glycol
PF4	Platelet factor 4
PNPP	p-nitrophenylphosphate
PPV	Positive predictive value
PVS	Polyvinyl sulfate
RBD	Receptor binding domain
rhPF4	Recombinant human platelet factor 4
ROC	Receiver operating characteristics
rpm	Revolutions per minute
SA	Streptavidin
scFv	Single-chain variable fragment
SD	Standard deviation
SDS-PAGE	Sodium dodecyl sulfate polyacrylamide gel electrophoresis
SERS	Surface-enhanced Raman spectroscopy
SRA	14C-serotonin release assay
TBS	Tris buffered saline
TXA_2	Thromboxane A_2
UFH	Unfractionated heparin
V_H	Variable heavy
VITT	Vaccine-induced thrombotic thrombocytopenia
V_L	Variable light
VEGF	Vascular endothelial growth factor
vWF	von Willebrand factor
WT	Wildtype
2xYT	Yeast Extract Tryptone

DECLARATION OF ACADEMIC ACHIEVEMENT

All the experiments outlined in this thesis were conducted by Anna-Lise Bissola, under the supervision of Dr. Ishac Nazy, Dr. Donald M. Arnold, and Dr. Colin Kretz, with the following exceptions: biolayer interferometry experiments using KKO-scFv was performed with the assistance of Andrea Huick and Rumi Clare, the serotonin-release assay using KKO-scFv was performed by James Smith, and KKO-scFv epitope mapping was performed by Mercy Daka and Angela Huynh.

1.0. INTRODUCTION

1.1. Platelets

Platelets are small, non-nuclear blood cells that have key hemostatic and thrombotic functions, such as helping to prevent excessive bleeding following vessel damage.[17] Human platelets have an average lifespan of 8–10 days and maintain normal levels between 150–400x10^9 platelets/L of blood.[17] The production of platelets from bone marrow megakaryocytes occurs by a process termed thrombopoiesis.[18] Thrombopoiesis is primarily regulated by the growth factor thrombopoietin, which stimulates proplatelet formation by inducing the thrombopoietin receptor on megakaryocytes when platelet counts are low in the blood.[18] Changes to the surface of aging platelets signal for their removal from circulation by macrophages, which is largely carried out in the liver and spleen.[19] Cycles of platelet production and senescence are required to maintain normal platelet counts in the blood.[18] Consequences related to an upset in platelet levels (e.g. thrombocythemia or thrombocytopenia) come from a disruption in hemostatic balance, which can lead to aberrant blood coagulation or uncontrolled bleeding events.[20]

Platelets circulate around the body in a resting, discoid state that become activated in response to blood vessel damage by the release of soluble agonists and exposed collagen.[17,21] Once activated, platelets undergo a globular shape change and form pseudopodia that not only allow them to adhere at sites of injury, but permit interactions with other activated platelets to form large aggregates that help control bleeding.[17] Large platelet aggregates form a “platelet plug” at sites of damage to help maintain vascular wall integrity.[22] Interactions between platelet surface glycoproteins (GP), such as GPIIbIIIa and GPIbIX, exposed collagen from the subendothelial matrix, and von Willebrand factor (vWF) help facilitate platelet adhesion under high shear conditions.[18,22,23] Platelet activation is further stimulated and upregulated by various signaling

molecules, including adenosine diphosphate (ADP), thromboxane A_2 (TXA_2), and serotonin, which are produced by damaged cells and released from surrounding activated platelets.[23] Activated platelets also secrete the contents of their intracellular granules, including alpha granules, dense granules, and lysosomes, to release proteins and small molecules that further promote coagulation.[17,18,23]

1.2. Anticoagulation and Heparin

Coagulation is tightly regulated to manage the formation and dissolution of blood clots.[20] Anticoagulants are a class of medications that inhibit blood clot formation and are prescribed as prophylaxis for high-risk individuals, such as surgical patients, and as thrombus treatments in clotting disorders, such as venous thromboembolism (VTE).[24,25] A commonly administered anticoagulant prescribed to patients undergoing procedures with high incidences of thrombosis, such as cardiac and orthopedic surgery, is heparin.[26,27] Heparin is widely used to prevent or treat clot formation because of its rapid onset of action, reversibility, and favorable pharmacodynamic properties.[26,28] Heparin is a negatively charged glycosaminoglycan (GAG) composed of linear, highly sulfated, and unbranched polysaccharides.[29] Chains of unfractionated heparin (UFH) molecules can be depolymerized to generate low molecular weight heparin (LMWH) fragments, which poses distinct pharmacokinetic and anticoagulant properties.[28,30] Through direct interactions with the serine protease inhibitor antithrombin, UFH and LMWH function by activating and upregulating its natural anticoagulant properties.[28]

The heparin-antithrombin complex exerts its anticoagulant effect by inhibiting thrombin and activated factor X (FXa) procoagulant activity.[29,30] Heparin-binding initiates a conformational change in the antithrombin reactive site loop that results in a 300-fold enhancement in the rate of antithrombin inhibitory activity.[31,32] Although the conformational change in antithrombin alone

can increase antithrombin activity against FXa, it is insufficient for upregulating thrombin inactivation.[29] Heparin enhances thrombin inhibition by forming a ternary complex responsible for bringing antithrombin and thrombin into proper orientation and proximity.[29] Therefore, chain length differences between different heparin variants are responsible for distinctions in their anticoagulant activity, as seen with unfractionated heparin (UFH), low-molecular weight heparin (LMWH), and the synthetic pentasaccharide, fondaparinux.[28,29] While UFH can inhibit both thrombin and FXa, LMWH and smaller heparin derivatives are unable to form the ternary complex required to successfully inactivate thrombin activity.[28] However, LMWH demonstrates superior anticoagulant activity against FXa and is more frequently used in various clinical scenarios due to a severe and potentially fatal complication associated with UFH administration called heparin-induced thrombocytopenia (HIT).[28,33]

1.3. Heparin-Induced Thrombocytopenia (HIT)

1.3.1. Clinical Features of HIT

Heparin-induced thrombocytopenia (HIT) is a prothrombotic immune-mediated adverse drug reaction that can develop in up to 1-5% of patients exposed to intravenous heparin.[34] The frequency of HIT depends largely on the clinical scenario, including factors such as heparin formulation, treatment duration, and patient population.[2,33-35] Surgical patients experience a significantly higher risk of HIT compared to medical patients, particularly those undergoing orthopedic or cardiac surgery.[2,34] HIT is primarily associated with the development of thrombocytopenia, observed as 50% decrease in platelets relative to a patient's baseline platelet levels or below normal counts ($>150x10^9$ platelets/L) occurring 5-10 days post-heparin exposure.[36] Thrombocytopenia has also been observed to fall outside the typical range in patients with rapid-onset HIT, which occurs within 24 hours of heparin exposure.[36,37] Despite the presence of

thrombocytopenia, HIT paradoxically causes an elevated risk of thrombosis due to increased platelet activation.[38] Platelet activation is triggered by pathogenic antibodies produced in response to heparin exposure that induces a hypercoagulable state in HIT patients.[1,39,40] Although HIT has an overall mortality rate of approximately 5-7%,[41,42] in patients who develop thrombotic complications (30-50%),[43] the risk of can fatality increase up to 30%.[42] Thrombosis most often manifests as venous clots in the form of deep vein thrombosis (DVT) and pulmonary embolism (PE), but they can also be arterial, likely effecting the distal aorta and lower limb arteries.[2,36,38] Arterial thrombosis can cause limb ischemia in HIT patients, which can give rise to peripheral artery embolism, myocardial infarction, or stroke in severe but uncommon circumstances.[36,38] Treatments for HIT include initiation of alternative anticoagulants after cessation of all heparin.[44,45] However, the development of new thrombosis is still reported in approximately 19-40% of HIT patients receiving treatment.[38]

1.3.2. HIT Pathophysiology

HIT is mediated by platelet activating antibodies that form in response to complexes formed between heparin and a self-protein, platelet factor 4 (PF4). All three classes of immunoglobulin (Ig) antibodies (IgG/A/M) are produced simultaneously in HIT, which can be detected within five days post-heparin therapy.[46] Although all Ig classes can be produced in response to heparin,[46] the presence of high affinity and high titer IgG isotypes are more frequently associated with platelet activation and the development of HIT. As previously mentioned, patients receiving heparin are at a higher risk of developing anti-PF4/heparin antibodies in surgical settings. This is likely due to the amount of endothelial damage that occurs during surgery, which causes extensive platelet activation and increases the amount of PF4 available to form complexes.[2] When PF4 is released from activated platelets, it can form tetramers that are stabilized by the binding of

negatively charged heparin molecules. Heparin binding induces a conformational change in PF4 to reveal neoepitopes that can trigger anti-PF4/heparin antibody production.[47,48] Antibodies bound to PF4/heparin form immune complexes in HIT patients that can facilitate interactions with platelets and monocytes through surface Fc-receptors.[49-51] The FcγRIIA receptor on platelets is a transmembrane glycoprotein that recognizes the Fc moiety of IgG with a low affinity, but binds more favorably to immune complexes that form between an antibody and their target antigen.[52,53]

Immune complexes are highly reactive antibody-antigen structures that circulate throughout the body and can stimulate various immune responses. Improper production or clearance of immune complexes can lead to the development of diseases caused by erroneous receptor binding and immune activation.[54] In HIT, anti-PF4/heparin-IgG immune complexes contribute to hypercoagulation through their ability to bind and crosslink platelet FcγRIIA receptors, which triggers platelet activation and aggregation.[51,52,55] Platelet activation leads to the generation of pro-coagulant microparticles and thrombin,[56] increasing the risk of HIT-associated thrombosis.[5,57] The cascading effect of platelet activation prompts a positive feedback cycle of further platelet activation and new thrombosis, which can have detrimental consequences for HIT patients who continue to receive heparin. Platelet activation also stimulates signaling pathways that result in platelet degranulation and secretion of pro-inflammatory cytokines, including PF4, consequently upregulating further immune complex formation.[55,57]

1.4. The Role of Platelet Factor 4 (PF4) and Heparin Complexes in HIT

Platelet factor 4 (PF4) is a positively charged CXC chemokine that plays a principal role in the pathogenesis of HIT. Levels of circulating PF4 in plasma are low (1.8 ng/mL) but increase significantly following platelet activation (>600 ng/mL).[58,59] During activation, PF4 is released from the alpha granules of platelets and megakaryocytes along with other proteins and molecules

that promote coagulation.[60] PF4 is a monomer composed of 70 amino acids with an approximate molecular weight of 7.8 kDa that exists in equilibrium between monomeric, dimeric, and tetrameric states.[60] The PF4 tetramer contains a ring of positively charged amino acids that come together to form a binding pocket for negatively charged molecules, such as glycosaminoglycans (GAGs) expressed by endothelial cells and/or chondroitin sulfates on other platelets.[58] However, PF4 has a much stronger affinity for the anticoagulant heparin compared to other GAGs causing it to preferentially bind to PF4 following platelet activation.[60] Therefore, heparin can both displace PF4 from membrane surfaces or other proteoglycans as well as bind to PF4 secreted by platelets to form stable protein complexes.[58,60]

Heparin binding plays a key role in HIT antigen formation through electrostatic interactions with PF4 that stabilize its tetrameric state. PF4 undergoes a significant conformational change when bound to heparin that exposes neo-epitopes recognized by anti-PF4/heparin antibodies.[47,48] Heparin brings together PF4 monomers by binding to the 'closed' end of PF4, orienting the 'open' end for pathogenic antibody binding.[47] The significance of stable tetrameric PF4 clusters to immunogenicity is also highlighted by antibodies that bind to PF4 in the absence of heparin and activate platelets. This behaviour is observed in a small fraction of heparin-independent antibodies detected in some HIT patients (see section 1.7)[61] as well as in other HIT-like disorders, such as vaccine-induced thrombotic thrombocytopenia (VITT).[62] Heparin-independent antibodies in these patients bind to PF4 at the heparin-binding site and are thought to mimic the stabilizing action of heparin.[63,64]

PF4/heparin antigenicity is further influenced by heparin chain length, as shown by the differences in reactivity between PF4 when complexed with UFH, LMWH, or fondaparinux.[3,4] This is emphasized by the fact that platelet Fc receptor crosslinking is not observed as frequently

with shorter heparin derivatives, such as LMWH or fondaparinux, when compared to UFH.[3,8,33] Only long chains of heparin (such as UFH) can stabilize tetrameric PF4 and bridge together several tetramers forming the ultra-large complexes crucial for HIT pathogenesis.[4,47,65] When heparin binds to PF4 it becomes linearized, which mediates the binding of a second PF4 tetramer.[47] The repulsive forces between two or more positively charged PF4 tetramers are neutralized when bound by negatively charged heparin, allowing several tetramers to closely interact.[3] Eventually, large macromolecular clusters of heparin and tetrameric PF4 are formed.[3,47]

1.5. Clinical and Laboratory Diagnosis of HIT

As a clinical-pathological disorder, medical assessments and laboratory testing are used in tandem to diagnose HIT. The 4T's score is a clinical scoring system used by physicians to recognize HIT based on four essential criteria: the magnitude of thrombocytopenia (>50%), timing of platelet count fall (onset after 5-10 days), thrombosis, and likelihood of other causes of thrombocytopenia.[15,66] Following evaluation by a physician, a predictive value ranging from low (1-3), intermediate (4-5), and high (6-8) is generated to determine the probability of HIT.[66] However, clinical criteria alone is a poor predictor of disease presence and a sole reliance on these evaluations can lead to disease overcall.[66] Previously, it was reported that most patient samples received for HIT testing are negative (65.6% true-negative, 20.9% false-positive), indicating high rates of clinical suspicion based on such criteria.[10] To reduce over-diagnosis and over-treatment, a clinical suspicion of HIT is confirmed using laboratory assays that detect anti-PF4/heparin antibodies, including enzyme immunoassays (EIAs), automated and/or rapid assays, and functional platelet activation assays.

Immunoassays are performed to determine if circulating anti-PF4/heparin antibodies are present in sera using a capture antigen, comprising either a complex of PF4/heparin or

PF4/polyvinylsulfate (PVS). There are a wide variety of commercially available or laboratory derived EIAs that are used to detect either all Ig class (IgG/A/M) HIT antibodies or IgG-specific antibodies, such as the anti-PF4/heparin IgG-EIA.[67] Commercial rapid assays are also available for the purpose of HIT diagnosis, such as the chemiluminescence immunoassay (CLIA),[68] latex immunoturbidimetric assay (LIA),[69] particle gel immunoassay (PaGIA),[70] and lateral flow assay (LFA).[71] The ability of immunoassays to correctly identify individuals with (sensitivity) or without (specificity) HIT has been extensively studied. Typically, both EIAs and rapid assays have high sensitivities (~99%)[67,72] for all anti-PF4/heparin antibodies but show reduced specificities (~50-70%)[2,15] for clinically significant HIT antibodies.[68-70,73,74] As such, EIAs and rapid assays are most frequently used to rule-out HIT followed by secondary tests to confirm the functional activity of anti-PF4/heparin antibodies.

Functional platelet activation assays have a much higher diagnostic specificity for HIT compared to both EIAs and rapid assays. Functional assays, such as the C^{14}-serotonin release assay (SRA), heparin-induced platelet activation assay (HIPA), and p-selection expression assay (PEA), operate by measuring endpoints indicative of platelet activation. In the SRA, patient sera is tested for its ability to induce platelet activation in the absence of heparin (0 U/mL), at pharmacological concentrations of heparin (0.1-0.3 U/mL), and at high heparin concentrations (100 U/mL), which disrupt the stoichiometric ratios necessary to form PF4/heparin complexes.[15,75] This assay quantifies radiolabeled serotonin release from activated platelets to achieve specific (~95%) and sensitive (~95%) detection of clinically significant HIT antibodies.[15,75] However, functional platelet activation assays are technically demanding and only performed by specifically designated reference laboratories, which decreases the accessibility of these tests.

1.6. Diagnostic Limitations of Laboratory Assays

Diagnostic laboratory assays for HIT face limitations surrounding either detection specificity or performance feasibility due to the prevalence of clinically insignificant anti-PF4/heparin antibodies. Approximately 50-70% of patients exposed to heparin can produce anti-PF4/heparin antibodies depending on the clinical situation, but only a fraction of these antibodies are able to activate platelets and cause HIT.[2,9,76-79] For instance, anti-PF4/heparin antibody production is remarkably common in patients undergoing cardiopulmonary bypass surgery, but the frequency of HIT in these patients is low.[2] Moreover, heparin-independent antibodies have also been detected by functional assays, which activate platelets in the absence of heparin and further highlights antibody complexity in HIT (see section 1.7).[64] Therefore, the polyclonal and polyspecific HIT immune response creates difficulties distinguishing between platelet-activating (pathogenic) and non-activating (non-pathogenic) antibodies.[11] Although immunoassays, like the anti-PF4/heparin IgG-EIA, are easy to perform and offer high sensitivity (~90%)[67] detection of anti-PF4/heparin antibodies, they have a low specificities (~50-70%)[2,15] for platelet activating pathogenic HIT antibodies.

Low specificity tests exacerbate these diagnostic challenges as many patients referred for testing are falsely positive in immunoassays (20.9%; EIA-positive/SRA-negative).[10] Although most suspected patients do not have HIT (65.6%; EIA-negative/SRA-negative),[10] the reliance on immunoassays or rapid assays for diagnosis contribute to over-diagnosis and over-treatment.[10,14] Unnecessary HIT treatments increase the risk of bleeding events, which can have detrimental consequences for patients.[10,14] Furthermore, alternative anticoagulant use and increased hospital stays account for 19.7% and 70.3% of additional medical costs related to over-treatment, respectively.[80,81]A global study conducted in 2016 found that speculative treatment of HIT with a

replacement medication ahead of laboratory confirmation is associated with maximum total costs of $39,616, $11,839, and $6833 USD per patient in the US, UK, and Germany, respectively.[80] However, the risk of thrombosis makes these additional expenditures unavoidable due to the severity of HIT when left untreated. HIT patients experience a 5-10% daily increased risk of experiencing severe thrombotic events, which necessitates immediate treatment.[35,82] Despite the improved diagnostic specificity provided by platelet activating assays, they are laborious, technically challenging, and can further delay diagnosis.[10,15,75]

In Canada, only a small number of laboratories are equipped to perform HIT testing and even fewer that perform functional platelet activation assays. This can lead to longer turnaround times for referring hospitals, leading doctors to begin treatment ahead of laboratory confirmation. An more accurate and reliable test for HIT would reduce the reliance on a clinical or immunoassay diagnosis alone, which currently have poor specificity and lead to disease overcall.[10] Furthermore, accessible testing would allow clinicians to receive laboratory results faster without compromising diagnostic accuracy, not only improving patient clinical outcomes by implementing earlier treatment but shortening hospital stays and reducing associated costs of treatment. However, availability of an accurate and rapid assay with the ability to differentiate between platelet activating (pathogenic) and non-activating (non-pathogenic) antibodies remains a key challenge when diagnosing HIT.

1.7. Reactivity of Polyclonal HIT Antibodies

Significant diagnostic challenges can be attributed to the HIT immune response and disease heterogeneity, which is emphasized by the diverse antibody response in patients receiving heparin. Three groups of anti-PF4/heparin antibodies have been classified based on distinct functional characteristics previously observed in laboratory assays. Non-HIT antibodies (group 1) are anti-

PF4/heparin antibodies that are positively detected by EIAs but are unable to induce platelet activation in functional assays.[64] Individuals with only group 1 antibodies are asymptomatic and the production of these antibodies is unlikely to cause HIT.[64,83] Typical HIT antibodies (group 2) are EIA-positive anti-PF4/heparin antibodies that trigger heparin-dependent platelet activation in functional assays through HIT immune complex formation.[8,64,75] The positive detection of pathogenic group 2 antibodies is required to confirm diagnosis of typical HIT. Atypical HIT antibodies (group 3) are detected at high titers in EIAs and strongly induce heparin-independent platelet activation in functional assays, despite being produced in the setting of heparin treatment.[64] An important characteristic of group 3/heparin-independent antibodies is their ability to bind and stabilize PF4 tetramers without the addition of heparin to cause platelet activation and aggregation.[61,64] Examining the HIT immune complex has also illustrated how differences between polyspecific anti-PF4/heparin antibodies may be related to their PF4 epitopes.

1.8. Pathogenic Epitopes on PF4

Previous studies of the polyclonal immune response in HIT have identified the existence of multiple antibody binding sites on PF4.[84,85] Epitope mapping of anti-PF4/heparin antibodies have reveled several clinically significant binding sites on PF4 using HIT patient sera and the murine monoclonal antibodies KKO,[16] 5B9,[86] and 1E12[86] as models for pathogenic HIT antibodies (Figure 1). This work revealed pathogenic antibodies against PF4/heparin from multiple HIT patients bind to a localized region on PF4.[13] The monoclonal antibodies KKO and 5B9 were also found to bind the same overlapping site as anti-PF4/heparin antibodies, despite having different PF4 epitopes (Figure 1a).[13] Further epitope mapping of sera containing false-positive anti-PF4/heparin antibodies (non-HIT; EIA+/SRA-) also showed that non-pathogenic antibodies do not bind any consistent region on PF4 (Figure 1b). This is unlike what is observed with pathogenic

HIT antibodies, suggesting a difference in their binding sites (Figure 1b).[13] Therefore, pathogenic antibodies recognize a specific region on PF4 that is also distinct from non-pathogenic antibody binding sites. This is further supported by previous inhibition experiments using HIT-positive and HIT-negative patient sera containing anti-PF4/heparin antibodies.[16] Sachais et al. (2013) demonstrated that only pathogenic antibodies from HIT-positive sera can inhibit KKO binding to PF4/heparin, whereas non-pathogenic antibodies from HIT-negative sera had little impact.[87]

Additionally, more than one clinically significant antibody binding site has been located on PF4. Docking model predictions and epitope mapping of 1E12 reveal that this antibody binds the same region on PF4 as heparin molecules (Figure 1a).[88] Unlike KKO and 5B9, 1E12 has been shown to activate platelets without the addition of heparin.[86,88] Based on these findings it is speculated that 1E12 mimics group 3/heparin-independent antibodies by binding to the heparin-binding site on PF4. This epitope is separate from the binding site recognized by antibodies that demonstrate heparin-dependent platelet activation as typically observed in HIT. Furthermore, anti-PF4 antibodies from patients with VITT (a disease pathologically similar to HIT) were also shown to bind the heparin-binding site on PF4.[63] Interestingly, both VITT and atypical HIT antibodies demonstrate heparin-independent platelet activation, illustrating the importance of epitope specificity to antibody activity.[63,64] Therefore, a useful strategy to improve the accuracy of current diagnostic assays for HIT could involve blocking pathogenic epitopes on PF4 (comprising heparin-dependent and -independent sites) to inhibit pathogenic antibody binding.

1.9. Single Chain Variable Fragments (scFv)

Inhibitors against the pathogenic regions on PF4 may allow us to distinguish between pathogenic and non-pathogenic antibodies based on their ability to prevent proper immune complex formation. One method of blocking immune complex formation could involve small

antibody fragments that bind to the same region on PF4 as pathogenic antibodies. IgG antibodies are composed of two heavy and two light chain domains linked by disulfide bonding, each with constant and variable peptide region.[89] The structure can be further divided into two segments, the fragment crystallizable (Fc) and fragment antibody binding (Fab) moieties, which are covalently joined by a hinge region.[89] The Fc domain exerts effector functions, such as Fc receptor binding and immune system communication, while the Fab domain contains the epitope recognition site responsible for antigen binding.[89] Single chain variable fragments (scFv) are generated from the variable heavy (V_H) and light (V_L) chain Fab domains of an antibody held together by a short and flexible glycine-serine linker, which allows it to retain the complete antigen-binding site.[90]

There is a growing clinical importance of scFvs, highlighted by the ongoing development of therapeutic antibody fragments as prospective treatments for a wide range of illnesses (Table 1). The most notable targeted scFv-derived therapeutic is Brolucizumab,[91] which was approved for the treatment of age-related macular degeneration (AMD) in 2019. Brolucizumab is a humanized scFv that inhibits vascular endothelial growth factor A (VEGF-A), which is related to the development of AMD, and combats vison loss in affected patients.[91] Another promising drug candidate in phase III clinical trials for the treatment of non-muscle-invasive bladder cancer is Vicinium (VB4-845).[92,93] Vicinium is an scFv conjugated to Pseudomonas exotoxin A (ETA) that binds to epithelial cell adhesion molecule (EpCAM), which is over expressed in bladder tumors, and demonstrates tumor-killing activity.[92,93] Another recent study by Minekova et al. (2022) describes the neutralizing activity of scFvs against the receptor binding domain (RBD) on SARS-CoV-2 spike proteins derived from antibodies isolated from convalescent plasma donors.[94] These fragments demonstrated the ability to counteract COVID-19 infection *in vitro* and *in vivo* by blocking an epitope required from angiotensin-converting enzyme 2 (ACE2) receptor-mediated

viral entry into cells.[94] These examples demonstrate the utility of developing scFv-based drug candidates, which could also serve a similar function in HIT.

The usefulness of scFv antibodies have also be studied in the context of diagnostics for various cancers,[95-97] auto-immune disorders[98], and viruses,[99,100] including SARS-CoV-2.[101-104] In a recent study by Antoine et al. (2022), an scFv against the SARS-CoV-2 receptor binding domain (RBD) were used to design a rapid, point of care diagnostic assay for COVID-19.[104] The authors incorporated an anti-RBD scFv into a commercially available surface-enhanced Raman scattering (SERS) assay and was able to provide highly sensitive SARS-CoV-2 virus detection in approximately 30 minutes.[104] Similarly, Kim et al. (2021)[103] developed an scFv-Fc fusion protein with high affinity for the SARS-CoV-2 nucleocapsid protein (NP) to create a rapid lateral flow based diagnostic assay for COVID-19.[103] Another study by Duranti et al. (2018) utilized a targeted anti-hERG1 scFv to detect tumor biomarkers as an alternative to monoclonal antibodies, which cannot be implemented for molecular cancer imaging due to their size and long half-life.[105] The successful application of scFvs in a diverse range of clinical fields suggest these fragments could also be implemented as biomolecular tools in other disorders, such as HIT.

2.0. RESEARCH OUTLINE

2.1. Overall Objective

This work aims to develop a high affinity and epitope specific scFv that can inhibit pathogenic anti-PF4/heparin antibodies to be used to design a novel diagnostic assay with improved sensitivity and specificity for HIT.

2.2. Rationale

An improved understanding of pathogenic antibody binding sites on PF4 can allow us to develop an epitope targeted approach to diagnose HIT. Inhibitors against the pathogenic regions

on PF4 may be able to help distinguish between pathogenic and non-pathogenic antibodies based on preventing immune complex formation. Previous studies have shown that immune complex formation and platelet activation can be inhibited using small PF4 antagonists that disrupt tetramerization.[106] These findings support the use of high affinity PF4 inhibitors that prevent pathogenic HIT antibody binding. Particularly, using an epitope-targeted inhibitor against PF4 may allow us to more accurately identify pathogenic anti-PF4/heparin antibodies that cause HIT. Our group previously identified a pathogenic epitope on PF4,[16] which shows anti-PF4/heparin antibodies from HIT-positive patients and KKO bind to an overlapping region on PF4 that is distinct from antibodies produced in HIT-negative patients (Figure 1). Since the pathogenic antibody binding sites on PF4 have been identified, it may be possible to use an epitope-targeted strategy to diagnose HIT. Therefore, the goal of this study is to develop an inhibitor using an scFv derived from KKO to block the heparin-dependent pathogenic binding site on PF4. This inhibitor will be used to design a novel diagnostic EIA for HIT that is able to distinguish between pathogenic and non-pathogenic HIT antibodies based on their individual binding sites.

2.3. Hypothesis

Epitope-specific monoclonal antibody fragments (scFv) of KKO against the heparin-dependent pathogenic region on PF4 will inhibit pathogenic anti-PF4/heparin antibody binding and prevent immune complex formation in HIT.

2.4. Specific Objectives

(i) Improve the affinity of scFv derived from KKO towards the heparin-dependent pathogenic epitope on PF4 using random mutagenesis and phage display.

Random mutagenesis is an established method of improving antibody binding that works by introducing various DNA sequence mutations.[107-109] Random sequence mutations

are first introduced using error-prone, mutagenic PCR before selection.[107] The insertion of various mutations along the scFv sequence will produce a diverse antibody screening library with a range of affinities for a desired antigen.[110] Phage display is commonly utilized for the isolation of specific targets from large protein or antibody libraries.[90,111,112] A starting library of phage is generated by cloning the V_H and V_L chains of an antibody into a phagemid vector, allowing for the monovalent display of scFv on the M13 filamentous phage pIII coat protein.[109,112] Phagemid vectors containing scFv DNA inserts are then used to infect *E. coli* bacteria along with a helper phage, which exponentially grow and amplify the scFv library.[113,114] These large phage libraries are screened for mutant antibodies with enhanced affinity, which are isolated following multiple rounds of screening and amplification.[107,109] Affinity discrimination of mutant phages relies on the antigen specific selection of phage-displayed antibodies and elimination of non-specific binders.[90,115] Resulting libraries possess antibodies with improved binding specificity and affinity towards target antigens.[107,116,117] Sequencing is performed following each cycle to locate mutations that have become enriched after multiple rounds of selection, representing lead candidates that will be further characterized in binding experiments.

(ii) Characterize the binding of mutant KKO-scFv compared to wildtype KKO-scFv.

(iii) Screen KKO-scFv mutants against patient sera containing true-positive and false-positive anti-PF4/heparin antibodies to determine their usefulness as diagnostic tools.

3.0. MATERIALS AND METHODS

3.1. Phage Display Library Construction

The M13 filamentous phage display vector, pADL-22c, was purchased from Antibody Design Laboratories Inc. (San Diego, CA). A library of mutant KKO-scFv sequences was first

constructed for expression in the pADL-22c phage display system. In PCR reactions, primers S1 and AS1 (Table M1) were used to amplify the variable heavy and light chain regions of KKO using the BioRad T100 Thermal Cycler (BioRad, Hercules, CA). Mutagenic PCR was performed using Mutazyme II Polymerase (Agilent Technologies, Inc., Santa Clara, CA), according to manufacturer's instructions. KKO-scFv PCR products were digested with *Sfi*1 and cloned into the overlapping *Bgl*I restriction sites of pADL-22c using T4 DNA Ligase (New England Biolabs Ltd., Ipswich, MA). Ligated products were electroporated into TG1 Electrocompetent *E. coli* cells (Lucigen, Middleton, WI) using the BioRad Gene Pulser (BioRad). Library depth was quantified by determining the number of colony forming units per mL (CFU) on LB agar plates supplemented with 100 μg/mL ampicillin. Colonies were then randomly selected to confirm KKO-scFv insertion by sanger sequencing.

Table M1: Primers for KKO-scFv amplification from pADL-22c phagemid. Underlined amino acids represent the *Bgl*I/*Sfi*1 overlapping restriction enzyme recognition sites.

Primer"	Sequence
S1…Sense Primer	5' GTTATTACTCGCGGCCCAGCCGGCCATGGCTGATATCCA GATGATCCAGAGCC 3'
AS1…Anti-Sense Primer	5' CCATGATGGTGGTGATGGTGTTGGCCTCCCGGGCCACTA GTGGCAGACACGGTAACCAGG 3'

3.2. Phage Library Preparation and Purification

Phage library preparation and purification were performed using a polyethylene glycol (PEG)/NaCl precipitation method as described by Barbas *et al.* (2001)[118] and Kretz (2017).[119] A culture of transformed TG1 *E. coli* (Lucigen) was grown at 37°C while shaking at 250 rpm to the mid-exponential phase (OD_{600}= 0.5-0.6 nm) in LB media containing 100 μg/mL ampicillin. The helper phage M13K07 was then added and incubated with the *E. coli* culture for 1 h at 37°C while shaking at 250 rpm. Culture media was then centrifuged (6000 x g, 15 min) to pellet bacteria. The bacterial pellet was then resuspended in 2xYT media containing 100 μg/mL ampicillin and 50

μg/mL kanamycin and incubated overnight at 30°C while shaking at 250 rpm. The following day, culture media was centrifuged (6000 x g, 10 min) to remove cell debris and phages were precipitated from the supernatant with 0.15x vol of PEG/NaCl (4% w/v PEG-8000 + 3% w/v NaCl) at 4°C overnight. The phages were pelleted by centrifugation (6500 x g, 60 min, 4°C) and re-suspended in Tris buffered saline (TBS) (50 mM Tris-HCl, pH 7.5, 150 mM NaCl). The supernatant was cleared of debris by centrifugation (10 000 x g, 10 min) followed by an additional round of precipitation before storing in TBS with 0.1% v/w Tween-20 (TBS-T) at 4°C. Phage preparations were titered by first growing a fresh culture of K91 *E. coli* in LB media containing 50 μg/mL kanamycin followed by infection with eluted phages for 1 h at 37°C while shaking. Phage titers were calculated according to the following formula:

$$\frac{\#\ of\ colony\ forming\ units\ (CFU)}{100\ \mu L\ x\ dilution\ factor\ (d_f)} = C_f\ (phage/\mu L)$$

3.3. Fluid-Phase Phage Bio-Panning Using Streptavidin Coated Magnetic Beads

Streptavidin-coated magnetic beads were pre-washed with 0.1% v/w Tween-20 in Tris buffered saline (TBS-T, 50 mM Tris-HCl, pH 7.5, 150 mM NaCl). To immobilize the target antigen, biotinylated-heparin (0.5 U/mL) and PF4 (30 μg/mL) in TBS-T supplemented with 2% BSA were incubated with 25 μL streptavidin-coated magnetic beads (Dynabeads™ M-450 Streptavidin, ThermoFisher, Hercules, CA) for 1 h at room temperature while rotating. All wash steps were performed by adding 1 mL of TBS-T and incubating while rotating for 3 minutes before magnetically separating and discarding the supernatant. After washing 3x with TBS-T, beads were incubated with phage in TBS-T + 2% BSA for 2 h at room temperature while rotating. Beads were then washed 5 x 3 min with TBS-T and magnetically separated. After the final wash, phages were eluted in 0.1 M Glycine-HCl (pH 2) and incubated for 10 min at room temperature while rotating. The eluted phage solution was neutralized by adding Tris-HCl buffer (pH 9). A fresh culture of

K12 ER2738 F'pilus positive *E. coli* (New England Biolabs Ltd.) was grown simultaneously (OD_{600nm} = 0.5) in LB media containing 10 μg/mL tetracycline and infected with eluted phages for 1 h at 37°C while shaking. An aliquot of the infected culture was then incubated overnight on LB agar + 2% glucose (w/v) + 100 μg/mL ampicillin plates at 37°C and used for sequence analysis by PCR. The remaining culture was pelleted and resuspended into fresh LB media + 2% glucose (w/v) + 100 μg/mL ampicillin and grown up overnight to amplify the phage. The following day, a new phage library preparation was performed as described in section 3.2. Five rounds of selection were performed before selecting lead candidate KKO-scFv mutants based on sequence analysis.

3.4. Construction and Bacterial Expression of Wildtype and Mutant KKO-scFv

The vector pADL-22c expressing the heavy and light chain variable regions (scFv) of KKO was used for protein expression in bacterial cells. KKO-scFv was transformed into chemically competent *E. coli* One Shot® BL21 (DE3) cells (ThermoFisher) before induction. To overexpress KKO-scFv, bacterial cultures were grown at 37°C to the mid-exponential phase (OD_{600nm} = 0.7-0.8), before adding 0.5 mM isopropyl *β*-D-1-thiogalactopyranoside (IPTG) to induce protein production while shaking at 225 rpm and 37°C for 3 h. Following induction, culture media was centrifuged at 5000 rpm for 15 min to harvest cells. Protein expression was then assessed by examining the pellet of each *E. coli* strain on a 4-20% SDS polyacrylamide gradient gel (BioRad). Bacterial pellets collected from 1L of culture media were then re-suspended in 50 mL lysis buffer: 50 mM sodium phosphate, pH 8, 300 mM NaCl, 20 mM imidazole, 5% (v/v) glycerol, 1% (v/v) Triton-X 100 (ThermoFisher), and 0.5% (v/v) DOC (SigmaAldrich, Oakville, ON) with protease inhibitors (Roche cOmplete EDTA free protease inhibitor tablets, Roche, Laval, QC). Cell lysis was carried out by sonication in 5 s pulses at 60% amplitude with 5 s cooling cycles on ice for a

total of 4 min. The supernatant was then centrifuged at 12,000 x *g* for 30 min and collected for purification by Ni^{2+} affinity chromatography.

3.5. Ni-NTA Affinity Purification of KKO-scFv

Empty gravity flow chromatography columns (BioRad) loaded with 1 mL HisPur™ Ni-NTA Resin (ThermoFisher) were used for KKO-scFv purification. The supernatant collected following bacterial lysis was added to the Ni-NTA column followed by 2x50 mL washes with buffer (50 mM $NaPO_4$, pH 8, 300 mM NaCl, and 20 mM imidazole). Histidine-tagged KKO-scFv was then eluted in a buffer solution containing 50 mM $NaPO_4$, pH 8, 300 mM NaCl, and 500 mM imidazole. Eluted fractions with the highest absorbance at 280 nm were then pooled and concentrated using Amicon® Ultra-4 10K centrifugal filter units (MilliporeSigma, Burlington, MA). Purification was confirmed by examining a sample of each eluted fraction on a denaturing 4-20% SDS polyacrylamide gradient gel (BioRad) and visualized using Coomassie SimplyBlue™ SafeStain (ThermoFisher).

3.6. Inhibitory PF4/heparin IgG-specific Streptavidin Enzyme Immunoassay (EIA)

The binding activity of wildtype and mutant KKO-scFv antibodies to PF4/heparin complexes was be measured using an inhibitory PF4/heparin IgG-specific EIA with a streptavidin-biotin capture system. Before performing this protocol, 96-well NUNC Maxisorp plates (ThermoFisher) were coated with 10 μg/mL streptavidin for 24 h. Plates were then blocked with 3% bovine serum albumin (BSA) in phosphate buffered saline (PBS) for 2 h at room temperature. Plates were then coated with 1 U/mL biotinylated-heparin for 1 h followed by 30 μg/mL PF4 for 1 h. Binding of HIT patient sera in a 1:50 dilution or full-length KKO (2 μg/mL) in the presence of mutant or wildtype KKO-scFv at increasing concentrations (50, 25, 10, 5.0, 1.0, 0.5 μg/mL in PBS + 1% BSA) was performed for 1 h at room temperature. After washing, alkaline phosphatase-

conjugated anti-human or anti-mouse IgG (Jackson Immuno Research Laboratories, Inc., West Grove, PA) was added at a 1:4000 dilution and incubated for 1 h at room temperature. For detection, 1 mg/mL p-nitrophenylphosphate (PNPP, Sigma-Aldrich) substrate dissolved in 1 mol/L diethanolamine (DEA) buffer (pH 9.6) was added. The optical density (OD) was measured at 2 min intervals for 30 min at 405 nm (OD_{405nm}) using a BioTek 800 TS plate reader (BioTek Instruments Inc., Winooski, VT) to determine if anti-PF4/heparin antibody binding was inhibited. Results were reported as a decrease in OD (absorbance at 405nm) from baseline levels.

The percentage of inhibition relative to anti-PF4/heparin antibody binding in the absence of KKO-scFv was also calculated using the following formula:

$$\text{Percentage of inhibition } (\%) = \left[\frac{(\text{OD405nm}_{\text{sera}} - \text{OD405nm}_{KKO\ scFv\ +\ sera})}{\text{OD405nm}_{\text{sera}}}\right] x\ 100$$

The concentration of KKO-scFv achieving 50% inhibition (IC_{50}) of KKO binding was calculated using non-linear dose-response curve fitting analysis on GraphPad Prism version 9.1.2 (GraphPad Software, Inc).

3.7. Biolayer Interferometry (BLI) using Wildtype and Mutant KKO-scFv

PF4 was purified and biotinylated as previously described.[120,121] Briefly, PF4 was incubated with 5x Heparin Sepharose 6 Fast Flow Chromatography Medium (GE Healthcare, Chicago, IL) for 1 h while shaking before adding 20 molar excess EZ-link-Sulfo-NHS-LC-Biotin (ThermoFisher). The biotin-PF4-heparin-sepharose mixture was incubated for 1 h with shaking to allow for the biotinylating reaction to occur. Biotinylated-PF4 was eluted from the heparin sepharose at high sodium concentration (PBS + 2M NaCl) and the absorbance at 280 nm was measured on a spectrophotometer (Eppendorf, Hamburg, Germany) to determine the concentration. Biotinylation of PF4 was then confirmed in a streptavidin anti-PF4/heparin EIA using the murine monoclonal antibody KKO.

The Octet-QK Red 96 (FortéBio, Menlo Park, CA) instrumentation was used to conduct all BLI experiments. A 96-well microtiter plate (black, flat-bottom) was used to hold 200 µL per well of either sample or buffer. Pre-coated streptavidin biosensor tips (FortéBio) were hydrated in phosphate buffered saline (PBS) containing 1% bovine serum albumin (BSA, Sigma-Aldrich) before performing all kinetic assays. Each step was performed at an operating temperature of 23°C with agitation at 1000 rpm. Streptavidin tips were first equilibrated in PBS + 1% BSA to establish a baseline. Biosensors were then dipped into wells containing 7.5 µg/mL biotinylated-PF4 (7.5 µg/mL in PBS + 1% BSA) alone or complexed with 0.125 U/mL unfractionated heparin for 15 minutes for antigen immobilization. The PF4-coated tips were then dipped into PBS + 1% BSA for 13 minutes to re-establish a baseline. Tips were then incubated in an analyte solution containing half-fold dilutions of wildtype KKO-scFv (4.0, 2.0, 1.0, 0.5, 0.25 µg/mL in PBS + 1% BSA) for 10 minutes to measure association. For mutant KKO-scFv association, tips were incubated in an analyte solution containing 200 µL of each mutant and wildtype KKO-scFv at a final concentration of 1 µg/mL in PBS + 1% BSA. Antibody dissociation steps were performed by dipping sensors in wells containing PBS + 1% BSA for 56 minutes. The following negative controls included in these kinetic experiments were also measured: 200 µL of buffer to replace both the antigen and KKO-scFv and 200 µL buffer replacing KKO-scFv only. Each experiment was performed with PF4 or with PF4/heparin as the immobilized antigen.

3.8. BLI Data Acquisition and Kinetic Analysis

Data acquisition was performed using Octet® User Software version 3.1 and analyzed using the 1:1 homogenous ligand binding model. Results were processed by subtracting reference from control values and aligned to fit curves correctly according to the baseline. Average rate constants (± standard deviation) for association (k_{on}), dissociation (k_{off}), and affinity (K_D) along

with error and R^2 values were calculated automatically by the supplier's software. The binding profile of each analyte was also described in terms of an average wavelength shift (nm; response), representing the change in molecules bound to the biosensor surface for the duration of the association step.

3.9. Epitope Mapping of KKO-scFv Binding to PF4

Epitope mapping was performed as described in a modified streptavidin PF4/heparin IgG-specific EIA using a library of 70 PF4 mutants.[13,63] Previously, the DNA coding sequence of human PF4 was expressed in the pET22b expression vector at the *Nde*I and *Hind*III restriction enzyme sites (GenScript, Piscatawa, NJ). Mutants of PF4 were designed using alanine-scanning mutagenesis, where each residue of PF4 was mutated to alanine or valine in the case of an alanine residue.[13] The purification of mutant PF4 was also performed as previously described.[13,120] Mutant PF4 was transformed and over-expressed in ArcticExpress (DE3) *E.coli* cells (Agilent Technologies) at 37ºC before inducing at 37ºC for 3h in the presence of 0.5 mM IPTG. Cells containing mutant PF4 were lysed by sonication in a buffer (pH 7.2) containing 20 mM Na_2PO_4, 400 mM NaCl, 1.4 mM β-Me, 5% (v/v) glycerol, 1% (v/v) Triton X-100 (ThermoFisher), 0.5% (w/v) DOC (MilliporeSigma), 2 mM $MgCl_2$, 10 μg ml^{-1} DNaseI (MilliporeSigma), and EDTA-free protease inhibitor cocktail (Roche). Lysis supernatant was then centrifuged for 40 min at 40,000xg and purified in a two-step process first loading the supernatant on a HiTrap Q HP column (Cytiva Life Sciences, Marlborough, MA) followed by purification on a HiTrap Heparin HP column (Cytiva Life Sciences). Each PF4 mutant was eluted from the column on a linear gradient of 0.5 to 2M NaCl and fractions containing pure protein were concentrated and stored in PBS.

The binding of KKO-scFv to mutant or wildtype PF4 was then assessed in a modified streptavidin PF4/heparin IgG-specific EIA as performed by Huynh et al. (2019, 2021).[13,63] NUNC

Maxisorp 384-well microtiter plates (ThermoFisher) were coated with 10 μg/mL streptavidin for 24 h. Plates were then blocked with 3% BSA in PBS for 2 h at room temperature and coated with 1 U/mL biotinylated-heparin for 1 h. Wild-type or mutant PF4 using a concentration of 5 μg/mL were then incubated for 1 h at room temperature followed by diluted KKO-scFv (wildtype and mutant) at a concentration of 5 μg/mL. To detect KKO-scFv binding, an anti-6xhistidine-tag antibody (ThermoFisher) at a 1:10,000 dilution was added for 1 h at room temperature. After washing, alkaline phosphatase-conjugated anti-mouse IgG (Jackson Immuno Research Laboratories, Inc.) was incubated on plates for 1h at a 1:4000 dilution. Finally, 1 mg/mL PNPP (Sigma-Aldrich) substrate dissolved in 1 mol/L DEA buffer (pH 9.6) was added. The OD was measured at 2 min intervals for 30 min at 405 nm (OD_{405nm}) and 490nm (OD_{490nm}) using a BioTek 800 TS plate reader (BioTek Instruments Inc.) to determine if KKO-scFv binding was perturbed. An amino acid was defined as essential to the KKO-scFv epitope if it resulted in a greater than (≥) 50% reduction in binding when mutated to alanine or valine compared to the wildtype residue. The percentage of binding loss relative to wildtype PF4 was calculated using the following formula:

$$\%\ \text{binding relative to WT} - \text{PF4} = \frac{(\text{OD405nm}_{mutant\ PF4}/\text{OD405nm}_{WT\ PF4})_{Test\ ab}}{(\text{OD405nm}_{mutant\ PF4}/\text{OD405nm}_{WT\ PF4})_{Polyclonal\ HIT-ab}}\ x\ 100$$

3.10. Serotonin-Release Assay (SRA) using KKO-scFv

Previously tested EIA-positive/SRA-positive HIT patient samples (n=5) were tested in a modified SRA to determine if KKO-scFv can inhibit platelet activation. Platelets labelled with ^{14}C-serotonin were pre-incubated with 50 μg/mL and 75 μg/mL of wildtype or mutant KKO-scFv constructs for 15 min. Platelets and KKO-scFv were then incubated with patient sera in the presence of therapeutic heparin doses (0.2 U/mL) as previously described.[51] Plates were incubated for 1 hr with shaking, followed by the addition of PBS-EDTA before centrifuging. To determine

^{14}C-serotonin-release, an aliquot of supernatant was removed from each well and measured using a scintillation counter (Packard Topcount, Meriden, CT, USA). The ability of each KKO-scFv construct to inhibit immune complex formation resulting in a moderate (≥20%) or strong (≥50%) decrease in ^{14}C-serotonin release was determined relative to control wells containing patient sera in the absence of KKO-scFv.

3.11. Statistical Analysis

GraphPad Prism version 9.1.2 for Mac OS software (GraphPad Software, Inc) was used to create all graphs and perform statistical analysis. Differences between data sets were tested for statistical significance using an unpaired, two-tailed, *t*-test using Microsoft Excel for Mac version 15.37 where $p < 0.01$ was considered statistically significant.

4.0. RESULTS

4.1. KKO-scFv Phage Library Construction

4.1.1. Wildtype KKO-scFv Cloning and Mutant Library Preparation

Wildtype KKO-scFv was cloned in to the phagemid vector pADL-22c using restriction enzyme *Bgl*1 and *Sfi*1 and electroporated into TG1 *E. coli* cells (Appendix Figure 2). Phagemids were confirmed for KKO-scFv insertion by PCR screening of 12 randomly selected colonies using two sets of DNA specific primers that overlap at each ligation site (Supplementary Table 1). KKO-scFv bands were visualized at approximately 350 bp using the first primer set and 550 bp using the second primer set, corresponding with the expected fragment sizes (Appendix Figure 2). All PCR products were then purified and analyzed by Sanger sequencing to verify correct DNA sequence.

Mutants of KKO-scFv were designed by inserting random mutations along the DNA sequence by mutagenic PCR. Mutated KKO-scFv was then cloned into pADL-22c as previously

described. Phagemids were confirmed for correct DNA insertion following a screen of 20 randomly selected colonies by PCR using primers that overlap with the *Bgl*1/*Sfi*1 ligation site (Figure 2). Bands were visualized at approximately 890 bp, corresponding with expected fragment sizes of KKO-scFv (Figure 2). PCR products were then purified and analyzed by Sanger sequencing to verify the presence of mutations throughout the KKO-scFv sequence. The average DNA mutation frequency was 16 mutations per kilo base (kb).

4.2. Phage Bio-Panning Optimization and Mutant Library Screening

4.2.1. Characterizing Wildtype KKO-scFv Phage Binding

To assess proper binding of phage-displayed wildtype KKO-scFv and confirm its specificity for PF4/heparin, a fluid phase enrichment assay with PF4/heparin complexes coated on streptavidin (SA) magnetic beads was performed. Based on the known activity of full-length KKO,[16] we predicted that KKO-scFv will out compete a non-specific protein for binding to PF4/heparin complexes. Acting as a target-unrelated peptide in this assay, the D' domain of vWF provides the partial binding site for coagulation factor VIII and has no known interactions with PF4.[122] Phages displaying vWF D' domain and wildtype KKO-scFv were mixed in an unequal ratio of 10:1 and used to infect *E. coli*, establishing a baseline prior to selection.

The combined phage solution was then incubated on magnetic SA beads coated with either biotinylated heparin (b-heparin) and PF4, b-heparin alone, or uncoated beads alone to assess binding. Before selection, only 1/20 (5.0%) *E. coli* colonies were positive for phage displaying KKO-scFv and after one round of selection on PF4/heparin coated beads, the number of colonies positive for KKO-scFv phage increased to 19/20 (95.0%) (Figure 3). The number of *E. coli* colonies positive for KKO-scFv phage also remained unchanged when incubated with heparin coated (1/20, 5.0%) or uncoated beads (2/20, 10.0%), demonstrating any phage interference does

not impact KKO-scFv specificity for PF4/heparin (Figure 3). These results show KKO-scFv expressed on the surface of phage binds to PF4/heparin complexes with high specificity over a non-specific protein. Furthermore, this method represents the optimized assay used to screen for high-affinity mutant KKO-scFv antibodies.

4.2.2. Isolation of High Affinity KKO-scFv Clones from a Phage Display Library

Phage bio-panning against PF4/heparin complexes successfully captured five unique mutant KKO-scFv variants that became enriched after five rounds of selection (Table 2). At each cycle of bio-panning, input and output phage titers were monitored followed by Sanger sequencing to track mutation occurrences (Table 2). Sequence analysis was performed on 40 randomly chosen colonies at each round, identifying five frequently occurring KKO-scFv mutants with unique sequences. The lead candidate mutants observed include: KKO-scFv$^{(R18K,\ N152K,\ D180N)}$, KKO-scFv$^{(S50N,\ Y53H)}$, KKO-scFv$^{(Y156H)}$, KKO-scFv$^{(Y156H,\ D180G,\ Q233P)}$, and KKO-scFv$^{(E183V,\ E185K,\ G223R)}$, henceforth referred to as mutant B, C, D, E, and F, respectively (Table 3). After five rounds of selection, mutant B occurred with a frequency of 7.5% (3/40), mutant C occurred with a frequency of 7.5% (3/40), mutant D occurred with a frequency of 15.0% (6/40), mutant E occurred with a frequency of 12.5% (5/40), and mutant F occurred with a frequency of 4.0% (2/48) (Table 3). Additionally, an overlapping amino acid substitution (Y156H) was identified in both mutant D and E with a cumulative frequency of 27.5% (11/40), suggesting this mutation may contribute significantly to PF4/heparin binding (Table 3).

4.2.3. Expression and Purification of Wildtype and Mutant KKO-scFv

After identifying five novel KKO-scFv variants, each mutant and wildtype were expressed in BL21 *E. coli* and purified on a Ni-NTA column for further characterization (Supplementary Figures 5-10). After affinity purification, the protein yield for wildtype KKO-scFv was 2.16 mg,

mutant B was 6.00 mg, mutant C was 1.15 mg, mutant D was 5.29 mg, mutant E was 2.33 mg, and mutant F was 1.42 mg. Concentrated fractions containing pure protein as determined by measuring absorbance at 280 nm were separated on a 4-20% SDS PAGE gel. KKO-scFv migrated as a single band with relative mobility of approximately 28 kDa, which was observed following Coomassie SimplyBlue™ SafeStain analysis (Figure 4). An unknown protein was observed in each purified protein sample at approximately 65 kDa (Figure 4). However, the purity of KKO-scFv samples obtained here was deemed suitable for the purpose of this study and the unknown protein did not interfere with later binding studies.

4.3. Characterizing Wildtype and Mutant KKO-scFv Binding

4.3.1. Binding Kinetics Using Biolayer Interferometry (BLI)

BLI experiments were performed to evaluate binding responses and affinities of wildtype and mutant KKO-scFv. Biotinylated PF4 alone or complexed with heparin was immobilized on streptavidin biosensors and used to capture wildtype KKO-scFv. Half-fold serial dilutions of wildtype KKO-scFv ranging from 0.25 μg/mL to 4 μg/mL were used to determine the optimal concentrations for future experiments (PF4/heparin Supplementary Figure 11; PF4 Supplementary Figure 12). An optimal concentration of 1 μg/mL was selected and BLI was repeated with immobilized biotinylated PF4 alone (Figure 5) or complexed with heparin (Figure 6) to compare average binding responses [wavelength shift (nm) ± standard deviation (s.d.)] and kinetic rates [equilibrium constant (K_D) ± s.d.] of wildtype to each mutant KKO-scFv.

BLI analysis revealed that wildtype KKO-scFv had an average binding response of 0.0386 ± 0.01 nm against PF4 and 0.0758 ± 0.01 nm against PF4/heparin (Figure 5b, 6b). Mutant C showed comparable binding responses to wildtype KKO-scFv for PF4 (0.0399 ± 0.01 nm) but had 2-fold higher binding responses to PF4/heparin (0.0898 ± 0.06 nm) (Figure 5b, 6b). Mutant D

demonstrated at least 3-fold higher binding responses than wildtype when tested against PF4 alone (0.1450 ± 0.02 nm) and PF4/heparin (0.1325 ± 0.01 nm) (Figure 5b, 6b). Mutant E had a 2-fold higher binding response to PF4 (0.0986 ± 0.01 nm) and a similar binding response when tested against PF4/heparin (0.0907 nm s.d. ± 0.01 nm) (Figure 5b, 6b). The binding response of mutant B had a 7-fold increase against PF4 (0.2665 ± 0.03 nm) and 4-fold increase (0.2849 ± 0.01 nm) against PF4/heparin (Figure 5b, 6b). Lastly, mutant F had a 5-fold increase binding response (0.2110 ± 0.03 nm) against PF4 and 5-fold increase binding response (0.3787 ± 0.01 nm) against PF4/heparin compared to wildtype (Figure 5b, 6b).

The average K_D values for wildtype KKO-scFv were calculated using the k_{on} and k_{off} rates for PF4 ($K_D = 1.32x10^{-6} \pm 1.11x10^{-6}$ M) and PF4/heparin ($K_D = 5.87x10^{-7} \pm 1.01x10^{-7}$ M) (Figure 5b, 6b). Mutant C had a comparable affinity as wildtype KKO-scFv for PF4 alone ($1.66x10^{-6} \pm 1.49x10^{-6}$ M) and a 10-fold increased affinity for PF4/heparin ($9.48x10^{-8} \pm 1.59x10^{-8}$ M) (Figure 5b, 6b). Mutant D had a 1000-fold stronger affinity ($5.83x10^{-9}$ M ± $3.13x10^{-9}$ M) and a 100-fold stronger affinity ($3.77x10^{-9} \pm 3.95x10^{-9}$ M) compared to wildtype KKO-scFv, while mutant E had 10,000-fold ($9.54x10^{-10} \pm 6.59x10^{-10}$ M) and 100-fold ($2.75x10^{-10} \pm 1.56x10^{-9}$ M) stronger affinities when tested against PF4 and PF4/heparin, respectively (Figure 5b, 6b). The K_D for Mutant B against PF4 alone increased by 1000-fold ($1.69x10^{-9} \pm 5.14x10^{-10}$ M) and 100-fold ($1.36x10^{-9} \pm 1.51x10^{-11}$ M) against PF4/heparin (Figure 5b, 6b). Mutant B also demonstrated improved affinities, with a K_D of $6.07x10^{-10} \pm 3.12x10^{-10}$ M) against PF4 and $2.92x10^{-10} \pm 1.07x10^{-10}$ M against PF4/heparin (Figure 5b, 6b). The data presented here demonstrate at least four mutant variants of KKO-scFv out of the five isolated have stronger binding responses and increased affinity for PF4 and PF4/heparin, suggesting these mutants have an improved kinetic performance compared to wildtype.

4.3.2. Full-Length KKO Inhibition and Determining IC_{50} Values

To further evaluate the binding of mutant and wildtype KKO-scFv, their ability to inhibit full-length KKO from binding PF4/heparin complexes was assessed in a modified streptavidin-capture EIA. Biotinylated heparin was immobilized with PF4 on streptavidin-coated plates and incubated with KKO in the presence of KKO-scFv at half-fold serial dilutions from 0 to 160 μg/mL. The concentration that achieves 50% inhibition (IC_{50}) of KKO binding was then determined for wildtype and each mutant variant of KKO-scFv, where lower IC_{50} values reflect mutants with superior inhibitory strength (Table 4). Wildtype KKO-scFv and mutant C were unable to inhibit full-length KKO binding at these concentrations and IC_{50} values for these constructs were not calculated. Mutant B had an IC_{50} value of 57.3 nM (1.6 μg/mL), mutant D had an IC_{50} value of 111.1 nM (3.1 μg/mL), mutant E had an IC_{50} value of 292.8 nM (8.2 μg/mL), and mutant F had an IC_{50} value of 46.8 (1.3 μg/mL).

Wildtype KKO-scFv was unable to significantly prevent full-length KKO at any concentration, achieving a maximum inhibition of 24.2 ± 4.9% (Figure 7). Mutant B appeared much stronger than wildtype KKO-scFv, illustrated by the substantial improvement of KKO inhibition and effectiveness at low concentrations (IC_{50} = 1.6 μg/mL) (Figure 7). Mutant C had a similar response against KKO to the wildtype, with weak inhibitory activity at all concentrations and a maximum of only 38.0 ± 6.7% inhibition (Figure 7). Mutant D and E also showed improved inhibitory activity against KKO at high and low concentrations compared to wildtype, with low IC_{50} values (3.1 μg/mL and 8.2 μg/mL, respectively) (Figure 7). Mutant F demonstrated the strongest inhibitory activity against KKO at all concentrations with the lowest IC_{50} value (1.3 μg/mL). These results also suggest KKO-scFv mutant B, D, E, and F have improved binding

affinities for PF4/heparin as indicated by their stronger inhibitory effect on full-length KKO compared to wildtype, supported by earlier BLI data.

4.3.3. Epitope Mapping of the KKO-scFv Binding Site on PF4

Epitope mapping was then done by Angela Huynh and Mercy Daka using a library of 70 PF4 mutants, previously generated by alanine-scanning mutagenesis, to identify the wildtype KKO-scFv binding site. Amino acids critical for KKO-scFv binding were identified as those causing a reduction in binding by 60% or greater when mutated to an alanine residue (or valine if the wildtype amino acid was alanine) compared to wildtype PF4. Epitope mapping identified thirteen key amino acids (L8, C10, V13, A32, K31, C36, A39, I41, C52, L55, Q56, L67, and L68) that compose the binding site for wildtype KKO-scFv. Comparing the binding site also revealed eight critical amino acids (C10, V13, A32, C36, C52, L55, Q56, and L68) overlap between the wildtype KKO-scFv and full-length KKO binding site on PF4[13,47] (Figure 8b). As predicted based on previous epitope mapping studies with KKO,[13] these key amino acids were also localized to the same region when displayed on the PF4 tetramer (Figure 8a).

To show any changes to the wildtype KKO-scFv binding site, epitope mapping of each mutant construct was then performed (Figure 8). The epitope for mutant C was found to contain eight amino acids on PF4 (C10, V13, A32, C36, C52, L55, Q56, L67), seven of which correspond to amino acids on PF4 bound by both full-length KKO and wildtype KKO-scFv. Epitope mapping further identified 20 amino acids on PF4 that make up the mutant D binding site (N7, C10, L11, C12, V13, Q18, I30, C36, L45, K46, I51, C52, L55, Q56, A57, Q56, L67, L68, Q69, S70), of which eight amino acids were shared by both full-length KKO and wildtype KKO-scFv and overlapped with the same region on PF4 (Figure 8). Epitope mapping of mutant B revealed this construct bound different amino acids on PF4 compared to wildtype KKO-scFv (Figure 8). None

of the 11 identified residues (L11, K14, H23, I24, I30, K31, Q40, K46, K50, I63, and I64) were common between either the KKO-scFv or full-length KKO epitope (Figure 8b).

However, the mutant B binding site did appear to overlap with the region on PF4 bound by both full-length KKO and KKO-scFv, which is also recognized by pathogenic HIT antibodies[13] (Figure 8a). Interestingly, we found that two amino acids in the mutant B epitope (H23 and K46) overlapped with the heparin-binding site on PF4 (Supplementary Figure 14).[63,123] This site is also known to bind group 3/heparin-independent antibodies that are produced in combination with group 2/heparin-dependent antibodies by a subset of HIT-positive patients.[63] Mutant B similarly bound to two amino acids on PF4 (H23 and Q40) that were previously reported as critical for the binding of HIT patient sera that contained a polyclonal mixture of heparin-dependent and -independent antibodies (Supplementary Figure 14).[63,123]

4.4. Inhibiting HIT-Positive (EIA+/SRA+) and HIT-Negative (EIA+/SRA-) Antibody Binding

Sera (n=10) from confirmed HIT-positive patients (EIA-positive/SRA-positive) containing anti-PF4/heparin antibodies were used in a modified streptavidin-biotin based anti-PF4/heparin IgG EIA (streptavidin anti-PF4/hep EIA) with KKO-scFv at concentrations from 0 to 50 μg/mL. On average, antibody binding to PF4/heparin was reduced in the presence of increasing KKO-scFv concentrations in a dose-dependent manner (Figure 9). HIT-positive patients were also sub-divided into two cohorts: 1) those with a mixture of both heparin-dependent and -independent antibodies (n=5) and 2) only heparin-dependent antibodies (n=5). It is known that heparin-independent antibodies bind to a different region of PF4 compared to heparin-dependent antibodies (Supplementary Figure 14). It is possible that the ability of KKO-scFv to reduce antibody binding in HIT-positive patients who produce both heparin-dependent and -independent antibodies.

However, no difference in the degree of inhibition was observed between patients with both heparin-dependent and -independent antibodies or only heparin-dependent antibodies (Figure 9).

The ability of each KKO-scFv construct to inhibit antibody binding is shown as a decrease in absorbance (OD) at 405 nm where an $OD_{405nm} \geq 0.45$ in this assay is considered positive for anti-PF4/heparin antibodies. The weakest inhibitors in the streptavidin anti-PF4/hep EIA were wildtype KKO-scFv and mutant C, which also showed the worst performance in earlier characterization experiments. Only 2/10 (20.0%) HIT-positive patients became negative ($OD_{405nm} \leq 0.45$) with the addition of either wildtype KKO-scFv or mutant C at maximum concentrations, respectively (Figure 9a,c). KKO-scFv mutants D and E showed improved inhibition of pathogenic antibody binding, as 7/10 (70.0%) and 8/10 (80.0%) HIT-positive patients become negative in with the addition of either construct at 50 μg/mL, respectively (Figure 9d,e). The strongest inhibitors of pathogenic antibody binding in the streptavidin anti-PF4/hep EIA were KKO-scFv mutants B and F. When 50 μg/mL of either construct was added, 9/10 (90.0%) HIT-positive patients became negative and when 10 μg/mL was added, 7/10 (Mutant B, 70.0%) and 6/10 (Mutant F, 60.0%) HIT-positive patients became negative, further highlighting the strength of these constructs (Figure 9b,f). A significantly greater difference between antibody binding ($OD_{405nm} \geq 0.45$) was also observed in all HIT-positive patients with or without the addition of wildtype KKO-scFv (1.657 and 0.931, $p = 0.018$), mutant B (1.565 and 0.275, $p = 0.001$), mutant C (1.684 and 0.799, $p = 0.010$), mutant D (1.840 and 0.283, $p = 0.001$), mutant E (1.682 and 0.319, $p = 0.001$), and mutant F (1.723 and 0.281, $p = 0.002$) (Table 5).

Sera (n=10) from confirmed HIT-negative patients (EIA-positive/SRA-negative) containing anti-PF4/heparin antibodies were then used in the same EIA with KKO-scFv constructs to determine if antibody binding was decreased in this cohort (Figure 10). Neither wildtype nor

mutant KKO-scFv constructs were able to significantly inhibit antibody binding to PF4/heparin at any concentration (Figure 10, Table 5). The mean OD_{405nm} at 50 μg/mL for all HIT-negative patients with and without the addition of wildtype KKO-scFv was 1.983 and 1.407 (p = 0.303), mutant B was 0.893 and 1.102 (p = 0.438), mutant C was 0.932 and 1.235 (p = 0.285), mutant D was 0.910 and 1.002 (p = 0.700), mutant E was 0.876 and 1.080 (p = 0.430), and mutant F was 0.841 and 1.189 (p = 0.195) (Table 5).

The percentage of inhibition for each KKO-scFv construct was also determined against sera from confirmed HIT-positive (n=10) and HIT-negative (n=10) patients at an optimal concentration of 50 μg/mL (Figure 11). Better diagnostic discrimination between HIT-positive and HIT-negative patients in the streptavidin anti-PF4/hep EIA was observed in the presence of each KKO-scFv construct. Wildtype KKO-scFv inhibited HIT-positive and HIT-negative antibodies by an average percentage of 44.7% and -38.3% (p=0.0002), respectively (Table 6). Mutant B inhibited HIT-positive and HIT-negative antibodies by an average percentage of 77.8% and -31.4% (p<0.0001), respectively (Table 6). Mutant C inhibited HIT-positive and HIT-negative antibodies by an average percentage of 50.6% and -42.5% (p=0.0004), respectively (Table 6). Mutant D inhibited HIT-positive and HIT-negative antibodies by an average percentage of 78.3% and -17.3% (p<0.0001), respectively (Table 6). Mutant E inhibited HIT-positive and HIT-negative antibodies by an average percentage of 76.5% and -34.0% (p=0.0001), respectively (Table 6). Mutant F inhibited HIT-positive and HIT-negative antibodies by an average percentage of 80.0% and -57.0% (p=0.0005), respectively (Table 6). While each construct of KKO-scFv was able to decrease antibody binding to varying degrees, mutants B, D, E, and F remained the strongest inhibitors compared to wildtype. Furthermore, antibody binding in HIT-negative patient samples was not significantly altered in the presence of any KKO-scFv construct in this assay.

4.5. Assessing the Clinical Applications of High-Affinity KKO-scFv Mutants

4.5.1. Large-Scale Screening of HIT-Positive (EIA+/SRA+) and HIT-Negative (EIA+/SRA-) Patient Sera

A large-scale screening of HIT patient sera was performed to further evaluate the utility of this assay as a diagnostic test. Based on previous characterization experiments, mutant B and mutant F were chosen as lead candidate mutants because they had stronger affinities in BLI, superior inhibitory activities against KKO full-length, and provided the best separation between pathogenic and non-pathogenic anti-PF4/heparin antibodies. Sera from confirmed HIT-positive (n=20) and HIT-negative (n=20) patients were then tested to further determine if mutant KKO-scFv can improve the diagnostic performance of the streptavidin anti-PF4/hep EIA by eliminating the high rate of false-positive results typically generated in this assay. Wildtype KKO-scFv was tested alongside mutant B and F KKO-scFv as a control to compare performances.

The ability of KKO-scFv to inhibit antibody binding at an optimal concentration of 50 μg/mL was determined based on the ability of these constructs to decrease antibody absorbance levels in a particular sample to negative threshold levels ($OD_{405nm} \leq 0.45nm$). Levels of pathogenic and non-pathogenic anti-PF4/heparin antibody binding remained significantly different between the upscaled HIT-positive and HIT-negative patient cohorts before and after the addition of KKO-scFv wildtype (p=0.019, Figure 12), mutant B (p=0.0001, Figure 13), and mutant F (p=0.0007, Figure 14). Furthermore, HIT-positive patients almost always became negative ($OD_{405nm} \leq 0.45nm$) in this assay with the addition of either mutant B (Figure 13) or mutant F (Figure 14), providing superior separation between pathogenic and non-pathogenic antibodies compared to wildtype KKO-scFv (Figure 12). Only 4/20 (20.0%) and 6/20 (30.0%) patients remained positive in the presence of KKO-scFv mutant B or mutant F, respectively compared to 17/20 (85.0%)

patients in the presence of wildtype KKO-scFv (Figure 12-14). A significant difference between pathogenic and non-pathogenic anti-PF4/heparin antibody binding was also observed in the presence of mutant B (mean inhibition; 75.8% vs. -4.4%, $p<0.0001$, Figure 15) and mutant F (mean inhibition; 76.0% vs. -13.0%, $p<0.0001$, Figure 15).

4.5.2. Determining New Positivity Thresholds and Diagnostic Performance of a Novel HIT Diagnostic Assay

Using previously tested patient samples (HIT-positive, n=20; HIT-negative, n=20), receiver operating characteristic (ROC) curves for the streptavidin anti-PF4/heparin IgG EIA using wildtype KKO-scFv, mutant B, or mutant F were generated to further assess the diagnostic performance of this assay (Figure 16). The ideal measurement for this assay was determined to be the percentage of inhibition rather than absorbance levels because they provide a better diagnostic sensitivity and specificity (data not shown). Based on ROC curve analysis, the positivity thresholds for this assay when using KKO-scFv wildtype, mutant B, and mutant F was a percentage of inhibition greater or equal to (≥) 42.0%, ≥ 39.8%, and ≥ 54.6%, respectively (Table 7). The area under the curve (AUC) value, which measures the ability of an assay to discriminate between patients with or without the disease,[124] was then determined. KKO-scFv wildtype had an AUC value of 0.84 (95% Confidence Interval [CI] 0.71-0.97), mutant B had an AUC of 0.98 (95% CI 0.95-1.00), and mutant F had an AUC of 0.98 (95% CI 0.94-1.00) (Table 7).

The sensitivity and specificities of this assay were then determined using each KKO-scFv construct at the ROC determined optimal thresholds (Table 8). The EIA with wildtype KKO-scFv at a positivity threshold of ≥42.0% inhibition had a sensitivity and specificity of 70% (95% CI 45.7-88.1) and 95% (75.1-99.9), respectively with a positive predictive value (PPV) of 93.3% (95% CI 67.0-99.0) and negative predictive value (NPV) of 76.0% (95% CI 61.7-86.2). When

using Mutant B at a positivity threshold of ≥39.8% inhibition, this assay had a sensitivity and specificity of the EIA was 100.0% and 90.0% (95% CI 68.3-88.8), respectively with a PPV of 90.9% (95% CI 72.8-97.4) and NPV of 100.0%. Lastly, the addition of mutant F in this assay at a positivity threshold of ≥54.6% inhibition had a sensitivity and specificity of 95.0% (95% CI 75.1-99.9) and 90.0% (95% CI 68.3-98.8), respectively with a PPV of 90.5% (95% CI 71.8-97.3) and NPV of 94.7% (95% CI 79.6-98.4). Therefore, mutant KKO-scFv was not only able to distinguish between pathogenic and non-pathogenic anti-PF4/heparin antibodies, but significantly improved the specificity (90.0%) of the streptavidin anti-PF4/hep EIA without sacrificing sensitivity (95.0-100.0%). A schematic diagram illustrating the inhibitory EIA using KKO-scFv compared to the original assay is shown in figure 18.

4.5.3. Inhibiting Immune Complex-Mediated Platelet Activation

To help inform future clinical studies using KKO-scFv, preliminary experiments were then performed to determine if wildtype and mutant KKO-scFv can inhibit the functional activity of pathogenic antibodies in an SRA. The ability of each KKO-scFv variant to inhibit platelet activation resulting in a moderate (≥20%) or strong (≥50%) decrease in the percent of ^{14}C-serotonin release was tested using strongly reactive (^{14}C-serotonin release > 85%) HIT-positive (EIA+/SRA+) patient sera (Figure 17).

Baseline platelet activation was assessed before the addition of any construct and in the presence of wildtype or mutant KKO-scFv at 50 and 75 μg/mL concentrations (Figure 17). Wildtype KKO-scFv inhibited platelet activation moderately in 2/5 (40%) HIT-positive samples and strongly inhibited platelet activation in 0/5 (0.0%) samples at both 50 and 70 μg/mL concentrations (Figure 17a). Comparatively, mutant B strongly inhibited platelet activation in 4/5 (80.0%) HIT-positive samples at either one or both concentrations (Figure 17b). Mutant C

performed similarly to wildtype, moderately inhibiting 3/5 (60.0%) HIT-positive samples and strongly inhibiting 0/5 (0.0%) HIT-positive samples at all concentrations (Figure 17c). At one or both concentrations, mutant D inhibited platelet activation moderately in 3/5 (60.0%) HIT-positive samples and strongly in 2/5 (40%) HIT-positive samples (Figure 17d). Platelet activation was moderately inhibited by mutant E in 1/5 (20.0%) HIT-positive samples and strongly inhibited in 1/5 (20.0%) HIT-positive samples at 75 μg/mL (Figure 17e). Although mutant F was only tested at one concentration (50 μg/mL) due to insufficient sample volume, this construct was able to strongly inhibit platelet activation in 3/5 (60.0%) HIT-positive samples (Figure 17f).

These findings demonstrate platelet activation was inhibited to varying degrees with each patient sample by different KKO-scFv constructs. However, mutants B and F caused the largest decrease in platelet activation when compared to other constructs, aligning with findings from previous experiments that further highlight the improved performance of these mutants.

5.0. DISCUSSION

HIT is an antibody-mediated drug disorder arising in patients receiving heparin as an anticoagulant medication, often following major surgical procedures.[1,2] Heparin binds favourably to PF4 tetramers and forms structurally stabilized complexes, which can trigger anti-PF4/heparin antibody production and lead to the formation of large immune complexes.[1,3-6] Although the development of anti-PF4/heparin antibodies is common in heparin-treated patients, only a small percentage of individuals develop HIT.[2,6-9] This is because PF4/heparin induces a highly polyclonal and polyspecific antibody response where most antibodies produced are non-pathogenic and cannot cause HIT.[10-12] Rapid and accurate differentiation between anti-PF4/heparin antibodies that can and cannot cause platelet activation remains a significant diagnostic challenge due to the reduced specificity and limited availability of current laboratory assays.[10,14] Recently, it

was shown that pathogenic antibodies bind to a restricted region on PF4 distinct from sites bound by non-pathogenic antibodies.[13] Based on these different binding sites, this work aims to use an epitope-targeted strategy to distinguish between pathogenic and non-pathogenic antibodies in an EIA using KKO-scFv mutants by blocking the heparin-dependent pathogenic epitope on PF4.

5.1. Improving the Affinity of KKO-scFv Using Random Mutagenesis and Phage Display

5.1.1. Preparation and Identification of KKO-scFv Mutant Constructs

Phage display remains a useful approach for the discovery of novel scFv antibodies with high affinity for a desired target antigen. To characterize phage-displayed KKO-scFv, we first designed and optimized a fluid-phase enrichment assay that has reduced background phage binding and unrelated antigen associations.[118] Solid phase capture assays, such as ELISAs, are commonly used for phage bio-panning to assess scFv binding activity and offer many advantages, such as large-scale rapid library screening and technical ease.[125] However, phage can hinder these assays by contributing to non-specific binding, increasing background signals and interfering with high affinity scFv binding.[118,126-128] The assay described here utilizes the streptavidin-biotin association to immobilize PF4/heparin on magnetic beads rather than polystyrene surfaces, which can reduce antigen availability and binding site confirmation.[125] We also incorporated a target unrelated protein, the vWF D' domain, to determine the binding specificity of our assay. We found phage displaying KKO-scFv could outcompete phage displaying the vWF D'domain for binding when incubated with PF4/heparin coated beads. Whereas incubating with heparin-only coated beads or uncoated beads yield no change in KKO-scFv-phage enrichment compared to vWF D'domain-phage. These data confirm KKO-scFv expressed on the surface of phage binds to PF4/heparin complexes with high specificity over an indiscriminate peptide and shows non-specific phage binding does not increase background signal. Therefore, this assay not only

characterizes KKO-scFv binding but offers a reliable method of screening phage libraries for the identification of high-affinity and specificity mutant constructs.

Using our optimized bio-panning method, five unique mutants of KKO-scFv specific to PF4/heparin were captured from a starting phage library containing $1.5x10^7$ diverse sequences (Table 3). These variants of KKO-scFv were named mutant B KKO-scFv$^{(R18K,\ N152K,\ D180N)}$, mutant C KKO-scFv$^{(S50N,\ Y53H)}$, mutant D KKO-scFv$^{(Y156H)}$, mutant E KKO-scFv$^{(Y156H,\ D180G,\ Q233P)}$, and mutant F KKO-scFv$^{(E183V,\ E185K,\ G223R)}$. To achieve this, random mutagenesis was performed to generate a large library of KKO-scFv mutants with the intent to isolate variants with enhanced affinity for PF4/heparin. A structure-guided approach to mutagenesis has the potential to yield site specific mutants with heightened affinity at the antibody-antigen interface. However, the benefit of random mutagenesis over other methods is the potential to identify mutations distant from antigen contact residues that improve binding affinity.[129] Such mutations could indirectly enhance the antibody-antigen association by strengthening electrostatic interactions or contributing to proper protein folding and stability.[130,131] Therefore, it is important to identify and locate individual mutations to establish how they contribute to antigen recognition and binding.

Sequence analysis of each KKO-scFv variant revealed that the distribution of random mutations was more frequently located on the V_H chain, which plays a predominant role in antigen recognition (Appendix 2).[129-131] Interestingly, an identical mutation (Y156H) was observed in both mutant D and mutant E along with another overlapping mutation at position D180 between mutant B (D180N) and mutant E (D180G). This observation suggests these two positions (Y156 and D180) may be important sites within the KKO-scFv paratope and could be explored further as potential 'hot-spot' residues.[132-134] Previous studies have successfully targeted known amino acid hot-spots to provide additional enhancements in binding affinity using semi-random mutagenesis

and phage display.[133,135] However, a better structural understanding of the interface between KKO-scFv and PF4/heparin is required for a more comprehensive analysis of the contribution these amino acids may make to PF4 binding interactions.

A number of key mutations also appeared within the complementary determining regions (CDR), which are six hypervariable loops located between both the V_H and V_L domains that form the primary antigen binding site.[130] The two previously highlighted mutated residues of interest (Y156 and D180) were both located within the CDR, specifically CDR1 and CDR2, respectively. In fact, the four strongest affinity KKO-scFv variants (mutant B, D, E, and F) had at least two or all mutations identified on the CDR loops found within the V_H domain, which are primarily involved in antigen binding. This could explain why these mutants demonstrated an improved affinity for PF4 and PF4/heparin, while mutant C, which only contained two V_L mutations, was most comparable to wildtype. In a study by Oyama et al. (2020), a significant difference between the affinity of scFvs with V_L mutations compared to those with V_H mutations was also observed following random mutagenesis studies.[136] Previous work involving affinity maturation has also found success in specifically targeting the V_H region with site-directed mutagenesis approaches to enhance the antigen binding properties of an scFv, specifically within the CDR3 loop.[137-139]

5.1.2. Purification of Wildtype and Mutant KKO-scFv Constructs

After five novel KKO-scFv variants were identified, each mutant and wildtype were expressed and purified for further characterization. In this study, KKO-scFv production was performed successfully using an *E. coli* BL21 bacterial expression system. While mammalian expression systems are typically ideal for complex eukaryotic protein production because they require extensive post-translational modifications, they are difficult to maintain, are time-consuming, and give low yields of protein.[140] Therefore, a more efficient bacterial expression

system was utilized for KKO-scFv production in this work. Bacterial expression systems have rapid growth rates and high protein yields but lack the ability to process post-translational modifications.[140,141] However, this issue is not encountered with scFv production because they do not require any complex modifications, such as glycosylation.[142]

Despite the benefits of bacterial expression systems, scFv production is not without its challenges. Previous studies involving scFv expression in *E. coli* have encountered significant obstacles related to protein overproduction and aggregation.[141,143-146] The reducing cytoplasmic environment in bacteria makes disulfide bonding difficult, often leading to the formation of inclusion bodies containing misfolded protein.[140] Utilizing the pADL-22c phage expression vector appeared to alleviate these concerns due to the presence of a leader sequence, allowing for the purification of soluble KKO-scFv. While each KKO-scFv construct was successfully isolated from *E. coli*, mutant B demonstrated the highest yield (6.0 mg) and purity. This feature contributed to its eventual selection as the lead candidate for assay development when combined with later results obtained during characterization of each KKO-scFv variant.

5.2. Characterization Studies Using Wildtype and Mutant KKO-scFv

5.2.1. Full-Length KKO Inhibition and BLI Binding Kinetics

Characterization of all mutant KKO-scFv constructs was performed to evaluate binding function and activity to ultimately guide selection of a lead candidate for assay development. These studies showed that at least four mutant KKO-scFv variants isolated during phage bio-panning performed better than wildtype in various binding experiments. In a competitive EIA, both wildtype KKO-scFv and mutant C were unable to significantly inhibit KKO from binding to PF4/heparin whereas mutants B, D, E and F showed much stronger inhibition of KKO in a concentration dependent manner. These findings also support the data obtained using BLI that

demonstrate mutants B, D, E, and F exhibit improved binding affinity for PF4 and PF4/heparin compared to wildtype KKO-scFv. These four KKO-scFv mutants also demonstrated K_D values equivalent or stronger than full-length KKO ($K_D=10^9$) against PF4 and PF4/heparin (Supplementary Fig. 13). Despite differences in sizes (KKO: 150 kDa vs. KKO-scFv: 28 kDa), the affinity of mutant KKO-scFv was similar to full-length KKO.

Out of the four strongest mutant variants of KKO-scFv, mutants B and F were selected to develop an improved diagnostic assay for HIT because they demonstrate high affinity for PF4 and PF4/heparin and strongly inhibit anti-PF4/heparin antibody binding. In competition experiments using full-length KKO, mutants B and F inhibited KKO binding in an anti-PF4/heparin EIA with the lowest IC_{50} values of 1.6 μg/mL and 1.3 μg/mL, respectively. BLI data also revealed that mutant B and F KKO-scFv had significantly increased affinity compared to wildtype KKO-scFv for both PF4 and PF4/heparin. Mutant B bound with low nanomolar affinity ($K_D= 10^{-9}$ M) to PF4 and PF4/heparin with the strongest binding responses (PF4 = 0.267 nm and PF4/hep = 0.378 nm) while mutant F had K_D values in the high picomolar range ($K_D=10^{-10}$ M) and similarly strong binding responses (PF4 = 0.211 nm and PF4/hep = 0.285 nm) (Figure 5-6).

5.2.2. Identifying the KKO-scFv Epitope on PF4

Epitope mapping was also performed in this study to confirm that KKO-scFv bound to the heparin-dependent pathogenic binding site on PF4. Epitope specificity was an important aspect of this work, as it has been previously shown that pathogenic anti-PF4/heparin antibodies and KKO bind to a restricted region on PF4.[13] A library of 70 mutant PF4 clones, each differing by a single amino acid, were used to identify the KKO-scFv binding site compared to full-length KKO. Eight amino acids were common between KKO and wildtype KKO-scFv, which also demonstrated antibody binding was restricted to the same region on PF4. Wildtype KKO-scFv also bound to five

additional amino acids not recognized by KKO (L8, K31, A39, I51, and L66), but it is unclear if this is related to non-specific binding contributed by sample contaminants. It may also be possible KKO-scFv bound to more amino acids compared to KKO because this assay is designed for full-length antibodies and optimizing this protocol may reveal a more restricted KKO-scFv epitope.

Epitope mapping was then performed on KKO-scFv mutant B, C, and D to show any potential changes to the wildtype binding site. Mutant B was the only construct that bound different amino acids on PF4 than the other mutants tested for this work. Despite recognizing a different epitope, mutant B binding was still restricted to the same pathogenic site on PF4. This is not unlike what is observed with pathogenic HIT antibodies from different patient's sera, which recognize different amino acids but bind to a common region on PF4.[13] Interestingly, mutant B also recognized two amino acids on PF4 within the heparin binding site, which could have important implications for future work (Supplementary Figure 14).[123] Phage display selection is primarily dependent on affinity rather than binding specificity, making it difficult to isolate a high affinity scFv that also possesses inhibitory properties.[147] Comparing the wildtype and mutant KKO-scFv helps to further define and strengthen the relationship between PF4 binding sites, affinity, and inhibitory activity.

While we found that wildtype KKO-scFv binds to the same epitope as full-length KKO,[13] it is possible that mutagenesis altered how the other constructs interact with PF4. Therefore, changes observed to the KKO-scFv epitope could suggest that differences in affinity between each mutant and wildtype construct are related to their individual binding sites. KKO-scFv mutant B may possess an epitope adaptation that improves its affinity for PF4 while retaining its specificity for the heparin-dependent binding site. Characterization studies showed that mutant C was most comparable to wildtype in terms of affinity and inhibitory strength, which is also reflected by its

almost identical PF4 epitope. Furthermore, mutant D bound to amino acids on PF4 that overlap with both the KKO and mutant B epitope and demonstrated much stronger affinities. However, the epitope for mutant D is much larger than the other constructs, which may be related to sample purity and/or assay optimization as previously mentioned. Future studies should seek to map the remaining KKO-scFv mutants to determine their similarities and differences to the KKO epitope.

5.3. Evaluation of a Rapid and Accurate Diagnostic Assay for HIT Using KKO-scFv

The next stage of this work was to develop and optimize an assay using KKO-scFv mutants to help distinguish between pathogenic and non-pathogenic antibodies. To do this, a modified IgG-specific streptavidin-biotin based anti-PF4/hep EIA (streptavidin anti-PF4/hep EIA) was performed with each KKO-scFv variant. In this assay, high-affinity epitope specific KKO-scFv is pre-incubated with PF4/heparin to block only sites previously identified as important to the pathogenic epitope on PF4 (Figure 18).[13] Serial dilutions of mutant and wildtype KKO-scFv were then incubated with HIT-positive (EIA+/SRA+) and HIT-negative (EIA+/SRA-) patient sera. We found that increasing concentrations of all KKO-scFv constructs were able to block antibody binding in HIT-positive patient sera. Our results also showed that KKO-scFv had no inhibitory effect on antibodies in HIT-negative sera. These findings also provide further evidence to suggest pathogenic antibodies recognize a specific epitope on PF4 that contributes to their pathogenicity in HIT.[13,16] Therefore, KKO-scFv is not only a unique diagnostic tool, but can also be used to study binding sites and disease mechanisms in HIT. These results also confirm that high affinity mutant KKO-scFv are a successful means to distinguishing between pathogenic and non-pathogenic HIT antibodies.

We found that four KKO-scFv constructs, mutants B, D, E, and F, were able to reduce the false-positive rate of EIAs caused by the presence of non-pathogenic antibodies when testing HIT-

positive and HIT-negative patient sera. Only pathogenic antibody binding was reduced to negative detection levels (OD_{405nm} < 0.45) in this optimized assay in the presence of mutant B, D, E, and F. As predicted, these four mutants also had a stronger effect and higher mean percent inhibition of pathogenic antibody binding compared to both wildtype and mutant C (Table 5-6). The weaker activity of mutant C reflects the importance of V_H domains to antigen recognition and reveals the potential to target mutations at the V_H CDR for KKO-scFv affinity maturation in future work. These findings also show a correlation with previous BLI analysis and inhibition studies with KKO, which demonstrate mutant B, D, E, and F have superior performance and binding kinetics. Out of five mutant constructs of KKO-scFv, only two were chosen as lead candidates to move forward with to perform a large-scale screening of patient sera and evaluate the diagnostic performance of this assay.

Mutant B and F demonstrated the foremost ability to distinguish between pathogenic and non-pathogenic antibodies compared to all KKO-scFv constructs. Testing these mutants against a larger population of HIT-positive (n=20) and HIT-negative (n=20) patient samples revealed pathogenic antibody binding was almost always significantly reduced in the presence of KKO-scFv while non-pathogenic antibody binding was not. ROC curve analysis revealed a significant increase in the performance of the streptavidin anti-PF4/hep EIA with the addition of KKO-scFv. Whereas the streptavidin anti-PF4/hep EIA without KKO-scFv in this study had a much lower AUC [0.66 (95% CI 0.49-0.83)] with a reduced sensitivity to 81.0% and specificity to 52.4% when testing the same clinical cohort. Compared to previous literature reports of the anti-PF4/hep EIA diagnostic performance,[15,67] incorporating KKO-scFv showed an improvement in specificity to 90.0% while maintaining the high sensitivity of this assay. However, given the stronger performance of mutant B, this KKO-scFv construct should be utilized as the primary candidate for

assay development in future work. Overall, targeting clinically significant epitopes on PF4 proves to be an effective method of distinguishing between HIT antibodies based on their individual binding sites. The addition of mutant KKO-scFv also demonstrates improved diagnostic performance compared to the IgG-specific anti-PF4/heparin EIA for identifying clinically significant HIT antibodies.

In this work, mutants of KKO-scFv demonstrated an advanced diagnostic performance in EIAs used to identify HIT antibodies. Current EIAs designed to diagnose HIT have low specificities (~50-70%)[2,15] for clinically significant antibodies in HIT. Automated rapid assays are also frequently employed for HIT diagnosis,[68-70,72,73] but they often require costly and specialized equipment to perform, making them inaccessible to many labs despite their higher specificities. Another EIA-based HIT laboratory assay that was designed similarly to the inhibition assay described in this study detects pathogenic anti-PF4/heparin antibodies by their ability to inhibit KKO binding (KKO-I).[148] Cuker et al. (2013) report KKO binding was inhibited by anti-PF4/heparin antibodies by an average of 78.9% against HIT-positive patient sera and 26.5% by HIT-negative patient sera.[148] We found that KKO-scFv mutant B achieved a better separation between anti-PF4/heparin antibodies, achieving an average of 75.8% inhibition in HIT-positive patients compared to -4.4% inhibition in HIT-negative patients. This suggests our EIA with KKO-scFv has better diagnostic discrimination compared to the KKO-I EIA as there was less overlap between true- and false-positive anti-PF4/heparin antibodies. Additionally, our assay had an improved sensitivity (100.0%) compared to the KKO-I (90.0%) and nearly identical specificities (90.0% and 92.0%, respectively) using a similar patient population size.

Not only does this study have important implications for HIT diagnosis, but if these constructs are able to prevent the platelet activating ability of pathogenic antibodies, they may also

offer a novel therapeutic strategy for HIT. To evaluate the therapeutic potential of KKO-scFv, we tested each construct in the SRA with strongly reactive (^{14}C-serotonin release > 85%) HIT-positive (EIA+/SRA+) patient sera to determine their ability to inhibit platelet activation. This study found that each KKO-scFv mutant and wildtype demonstrated some ability to inhibit platelet activation to varying degrees, depending on the patient sample being tested. Despite inconclusive SRA data, this study reveals an intriguing trend regarding the ability of KKO-scFv to block platelet activation in a direct competition assay with HIT-positive antibodies. However, further experiments are required due to the small sample size of HIT patients selected for this study. It is possible that additional strategies to enhance the binding strength of certain mutants (such as KKO-scFv mutant B) could allow for the identification of a lead candidate for drug development. Antibody fragments have been explored extensively as possible therapeutics, many of which are currently under clinical development (Table 1). If further strengthening these constructs can allow them to prevent functional pathogenic anti-PF4/heparin antibody activity, this may substantiate the future development of KKO-scFv into a novel treatment for HIT.

5.4. Limitations

Bacterial systems can be used to generate scFvs with relative ease compared to full-length antibodies because of their smaller size and limited post-translational complexity.[149] However, a significant limitation scFv production in *E.coli* is insolubility due to protein overproduction, aggregation, and/or the formation of inclusion bodies.[150,151] We frequently observed the production of insoluble KKO-scFv using both pET-22b(+) and pET-30a(+) vectors in BL21(DE3) *E.coli* (data not shown). Attempts to improve solubilization and prevent aggregation using a combination of detergents (to increase solubility) and beta-mercaptoethanol (to reduce improper disulfide bonds) were unsuccessful at significantly increasing protein yields. Interestingly, the inclusion of a leader

sequence in the expression vector pET-22b(+) did appear to make a slight difference in soluble protein levels (data not shown). Protein export into the periplasm has been shown to increase protein solubility because this environment is less reducing compared to the cytoplasm, which causes improper disulfide bond formation and protein misfolding.[140,152] The phagemid pADL-22c also included a PelB leader sequence (Supplementary 1), which may contribute to the successful production of KKO-scFv in this study. Previous studies involving scFv have also explored ways to overcome this limitation that involve solubilization and recovery steps during purification.[143,144] This strategy can involve the production of scFv in inclusion bodies, which are denatured using high concentrations of a chaotropic reagent (e.g. urea) followed by a refolding step to recover functional protein.[143,144] However, these additional steps are complex and can significantly decrease protein yields. Molecular chaperones that aid in solubilization, such as maltose binding protein, have also been successfully used to improve scFv solubility[143,153] and represent another potential solution for KKO-scFv production.

Additional methods to produce KKO-scFv could involve using a different bacterial expression vector that aids in protein solubility. The phagemid vector pADL-22c was used to both produce phage-displayed KKO-scFv and pure KKO-scFv. Although this vector contains an amber stop codon (UAG), which can be read to suppress phage production and facilitate the generation of KKO-scFv free from pIII-fusion,[154] it is not optimized for protein production. Various vectors designed specifically for proteins prone to aggregation could be explored as options to improve KKO-scFv production. These are often low-copy number plasmids, which control expression levels to limit protein overproduction and aggregation.[155,156] Engineered host strains of *E. coli* designed to optimize soluble protein production by facilitating the formation of disulfide bonds could also be used to overcome limitations related to KKO-scFv production. Commercial *E. coli*

strains mutated to lack the thioredoxin reductase (*trxB*) and glutathione reductase (*gor*) enzymes, such as SHuffle (New England Biolabs) and Origami (Novagen), are optimal for promoting disulfide bond formation by eliminating the reducing potential of these enzymes in the cytoplasm.[151,157] The more oxidizing environment within the cytoplasm of these strains encourages the proper folding of proteins that rely on disulfide bonding for stability and solubility.[158-160]

Although the methods described here overcame some solubility issues, another limitation of this work was the purity of KKO-scFv samples. In each batch of purified KKO-scFv, we identified the presence of an unknown protein at approximately 65 kDa (Figure 2). It was initially thought this contaminant was caused by amber stop codon read-through, which normally prevents phage pIII minor coat protein expression in non-suppressor *E.coli* strains.[161,162] However, western blot analysis did not detect any KKO-scFv-pIII fusion proteins in these samples (data not shown). Therefore, another approach to improve sample purity may be by further optimizing the purification process. This could be achieved by incorporating an imidazole gradient elution step coupled with ion exchange or size exclusion chromatography to separate KKO-scFv from the unknown protein. Alternatively, the use of stronger affinity tags, such as hemagglutinin (HA), might also help eliminate any contaminate binding.[163] Any interference caused by the unknown protein did not appear to influence later binding studies and the purity of these preps was deemed suitable for the purpose of this study. However, improvements in purity that do not sacrifice yield will be required to produce KKO-scFv for any future clinical, laboratory, or commercial use, including any potential diagnostic and therapeutic applications.

6.0. FUTURE DIRECTIONS

The importance of binding site specificity to pathogenicity suggests that the mutant KKO-scFv constructs described here could function as potential diagnostic tools in similar disorders,

such as vaccine-induced thrombotic thrombocytopenia (VITT).[63] VITT is a rare but serious complication associated with adenoviral vector vaccines against severe acute respiratory syndrome coronavirus 2 (SARS-CoV-2).[62,164] VITT is associated with moderate to severe thrombocytopenia and thrombosis caused by platelet activating anti-PF4 IgG antibodies.[62,165] Immunoassays commonly used for HIT diagnosis have been adapted for a similar purpose in VITT due to their similar pathophysiologies and show a significantly improved specificity and sensitivity for detecting VITT antibodies.[166] However, a current limitation of these EIAs is their inability to distinguish between VITT and HIT antibodies,[167] which can have important implications for the diagnosis and treatment of either syndrome. It has been previously shown that VITT antibodies bind to a different region on PF4 compared to typical HIT antibodies,[13] which overlaps with the heparin binding site.[63] An epitope-directed approach may offer a viable solution to improve diagnosis by differentiating VITT and HIT antibodies by their PF4 binding sites. Thus, an investigation surrounding the ability of KKO-scFv to inhibit HIT but not VITT antibodies to help increase the diagnostic accuracy of EIAs should be the focus of future work.

The versatility of KKO-scFv and amenability of scFvs to genetic manipulation in general also makes these fragments ideal for advanced development compared to full-length antibodies.[149] While mutagenesis and phage display proved effective at producing several strong mutants of KKO-scFv, additional alterations to the methods could be made in future work to generate potentially stronger constructs that can inhibit platelet activation. Positive and negative selection strategies during the phage bio-panning selection process could be included to eliminate potential non-specific mutants and increase the likelihood of capturing higher affinity and more specific clones.[168] Additionally, selection of high affinity mutants can also be improved by increasing binding competition for PF4/heparin, which could be achieved by decreasing the amount of

available target antigen during bio-panning.[169] Subjecting these mutants to additional rounds of mutagenesis, either random or site-directed, that target the V_H CDR regions could also lead to the production of higher affinity scFvs. Another possible method to strengthen KKO-scFv would be to convert it into an alternative antibody format, such as a bivalent scFv or Fab.[91,170] In a study by Bertoglio et al. (2021), a native gene library of monoclonal scFvs was screened for human antibodies against the spike protein RBD using phage display to identify a SARS-CoV-2 neutralizing antibody.[102] Once isolated, the fully characterized scFv antibody was converted into a high affinity bivalent scFv-Fc fusion protein and is currently in phase Ib/II clinical trials as a potential anti-viral treatment for COVID-19.[171]

Therefore, another important direction for this work is to enhance the strength of KKO-scFv so that it can achieve inhibition of anti-PF4/heparin antibody mediated platelet activation. Antibody fragments are considered appealing formats for drug development due to their small size, which gives these molecules favourable pharmacokinetic properties, such as rapid blood clearance, enhanced tissue penetration, and fewer immune interactions.[93] Recently, a bivalent nanobody (ALX-0681; Caplacizumab) was approved for treatment of acquired thrombotic thrombocytopenic purpura (aTTP).[172-174] Caplacizumab prevents thrombosis by inhibiting a key interaction between platelets and vWF, which is central to the pathogenesis of aTTP.[172-174] Furthermore, the ongoing development of antibody fragments as drug candidates supports the advancement of these KKO-scFv mutants into a novel therapy for HIT (Table 1). Recently, Minenkova et al. (2022) isolated high affinity scFvs from COVID-19 convalescent plasma and performed two rounds of phage bio-panning with random mutagenesis to successfully increase their neutralizing activity against different SARS-CoV-2 variants.[94] The development of KKO-scFv into a potential therapeutic would have important implications for HIT patients receiving treatment. Current treatments often

have high rates of bleeding and other adverse side effects, which are associated with alternative anticoagulant use.[175,176] KKO-scFv can still bind to the pathogenic site on PF4, but unlike a full-length antibody, is unable to interact with surface FcγRIIa receptors and cause platelet activation because it lacks the Fc fragment. Thus, a drug derived from KKO-scFv would allow patients to continue receiving heparin without the risk of HIT-associated thrombosis by preventing immune complexes formation. This would lead to shorter hospital stays post-surgery and reduced hematological complications, such as bleeding, related to alternative anticoagulant use for patients with HIT.[24,175,177]

7.0. CONCLUSION

In this study, random mutagenesis was used to improve the affinity of an scFv derived from the monoclonal antibody KKO. Five mutant variants of KKO-scFv were identified using phage display after various rounds of bio-panning selection on magnetic beads coated with the target antigen for HIT antibodies, PF4/heparin. Functional studies were then carried out to assess the binding characteristics and affinity of each variant compared to wildtype. BLI was used for kinetic analysis of wildtype and mutant KKO-scFv and demonstrated mutant B, D, E, and F had substantially improved affinity towards PF4 alone and PF4 complexed with heparin compared to wildtype and mutant C. Binding inhibition experiments using KKO were also performed to evaluate the strength of each construct against a full-length antibody and determine approximate IC_{50} values. These studies revealed that the same four mutant variants of KKO-scFv were able to strongly inhibit KKO binding in a streptavidin anti-PF4/hep EIA. Epitope mapping revealed KKO-scFv wildtype, mutant C, and mutant D bound to the same amino acids as full-length KKO. Whereas mutant B recognized amino acids that differed from the other variants but still overlapped with the heparin-dependent binding site on PF4. A small sample of patient sera was then tested in

an anti-PF4/heparin EIA using wildtype and mutant KKO-scFv, which showed each construct inhibited HIT-positive antibodies but did not affect the binding of HIT-negative antibodies. These findings suggest KKO-scFv can eliminate false-positive signals in an EIA that arise from antibodies that do not cause HIT.

Mutant B and mutant F were selected as lead candidates and used in the same EIA to screen a larger number of HIT patient samples. We found that the addition of mutant B and F KKO-scFv to the streptavidin anti-PF4/hep EIA improved the diagnostic specificity to 90.0% in a cohort containing HIT-positive and HIT-negative patients without reducing sensitivity. The assay described here provides a promising alternative to functional and automated rapid assays for the diagnosis of HIT. We show that high affinity KKO-scFv mutants can accurately differentiate between pathogenic and non-pathogenic HIT antibodies in an EIA, thus providing a rapid and cost-effective solution to common limitations of HIT diagnostic assays. Furthermore, this EIA can be performed easily with standard laboratory equipment, increasing the overall availability of HIT testing. While the results of this work are promising, the assay described in this study still requires further testing on a blind prospective cohort of suspected patients to accurately determine diagnostic performance in a practical setting.

8.0. FIGURES

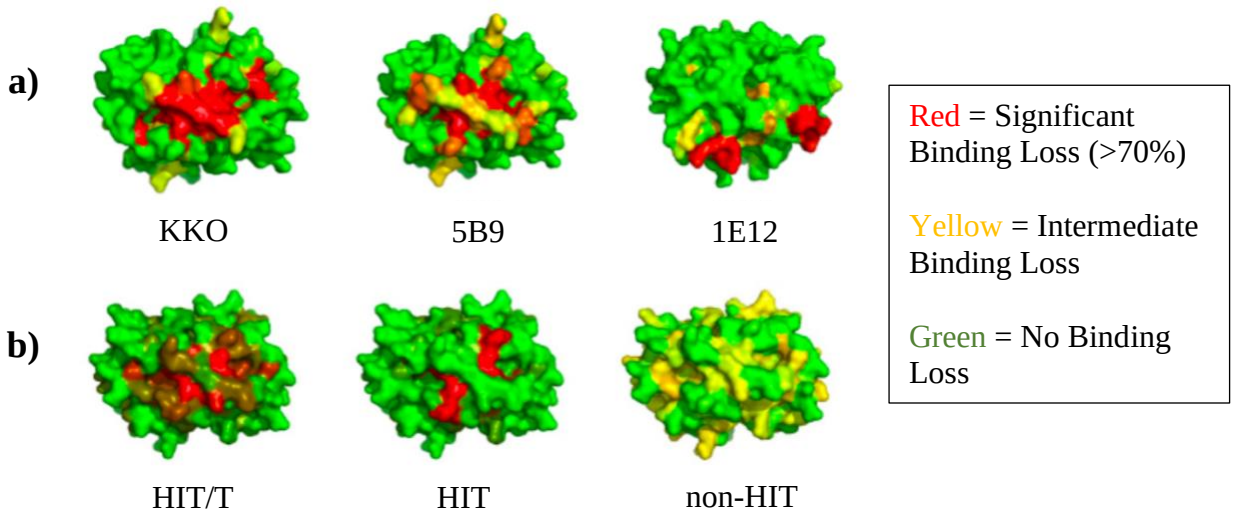

Figure 1. PF4 crystal structure with epitope mapping of antibody binding. Alanine-scanning mutagenesis was used to determine important amino acids recognized on PF4 by antibodies from HIT patient sera. Mutant PF4 was used to visualize surface binding data of **a)** murine monoclonal antibodies that mimic anti-PF4/heparin antibodies, KKO, 5B9, and 1E12 and **b)** HIT with thrombosis (HIT/T), HIT, and EIA-positive/SRA-negative (non-HIT; false-positive patient with non-pathogenic antibodies) patient samples relative to wildtype PF4 binding (Unpublished data and figure from A. Huynh and I. Nazy: Department of Medicine, McMaster University, 2019).

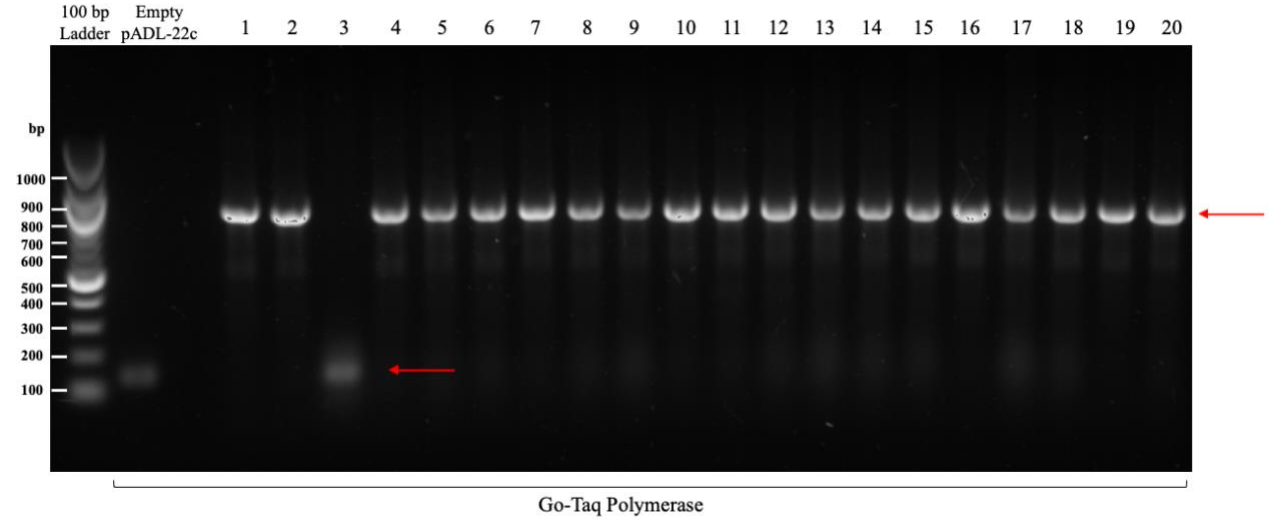

Figure 2. Mutant KKO-scFv phage library polymerase chain reaction colony screen. Agarose gel electrophoresis analysis of mutant KKO-scFv PCR products. After KKO-scFv was sub-cloned into the phagemid pADL22-c using Mutazyme II DNA polymerase, TG1 *E. coli* cells were electroporated and grown up overnight on LB + ampicillin agar plates. Following this, 20 random colonies were selected and used to validate KKO-scFv insertion. Gene-specific primers that overlap with the KKO-scFv ligation sites were used for each PCR reaction (Table 1A). PCR products were separated on a 1% agarose gel in 1X TAE buffer. Columns 1-20 represent high mutation frequency Mutazyme II polymerase PCR products. Bands at approximately 890 bp were visualized in 19 out of 20 selected colonies, which corresponds to the expected scFv fragment size (top arrow). Bands at approximately 139 bp were visualized in 1 out of 20 selected colonies, representing vectors that do not contain KKO-scFv (bottom arrow). The sizes of molecular weight standards are shown in the first lane (bp) followed by an empty pADL22-c vector as a negative control.

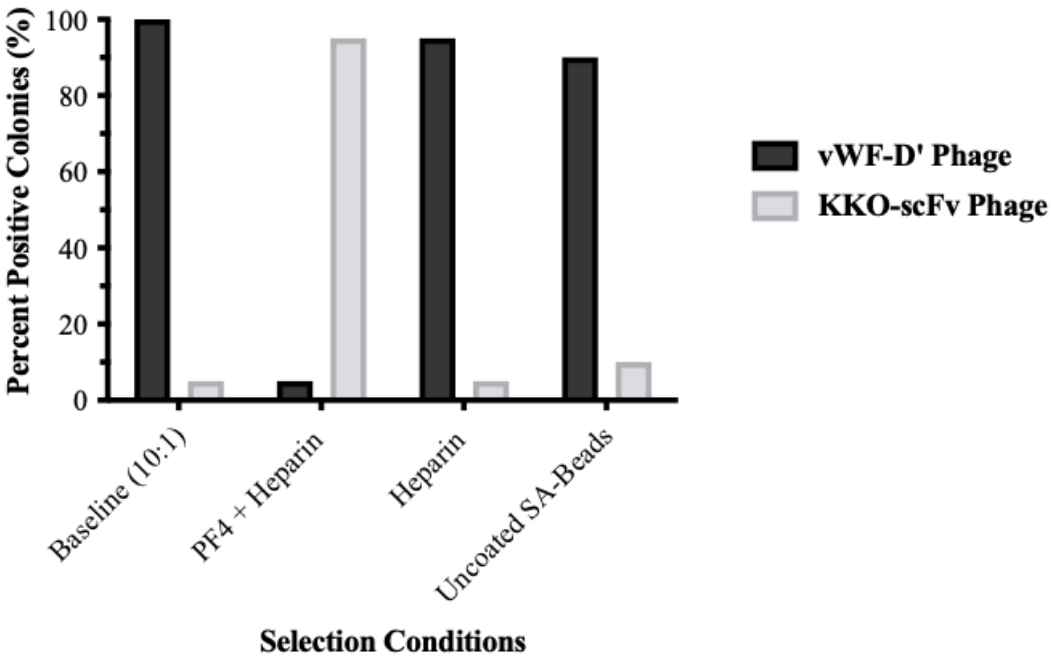

Figure 3. Binding characterization of phage displaying wildtype (WT) KKO-scFv to PF4/heparin. Enrichment of WT KKO-scFv phage was determined using a streptavidin (SA)-coated magnetic bead pulldown assay. Results are expressed as a percentage of colonies positive for either vWF D' (black) or WT KKO-scFv phage (grey) after selection. To determine baseline percentages, K91 *E. coli* cells were infected with a mixture of vWF D' and WT KKO-scFv phage in a 10:1 ratio and grown up overnight on LB + ampicillin agar plates. K91 *E. coli* cells were the infected with the same 10:1 phage mixture following selection on streptavidin magnetic beads coated with biotinylated-heparin/PF4, biotinylated-heparin, or uncoated SA-beads alone. Following this, 20 random colonies per selection condition were analyzed to assess WT KKO-scFv phage enrichment.

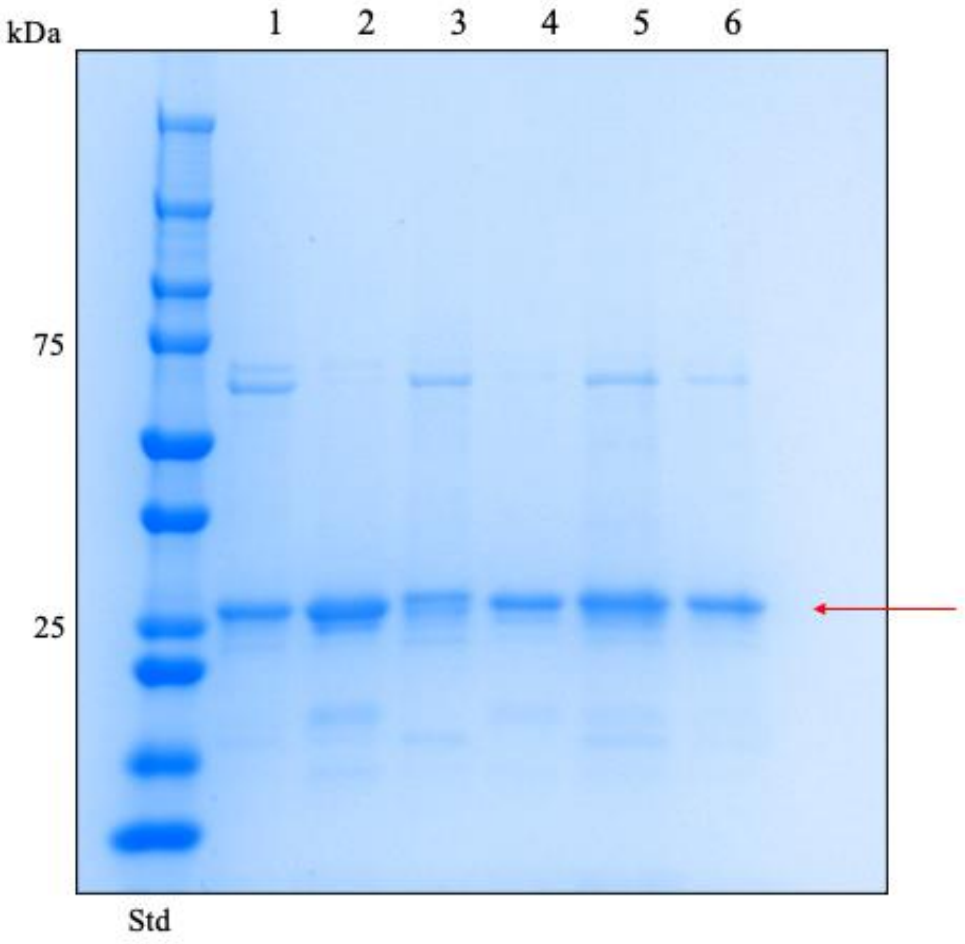

Figure 4. Purification of KKO-scFv from BL21 cells using Ni-NTA affinity chromatography. SDS-PAGE and Coomassie SimplyBlue™ SafeStain analysis of NI-NTA column purification of KKO-scFv wildtype and mutant constructs. Std represents protein ladder standards (kDa). Lanes 1-6 represent concentrated eluates containing KKO-scFv displaced from the column at 500 mM imidazole buffer. Lane 1 shows wildtype KKO-scFv, lane 2 shows KKO-scFv mutant B, lane 3 shows KKO-scFv mutant C, lane 4 shows KKO-scFv mutant D, lane 5 shows KKO-scFv mutant E, and lane 6 shows KKO-scFv mutant F. The red arrow indicates protein bands corresponding to purified KKO-scFv at approximately 28 kDa. All samples were separated on a denaturing 4-20% SDS polyacrylamide gradient gel followed by staining.

a)

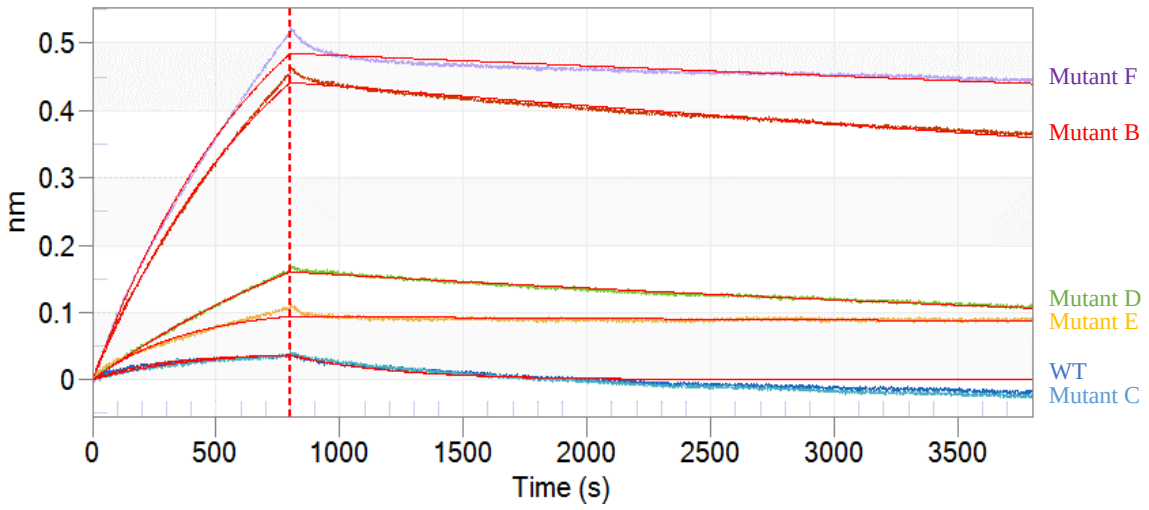

b)

Sample (KKO-scFv)	Response (nm) ± s.d.	K_D (M) ± s.d.	K_{on}($M^{-1}s^{-1}$) ± s.d.	K_{off}(s^{-1}) ± s.d.
Wildtype	0.0386 ± 0.01	$1.32x10^{-6} \pm 1.11x10^{-6}$	$1.25x10^{4} \pm 2.08x10^{4}$	$2.55x10^{-3} \pm 2.37x10^{-3}$
Mutant B	0.2665 ± 0.03	$1.69x10^{-9} \pm 5.14x10^{-10}$	$3.02x10^{4} \pm 7.86x10^{3}$	$5.07x10^{-5} \pm 1.78x10^{-5}$
Mutant C	0.0399 ± 0.01	$1.66x10^{-6} \pm 1.49x10^{-6}$	$1.69x10^{4} \pm 2.76x10^{4}$	$2.15x10^{-4} \pm 3.01x10^{-4}$
Mutant D	0.1450 ± 0.02	$5.83x10^{-9} \pm 3.13x10^{-9}$	$2.57x10^{4} \pm 2.38x10^{4}$	$1.03x10^{-4} \pm 3.51x10^{-5}$
Mutant E	0.0986 ± 0.01	$9.54x10^{-10} \pm 6.59x10^{-10}$	$6.93x10^{4} \pm 1.32x10^{4}$	$1.24x10^{-4} \pm 1.52x10^{-4}$
Mutant F	0.2110 ± 0.03	$6.07x10^{-10} \pm 3.12x10^{-10}$	$4.22x10^{4} \pm 6.17x10^{3}$	$2.52x10^{-5} \pm 1.25x10^{-5}$

Figure 5. BLI Binding response of KKO-scFv against PF4. a) Spectrogram representing the binding responses of wildtype and mutant KKO-scFv showing lines of best fit. BLI experiments were performed (n=3) using wildtype KKO-scFv (dark blue), mutant B (red), mutant C (light blue), mutant D (green), mutant E (yellow), and mutant F (purple) at 1 µg/mL. Binding was measured against immobilized biotinylated PF4 on streptavidin biosensors. **b)** Table showing kinetic data [mean ± standard deviation (s.d.); n=3] of wildtype and mutant KKO-scFv, including binding responses (nm), affinity constants (K_D), association rates (K_{on}), and dissociation rates (K_{off}). All data was analyzed using a 1:1 homogenous ligand binding model with Octet® User Software version 3.1.

a)

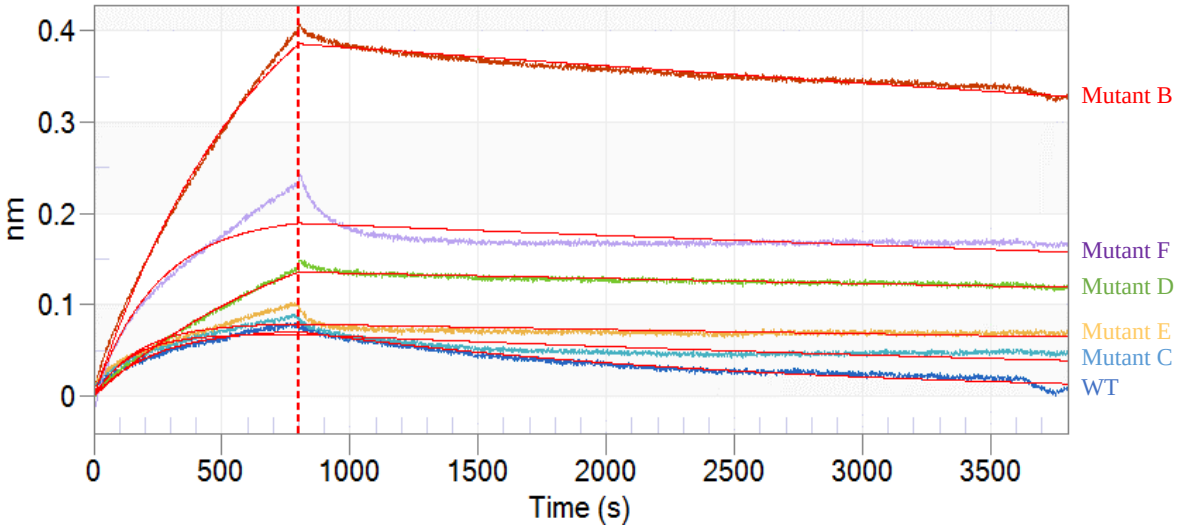

b)

Sample (KKO-scFv)	Response (nm) ± s.d.	K_D (M) ± s.d.	K_{on}($M^{-1}s^{-1}$) ± s.d.	K_{off}(s^{-1}) ± s.d.
Wildtype	0.0758 ± 0.01	$5.38x10^{-9} \pm 1.14x10^{-9}$	$9.67x10^{4} \pm 2.58x10^{3}$	$5.19x10^{-4} \pm 1.05x10^{-4}$
Mutant B	0.3787 ± 0.02	$1.36x10^{-9} \pm 1.51x10^{-11}$	$2.76x10^{4} \pm 2.85x10^{3}$	$3.91x10^{-5} \pm 6.95x10^{-6}$
Mutant C	0.1591± 0.01	$3.81x10^{-9} \pm 7.38x10^{-10}$	$8.58x10^{4} \pm 7.18x10^{3}$	$4.77x10^{-4} \pm 2.08x10^{-5}$
Mutant D	0.1325 ± 0.01	$3.77x10^{-9} \pm 3.95x10^{-9}$	$1.29x10^{4} \pm 1.56x10^{4}$	$3.47x10^{-5} \pm 1.67x10^{-5}$
Mutant E	0.0907 ± 0.01	$2.75x10^{-10} \pm 1.56x10^{-9}$	$7.92x10^{4} \pm 5.84x10^{4}$	$2.78x10^{-5} \pm 3.28x10^{-5}$
Mutant F	0.2849 ± 0.01	$2.92x10^{-10} \pm 1.07x10^{-10}$	$5.09x10^{4} \pm 1.05x10^{4}$	$1.41x10^{-5} \pm 2.66x10^{-6}$

Figure 6. BLI Binding response of KKO-scFv against PF4/heparin. a) Spectrogram representing the binding responses of wildtype and mutant KKO-scFv showing lines of best fit. BLI experiments were performed (n=3) using wildtype KKO-scFv (dark blue), mutant B (red), mutant C (light blue), mutant D (green), mutant E (yellow), and mutant F (purple) at 1 µg/mL. Binding was measured against immobilized biotinylated PF4/heparin complexes on streptavidin biosensors. **b)** Table showing kinetic data [mean ± standard deviation (s.d.); n=3] of wildtype and mutant KKO-scFv, including binding responses (nm), affinity constants (K_D), association rates (K_{on}), and dissociation rates (K_{off}). All data was analyzed using a 1:1 homogenous ligand binding model with Octet® User Software version 3.1.

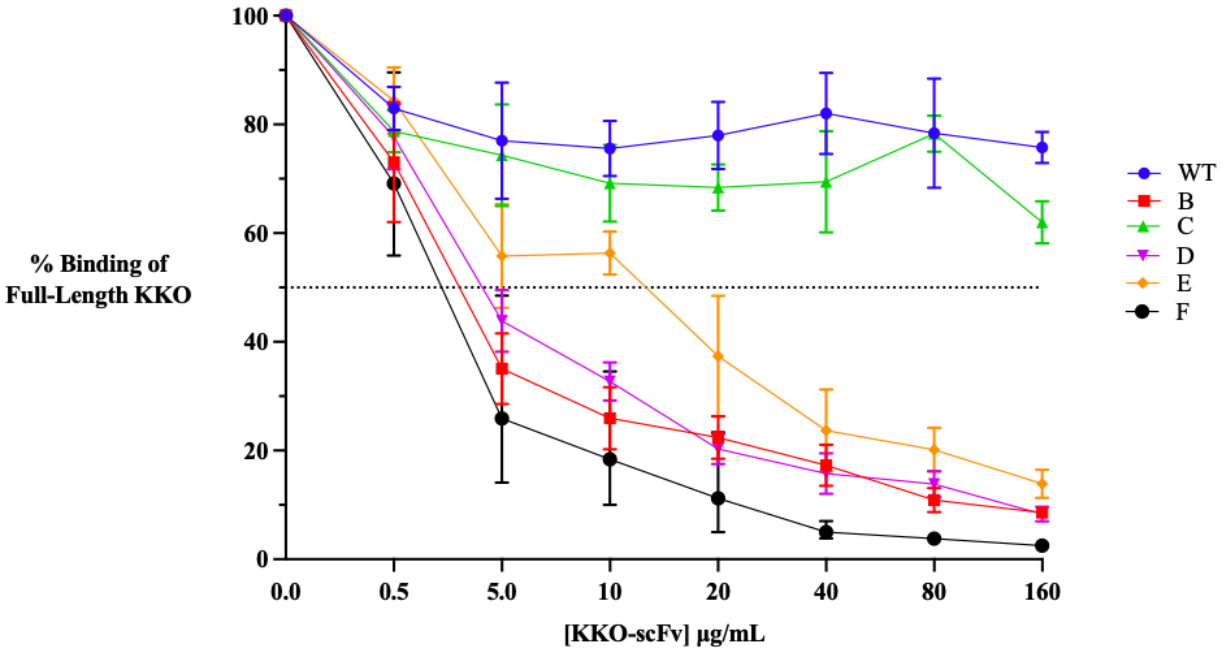

Figure 7. KKO-scFv inhibition of full-length monoclonal antibody KKO binding in a modified streptavidin enzyme immunoassay (EIA). Dose-dependent inhibition of KKO (2 µg/mL) from binding to PF4/heparin complexes using concentrations of KKO-scFv ranging from 0 to 160 µg/mL (n=3). Results are shown as the percentage (%) of KKO binding in the presence of wildtype (blue), mutant B (red), mutant C (green), mutant D (purple), mutant E (orange), and mutant F (black) KKO-scFv at increasing concentrations. The ability of each construct to inhibit KKO binding resulting in a >50% decrease (black dotted line) in absorbance (OD) at 405 nm was determined relative to control wells containing KKO in the absence of KKO-scFv.

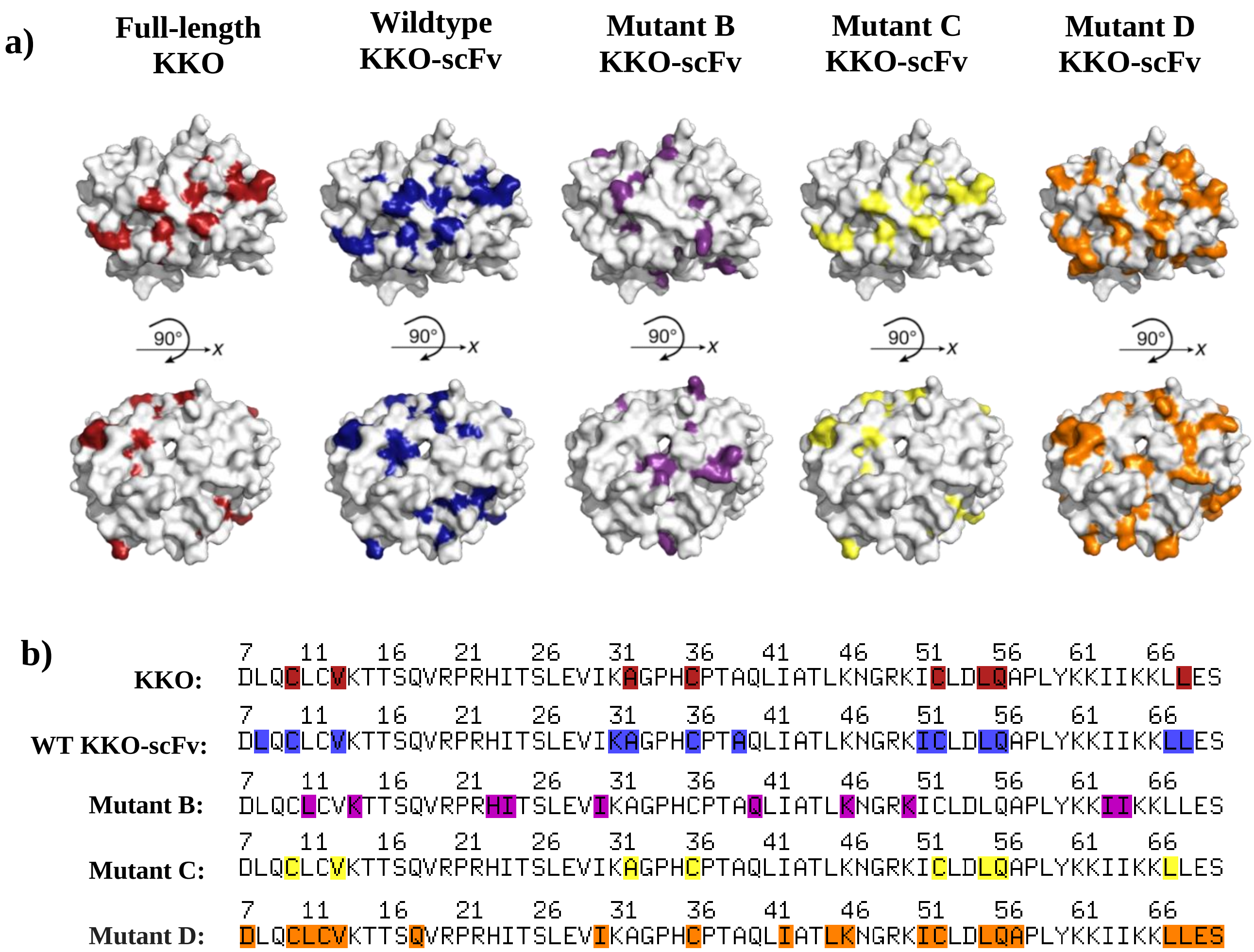

Figure 8. Identification of amino acids that are critical for the binding of KKO-scFv to PF4. a) PF4 tetramer showing full-length KKO (red**)**, wildtype KKO-scFv (dark blue), KKO-scFv mutant B (purple), KKO-scFv mutant C (yellow), and KKO-scFv mutant D (orange) surface antibody binding sites. **b)** The primary sequence of PF4 highlighting amino acids predicted to be make-up the binding sites for KKO-scFv wildtype (dark blue), KKO-scFv mutant B (purple), KKO-scFv mutant C (yellow), and KKO-scFv mutant D (orange) compared to full-length KKO (red). Images are modified from the Protein Data Bank (PDB) entry 1RHP.

a)

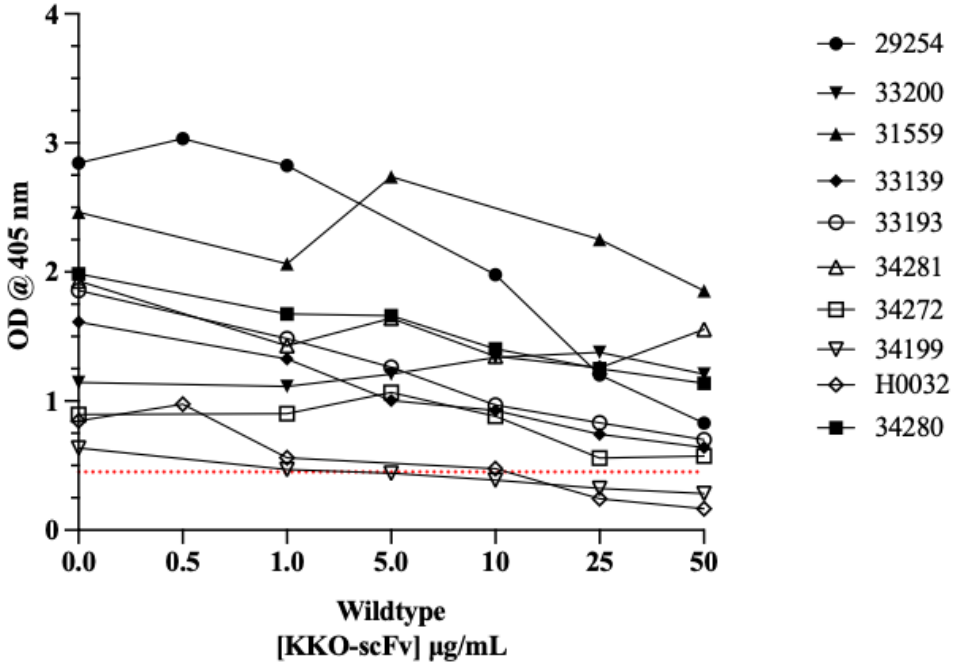
OD @ 405 nm
0
1
2
3
4
0.0
0.5
1.0
5.0
10
25
50
Wildtype
[KKO-scFv] µg/mL
29254
33200
31559
33139
33193
34281
34272
34199
H0032
34280

b)

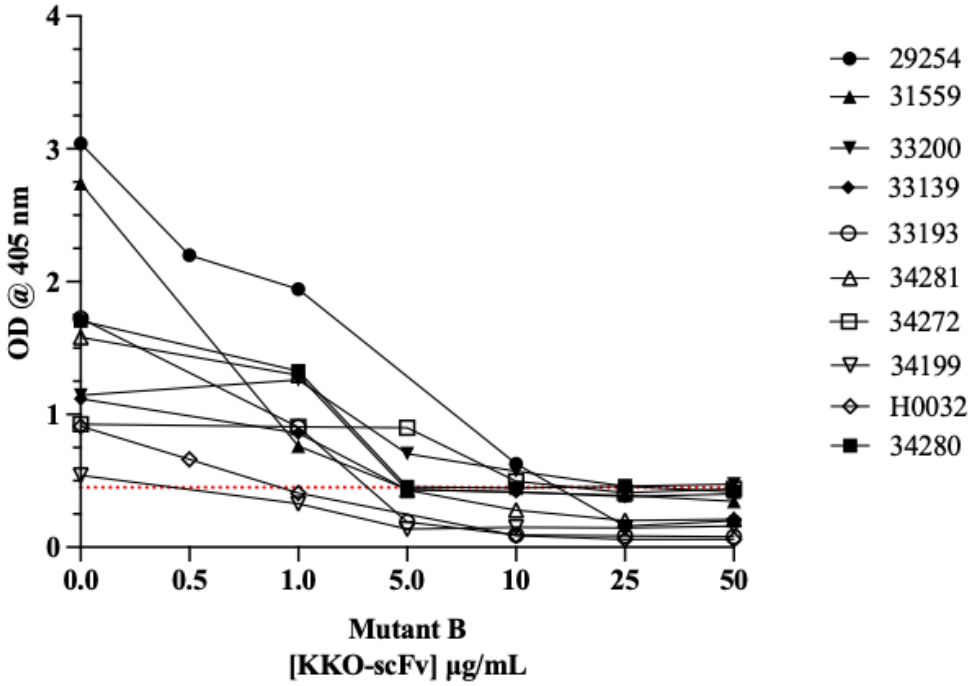
OD @ 405 nm
0
1
2
3
4
0.0
0.5
1.0
5.0
10
25
50
Mutant B
[KKO-scFv] µg/mL
29254
31559
33200
33139
33193
34281
34272
34199
H0032
34280

c)

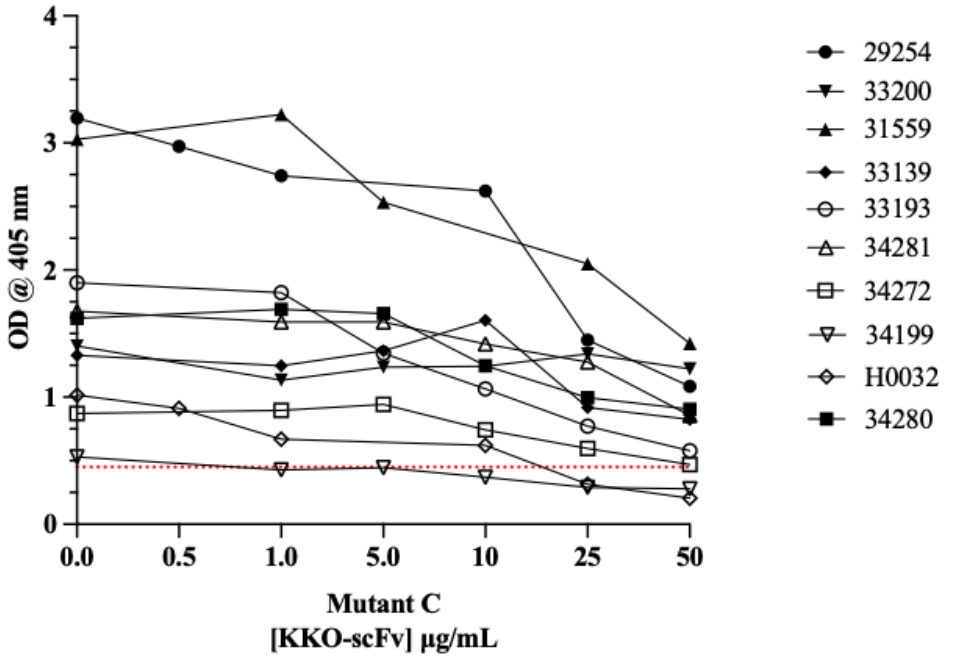
OD @ 405 nm
0
1
2
3
4
0.0
0.5
1.0
5.0
10
25
50
Mutant C
[KKO-scFv] µg/mL
29254
33200
31559
33139
33193
34281
34272
34199
H0032
34280

d)

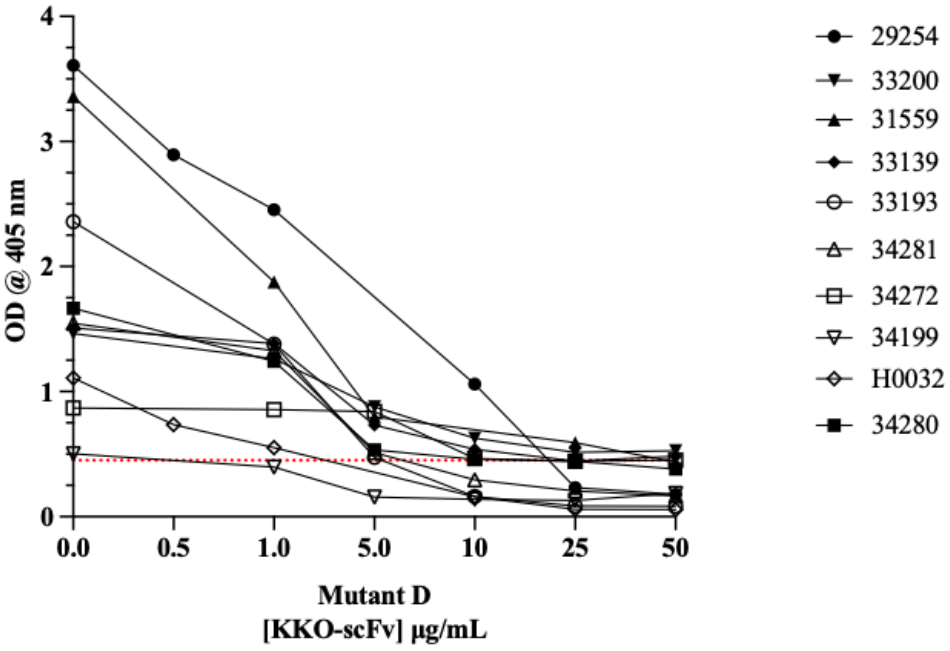
OD @ 405 nm
0
1
2
3
4
0.0
0.5
1.0
5.0
10
25
50
Mutant D
[KKO-scFv] µg/mL
29254
33200
31559
33139
33193
34281
34272
34199
H0032
34280

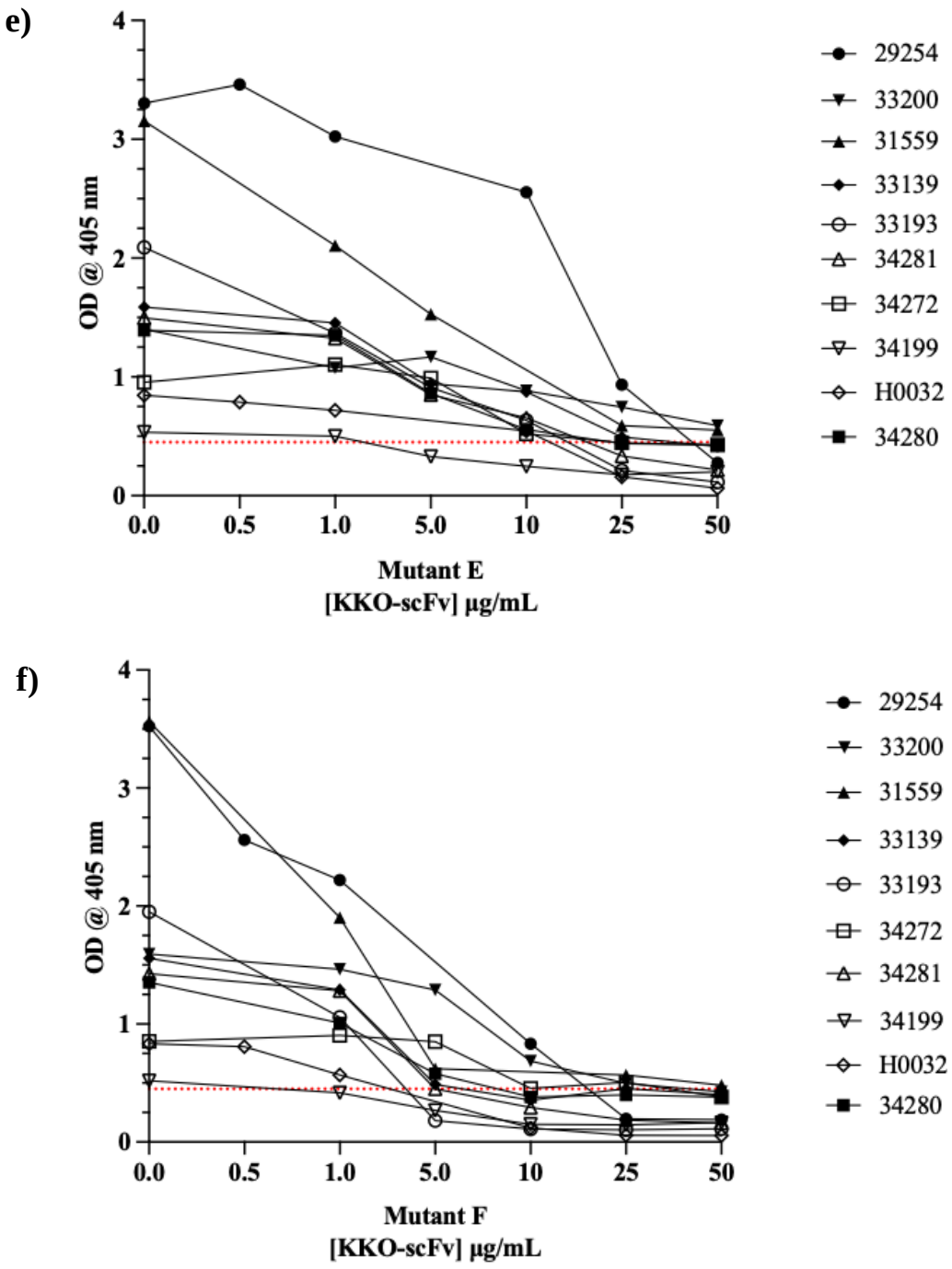

Figure 9. KKO-scFv inhibition of pathogenic anti-PF4/heparin antibody binding in a modified streptavidin enzyme immunoassay (EIA). Previously tested HIT patient samples (n=10) were tested in a modified streptavidin EIA in the presence of KKO-scFv **a)** wildtype, **b)** mutant B, **c)** mutant C, **d)** mutant D, **e)** mutant E, or **f)** mutant F at either 0, 1, 5, 10, 25, and 50 µg/mL concentrations. EIA-positive/SRA-positive patient samples with only heparin-dependent antibodies (black, n=5) or a mixture of heparin-dependent and -independent (white, n=5) were used in this assay. The ability of each KKO-scFv construct to inhibit antibody binding is shown as a decrease in absorbance (OD) at 405 nm. An $OD_{405nm} \geq 0.45$ in this assay is considered positive for anti-PF4/heparin antibodies, as shown by the dotted line.

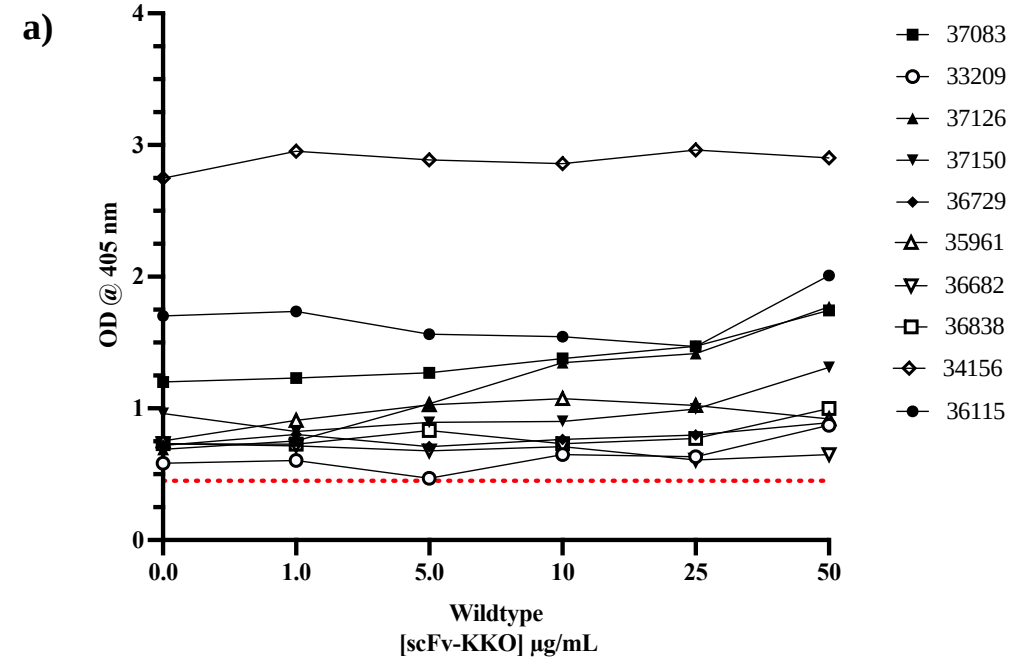
a)
OD @ 405 nm
0
1
2
3
4
0.0
1.0
5.0
10
25
50
Wildtype
[scFv-KKO] µg/mL
37083
33209
37126
37150
36729
35961
36682
36838
34156
36115

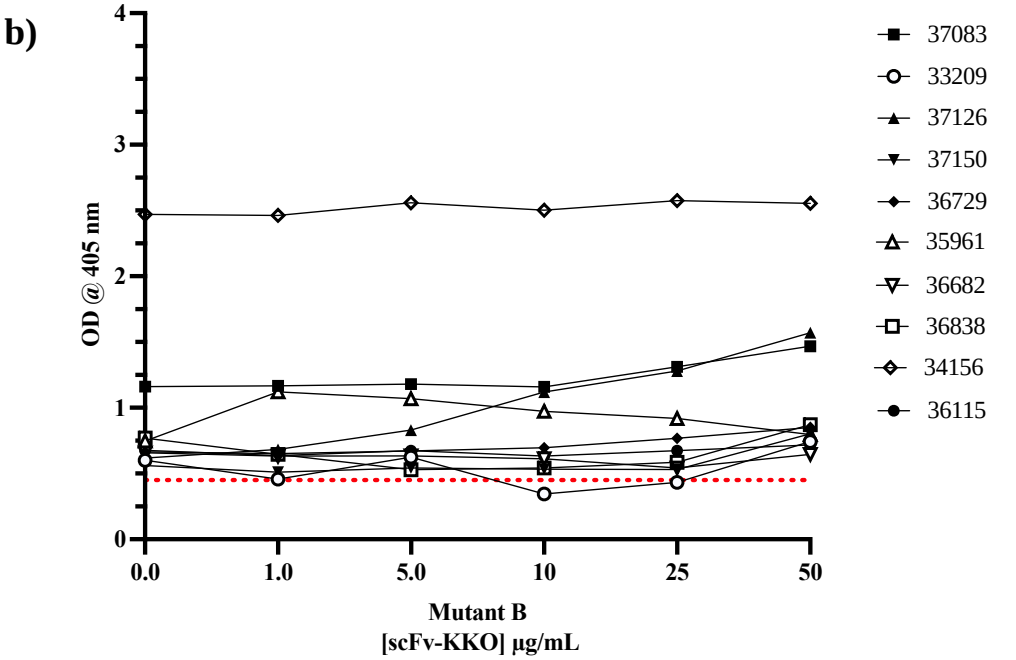
b)
OD @ 405 nm
0
1
2
3
4
0.0
1.0
5.0
10
25
50
Mutant B
[scFv-KKO] µg/mL
37083
33209
37126
37150
36729
35961
36682
36838
34156
36115

c)

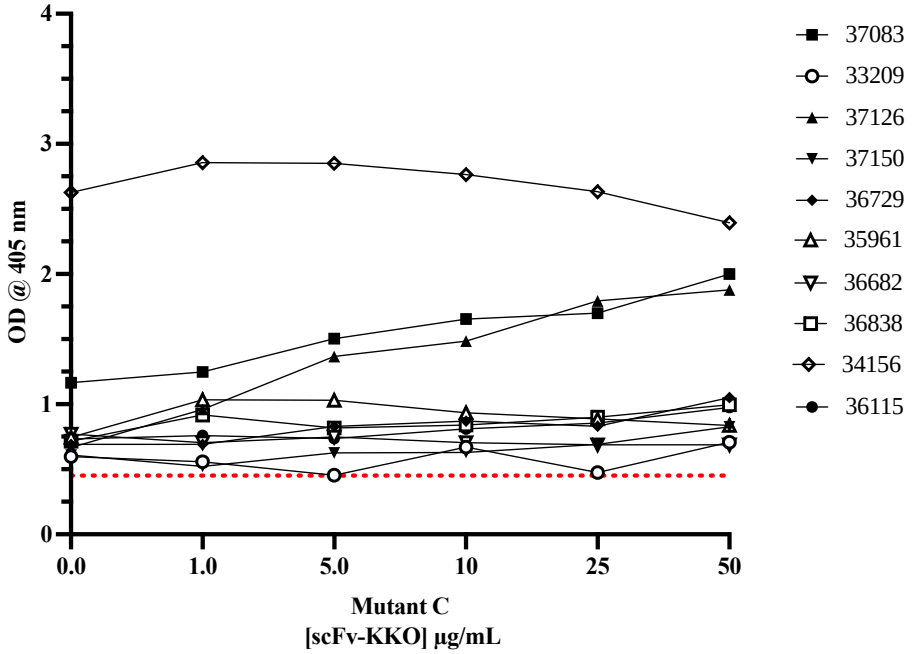
OD @ 405 nm
0
1
2
3
4
0.0
1.0
5.0
10
25
50
Mutant C
[scFv-KKO] µg/mL
37083
33209
37126
37150
36729
35961
36682
36838
34156
36115

d)

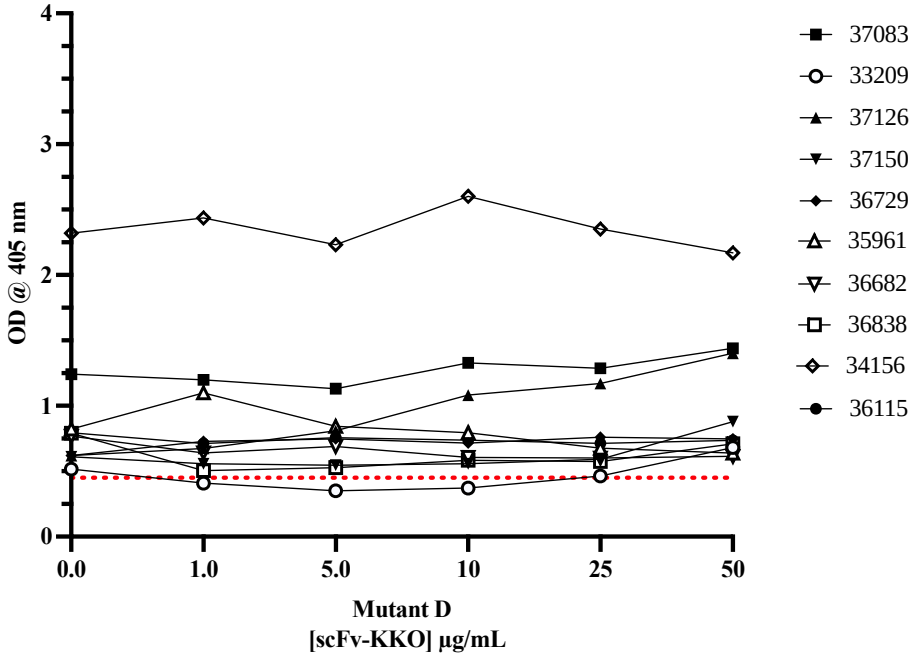
OD @ 405 nm
0
1
2
3
4
0.0
1.0
5.0
10
25
50
Mutant D
[scFv-KKO] µg/mL
37083
33209
37126
37150
36729
35961
36682
36838
34156
36115

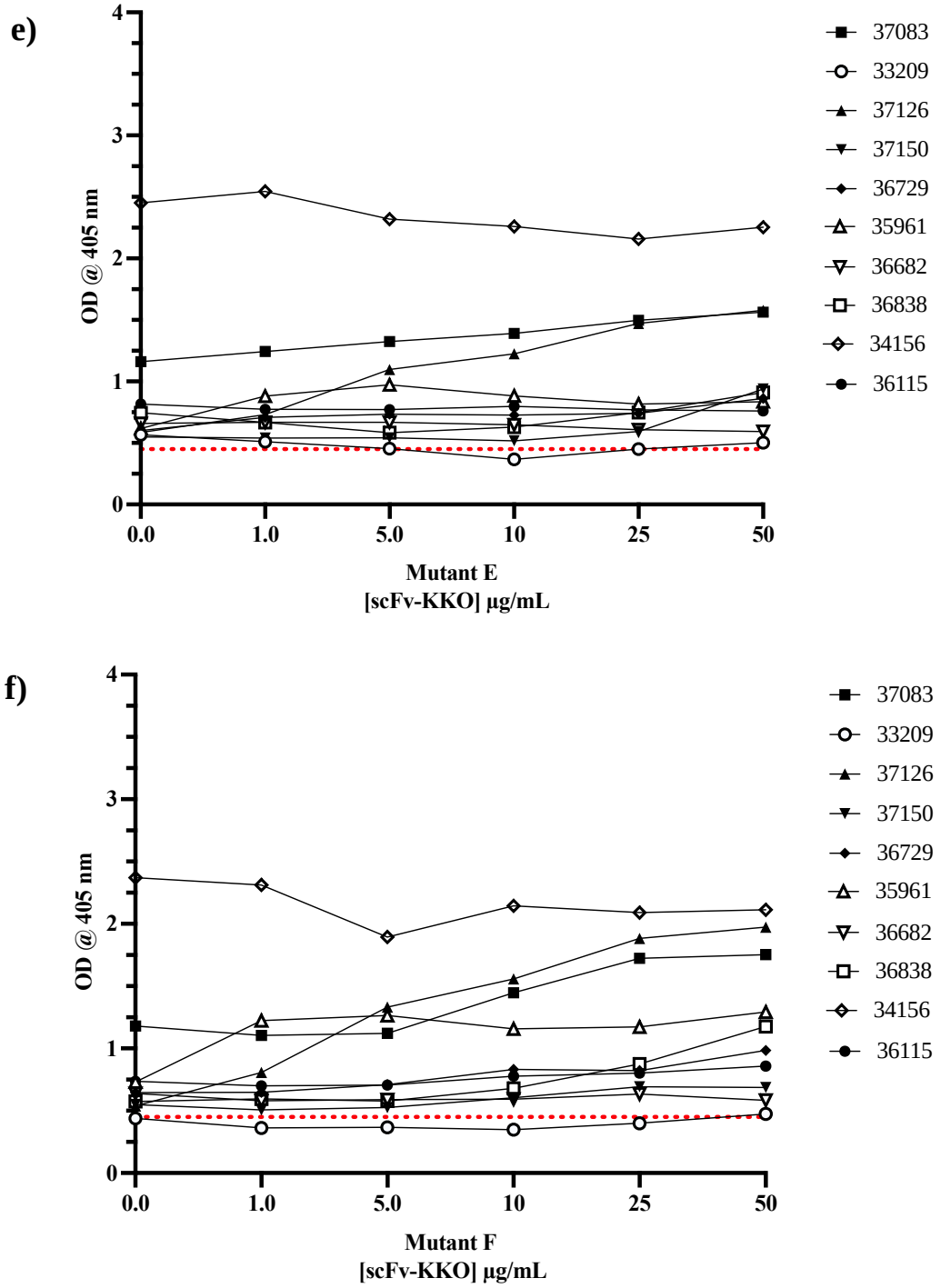

Figure 10. KKO-scFv inhibition of non-pathogenic anti-PF4/heparin antibody binding in a modified streptavidin enzyme immunoassay (EIA). Previously tested EIA-positive/SRA-negative HIT patient samples (n=10) were tested in a modified streptavidin EIA in the presence of KKO-scFv **a)** wildtype, **b)** mutant B, **c)** mutant C, **d)** mutant D, **e)** mutant E, or **f)** mutant F at either 0, 1, 5, 10, 25, and 50 µg/mL concentrations. The ability of each KKO-scFv construct to inhibit antibody binding is shown as a decrease in absorbance (OD) at 405 nm. An $OD_{405nm} \geq 0.45$ in this assay is considered positive for anti-PF4/heparin antibodies, as shown by the dotted line.

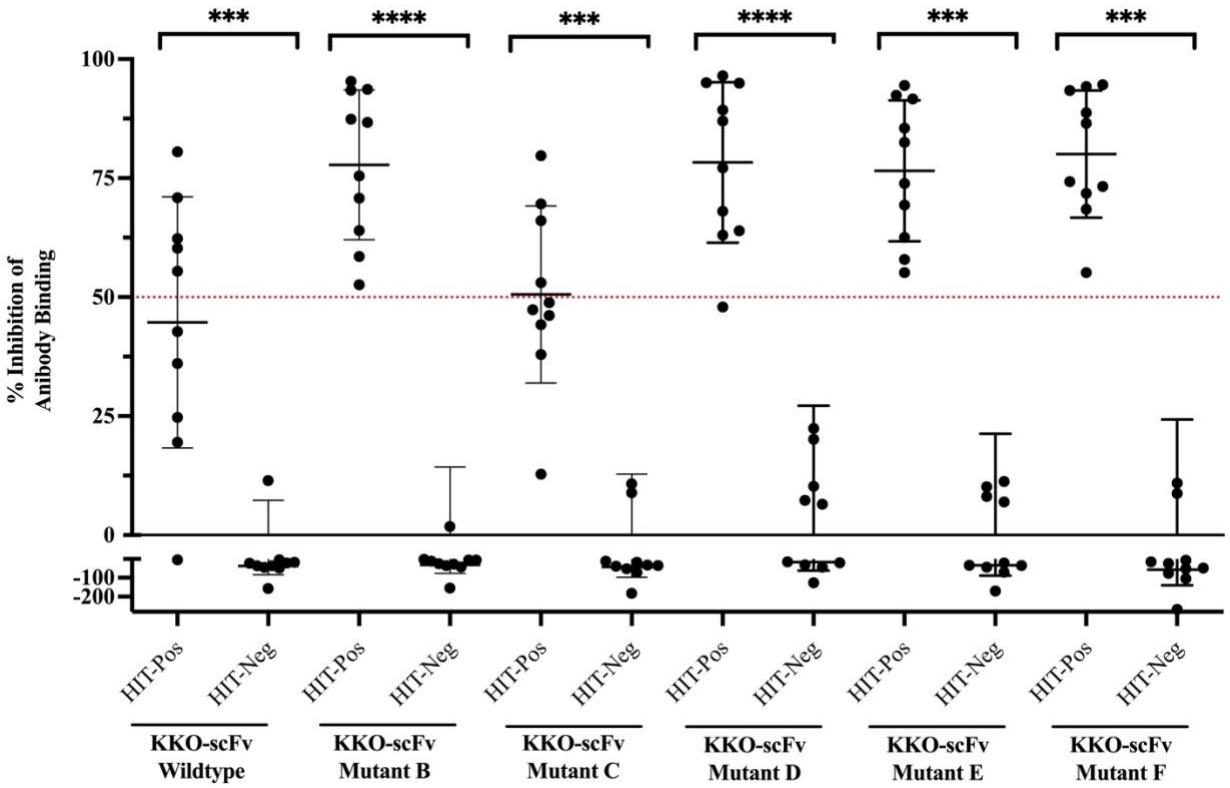

Figure 11. Percent inhibition of anti-PF4/heparin antibody binding from HIT-positive and HIT-negative patients by KKO-scFv in a streptavidin enzyme immunoassay (EIA). Previously tested EIA-positive/SRA-positive HIT patient samples (HIT-pos sera; n=10) and EIA-positive/SRA-negative (HIT-neg sera; n=10) were tested in a modified streptavidin EIA. Results are shown as the percent (%) inhibition of anti-PF4/heparin antibody binding in the presence of KKO-scFv wildtype, mutant B, mutant C, mutant D, mutant E, or mutant F at 50 μg/mL. The ability of each KKO-scFv construct to inhibit antibody binding resulting in a decrease in binding below 50% (red dotted line) was determined. Statistical significance was calculated using an unpaired t-test where (***) represents $p > 0.0005$ and (****) represents $p < 0.00005$. Error bars denoting mean inhibition ± standard deviation (s.d.) are shown.

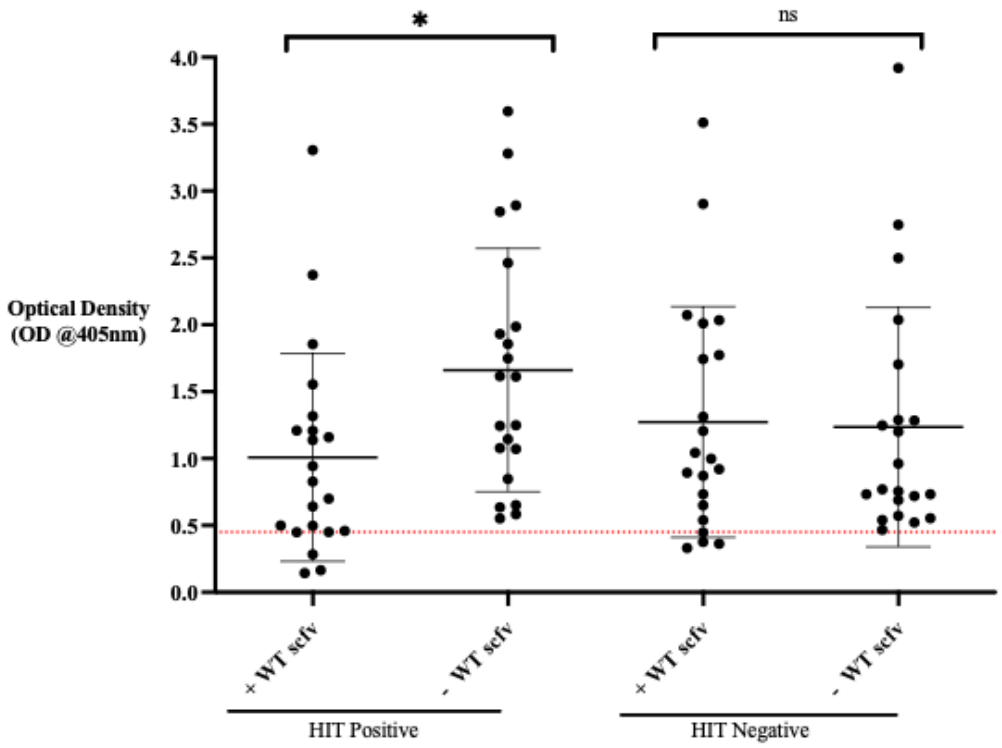

Figure 12. Large-scale screening of HIT-positive and HIT-negative patients in a streptavidin enzyme immunoassay (EIA) using wildtype KKO-scFv. Previously tested HIT patient samples (HIT positive sera, n=20; HIT negative sera, n=20) were tested in an anti-PF4 IgG-specific streptavidin inhibition EIA. Results are shown as the absorbance (OD) at 405 nm with (+scFv) or without (-scFv) the addition of wildtype KKO-scFv. The ability of wildtype KKO-scFv to inhibit antibody binding resulting in a decrease in absorbance below the negative cut-off (OD_{405nm}=0.45, red dotted line) was determined. Statistical significance was calculated using an unpaired t-test where (*) represents $p > 0.05$.

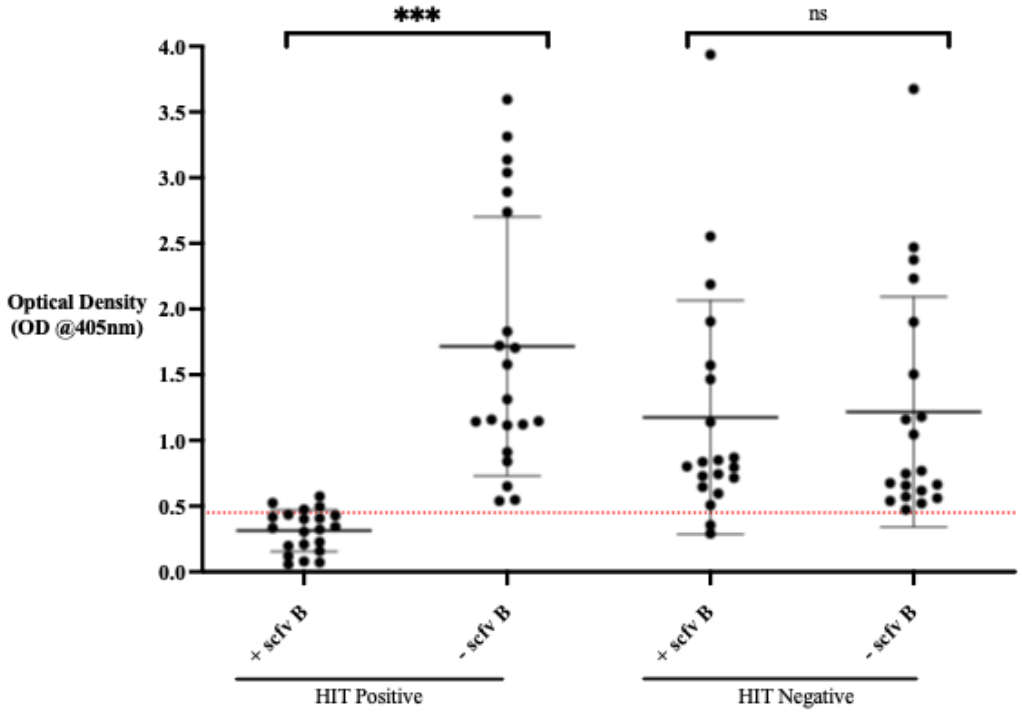

Figure 13. Large-scale screening of HIT-positive and HIT-negative patients in a streptavidin enzyme immunoassay (EIA) using KKO-scFv Mutant B. Previously tested HIT patient samples (HIT positive sera, n=20; HIT negative sera, n=20) were tested in an anti-PF4 IgG-specific streptavidin inhibition EIA. Results are shown as the absorbance (OD) at 405 nm with (+scFv) or without (-scFv) the addition of KKO-scFv mutant B. The ability of mutant B KKO-scFv to inhibit antibody binding resulting in a decrease in absorbance below the negative cut-off (OD_{405nm}=0.45, red dotted line) was determined. Statistical significance was calculated using an unpaired t-test where (***) represents $p > 0.0005$.

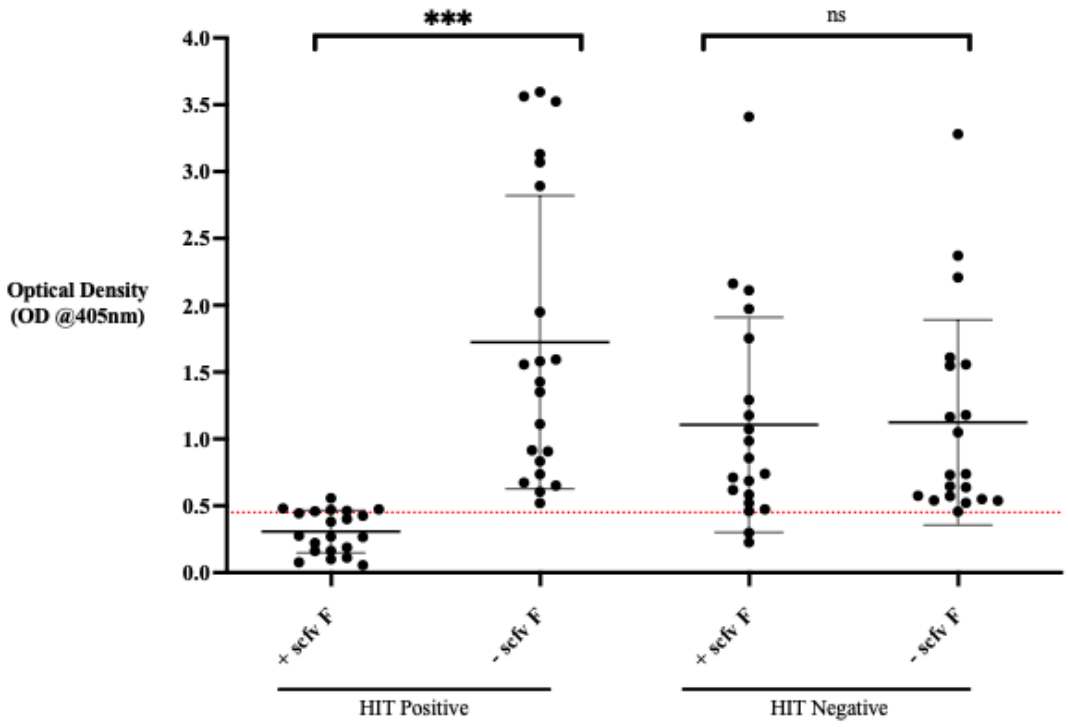

Figure 14. Large-scale screening of HIT-positive and HIT-negative patients in a streptavidin enzyme immunoassay (EIA) using KKO-scFv Mutant F. Previously tested HIT patient samples (HIT positive sera, n=20; HIT negative sera, n=20) were tested in an anti-PF4 IgG-specific streptavidin inhibition EIA. Results are shown as the absorbance (OD) at 405 nm with (+scFv) or without (-scFv) the addition of KKO-scFv mutant F. The ability of mutant F KKO-scFv to inhibit antibody binding resulting in a decrease in absorbance below the negative cut-off (OD_{405nm}=0.45, red dotted line) was determined. Statistical significance was calculated using an unpaired t-test where (***) represents $p > 0.0005$.

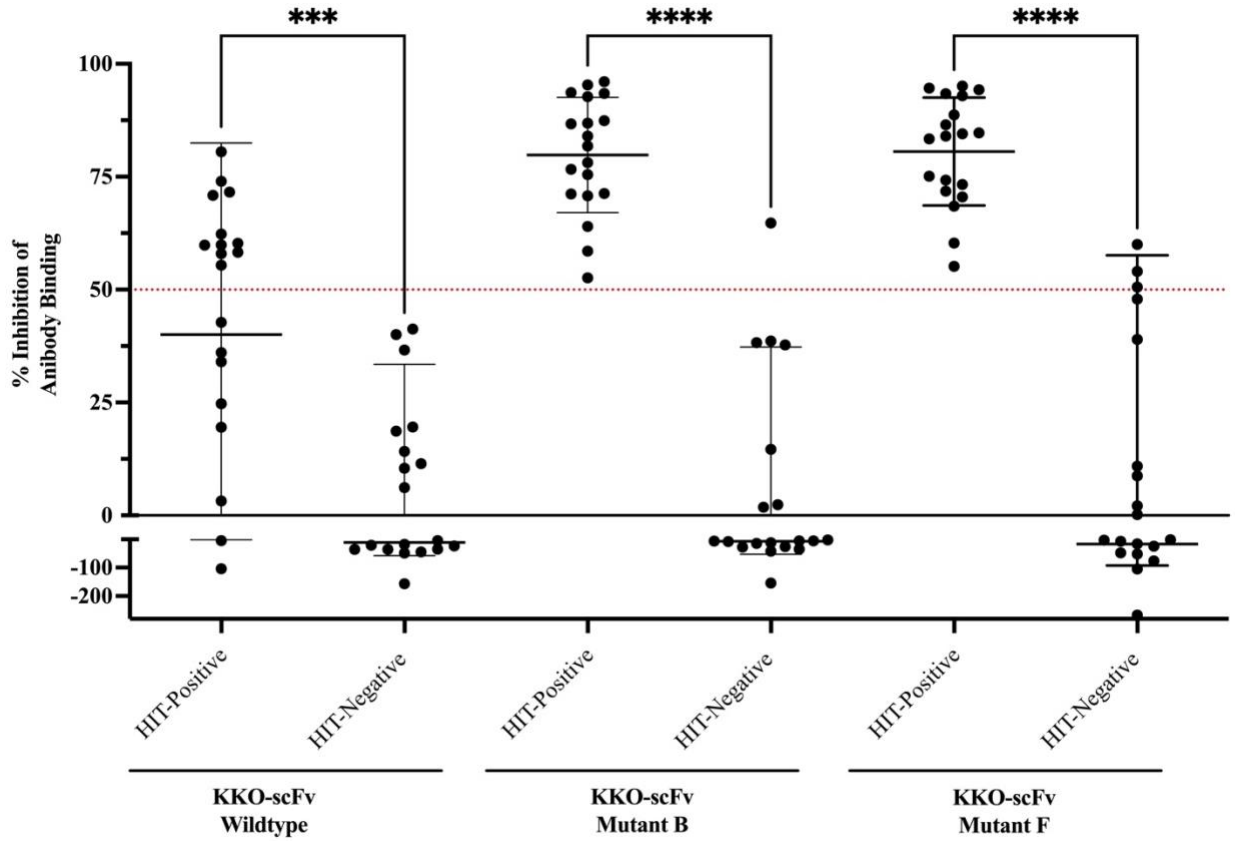

Figure 15. Distinguishing between pathogenic and non-pathogenic anti-PF4/heparin antibodies in a streptavidin enzyme immunoassay (EIA) using KKO-scFv. Previously tested EIA-positive/SRA-positive HIT patient samples (HIT positive sera; n=20) and EIA-positive/SRA-negative (HIT negative sera; n=20) were tested in a modified streptavidin EIA. Results are shown as the percent (%) inhibition of anti-PF4/heparin antibody binding in the presence of KKO-scFv wildtype, mutant B, or mutant F at 50 μg/mL. The ability of each KKO-scFv construct to inhibit antibody binding resulting in a decrease in binding below 50% (red dotted line) was determined. Statistical significance was calculated using a two-way ANOVA analysis where (***) represents $p > 0.0005$ and (****) represents $p < 0.00005$. Error bars denoting mean inhibition ± standard deviation (s.d.) are shown.

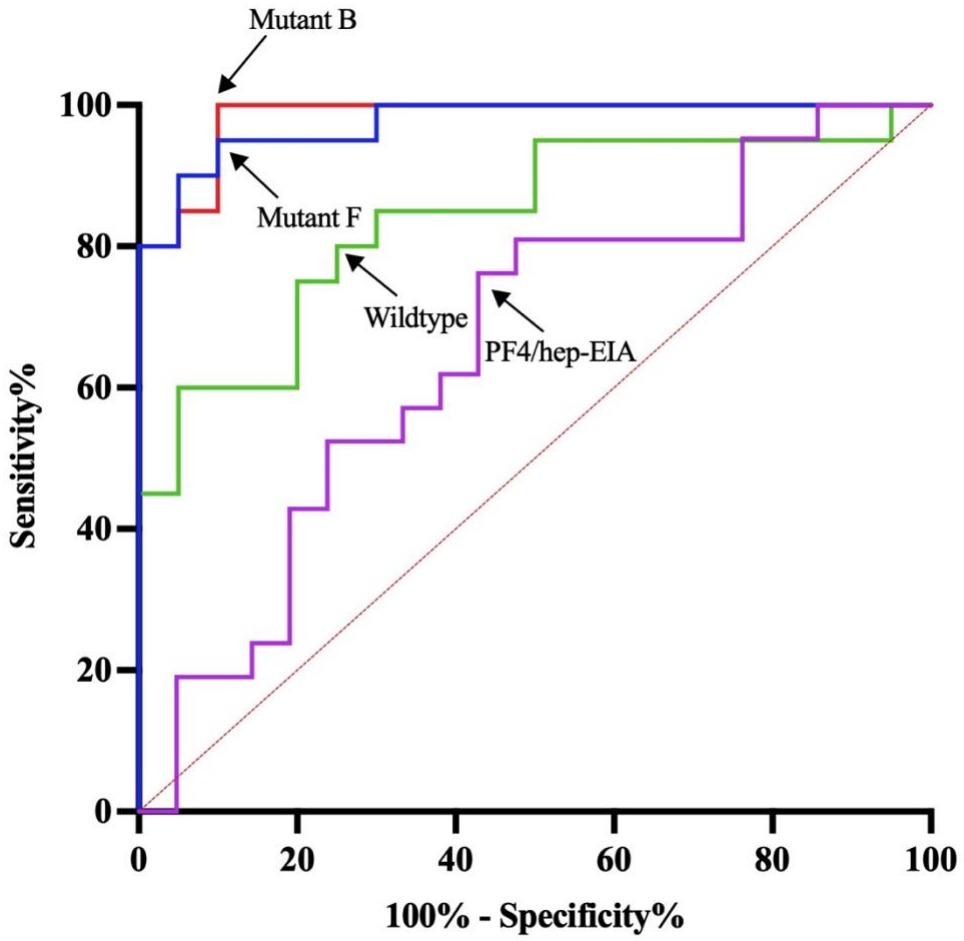

Figure 16. The receiver operating characteristics (ROC) curves of an IgG-specific streptavidin anti-PF4/heparin EIA using KKO-scFv. ROC curves were generated for the PF4/heparin IgG-specific streptavidin EIA alone (purple) and using KKO-scFv wildtype (green), mutant B (red), or mutant F (blue) obtained from testing two clinical cohorts of HIT-positive (n=20, EIA+/SRA+) and HIT-negative (n=20, EIA+/SRA-).

a)

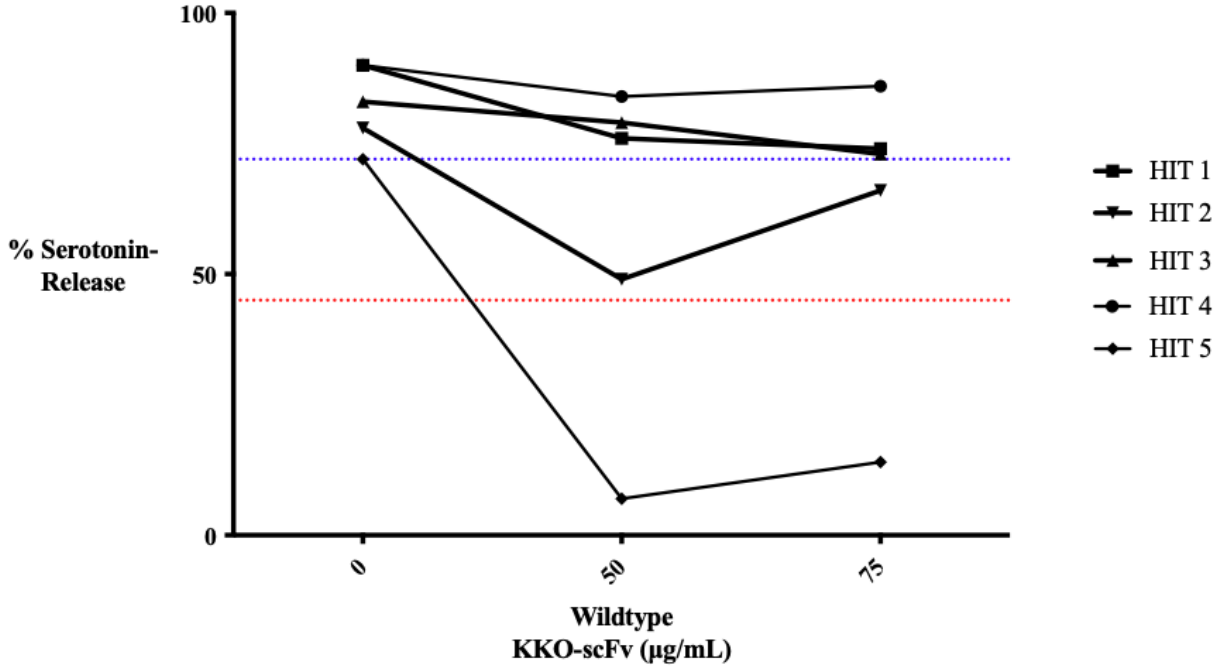
100
50
0
% Serotonin-Release
0
50
75
Wildtype
KKO-scFv (µg/mL)
HIT 1
HIT 2
HIT 3
HIT 4
HIT 5

b)

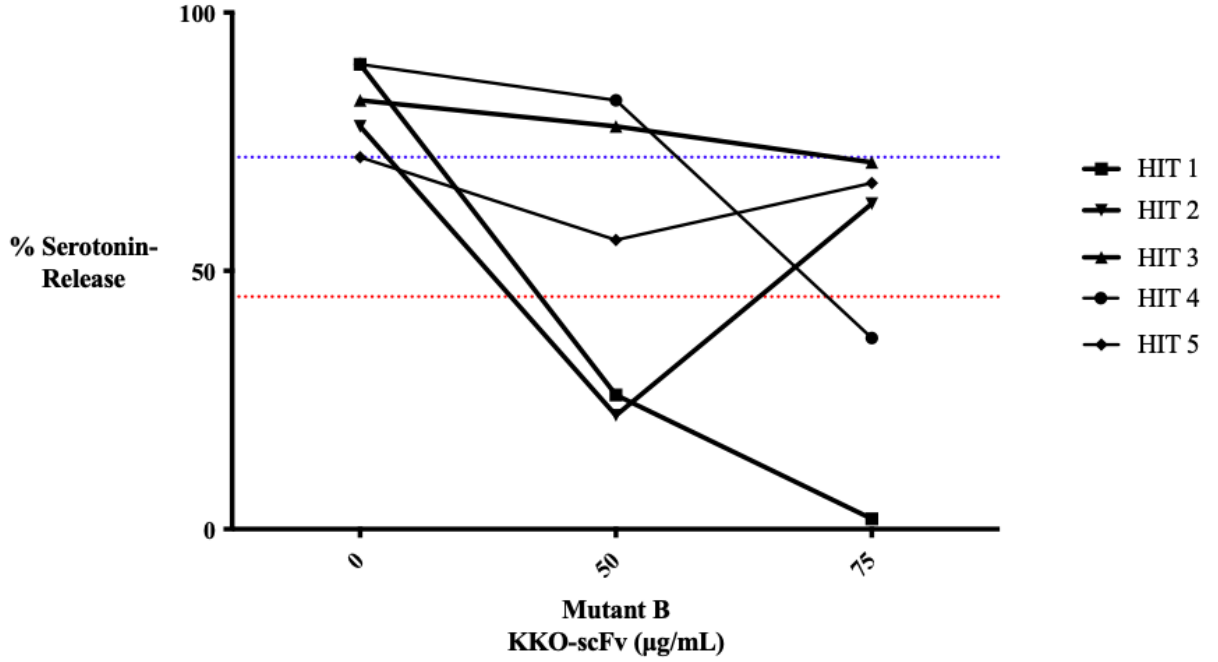
100
50
0
% Serotonin-Release
0
50
75
Mutant B
KKO-scFv (µg/mL)
HIT 1
HIT 2
HIT 3
HIT 4
HIT 5

c)

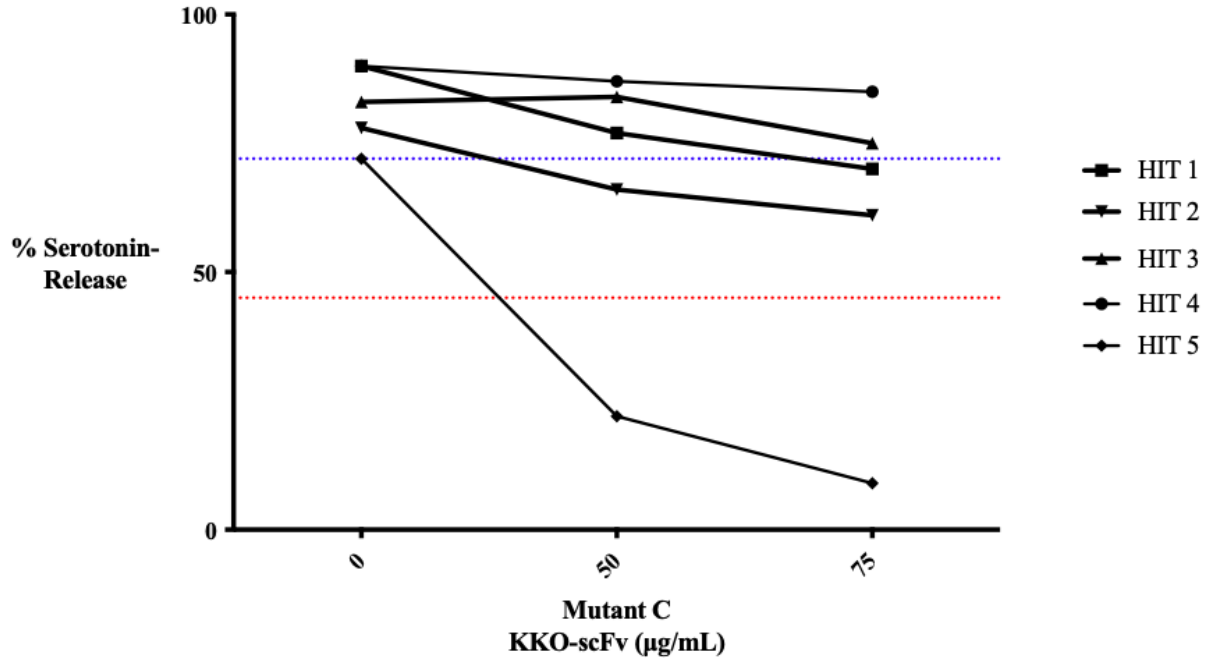
100
50
0
% Serotonin-Release
0
50
75
Mutant C
KKO-scFv (µg/mL)
HIT 1
HIT 2
HIT 3
HIT 4
HIT 5

d)

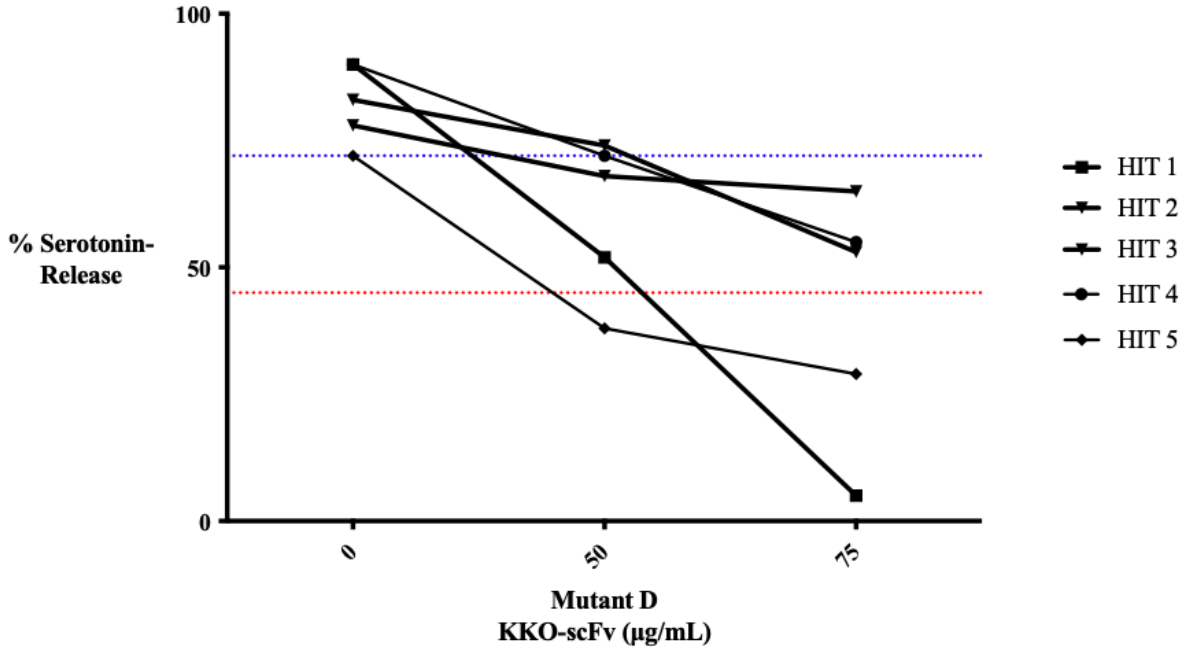
100
50
0
% Serotonin-Release
0
50
75
Mutant D
KKO-scFv (µg/mL)
HIT 1
HIT 2
HIT 3
HIT 4
HIT 5

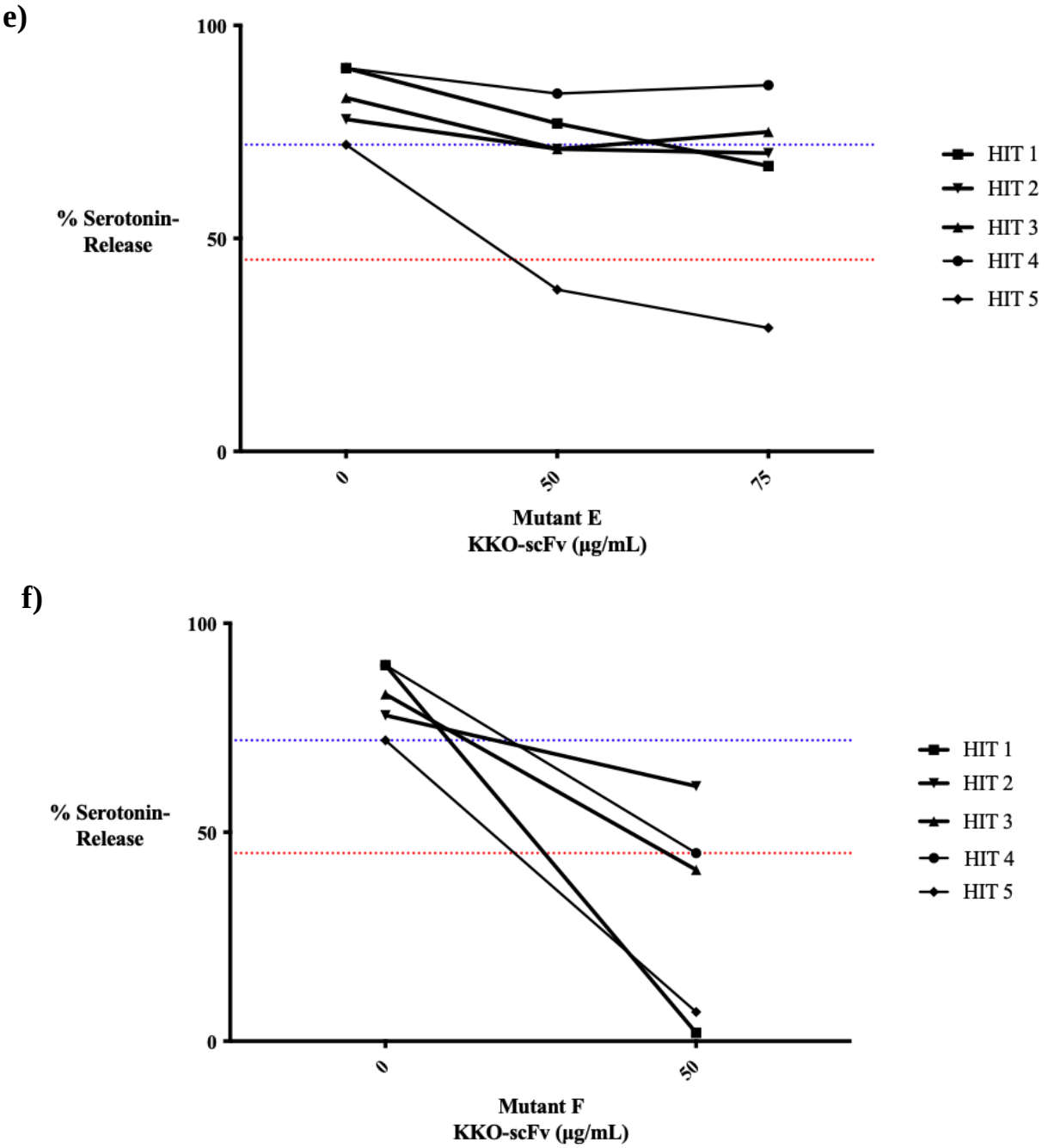

Figure 17. KKO-scFv inhibition of HIT antibody-mediated platelet activation in the ^{14}C-serotonin release assay**.** Previously tested EIA-positive/SRA-positive HIT patient samples (n=5) were tested in a modified ^{14}C-serotonin-release assay (SRA) in the presence of KKO-scFv **a)** wildtype, **b)** mutant B, **c)** mutant C, **d)** mutant D, **e)** mutant E, or **f)** mutant F at either 0, 50, or 75 µg/mL concentrations. The ability of each KKO-scFv construct to inhibit platelet activation resulting in a moderate (≥20%; blue line) or strong (≥50%; red line) decrease in percent (%) ^{14}C-serotonin release was determined relative to control wells containing patient sera in the absence of KKO-scFv.

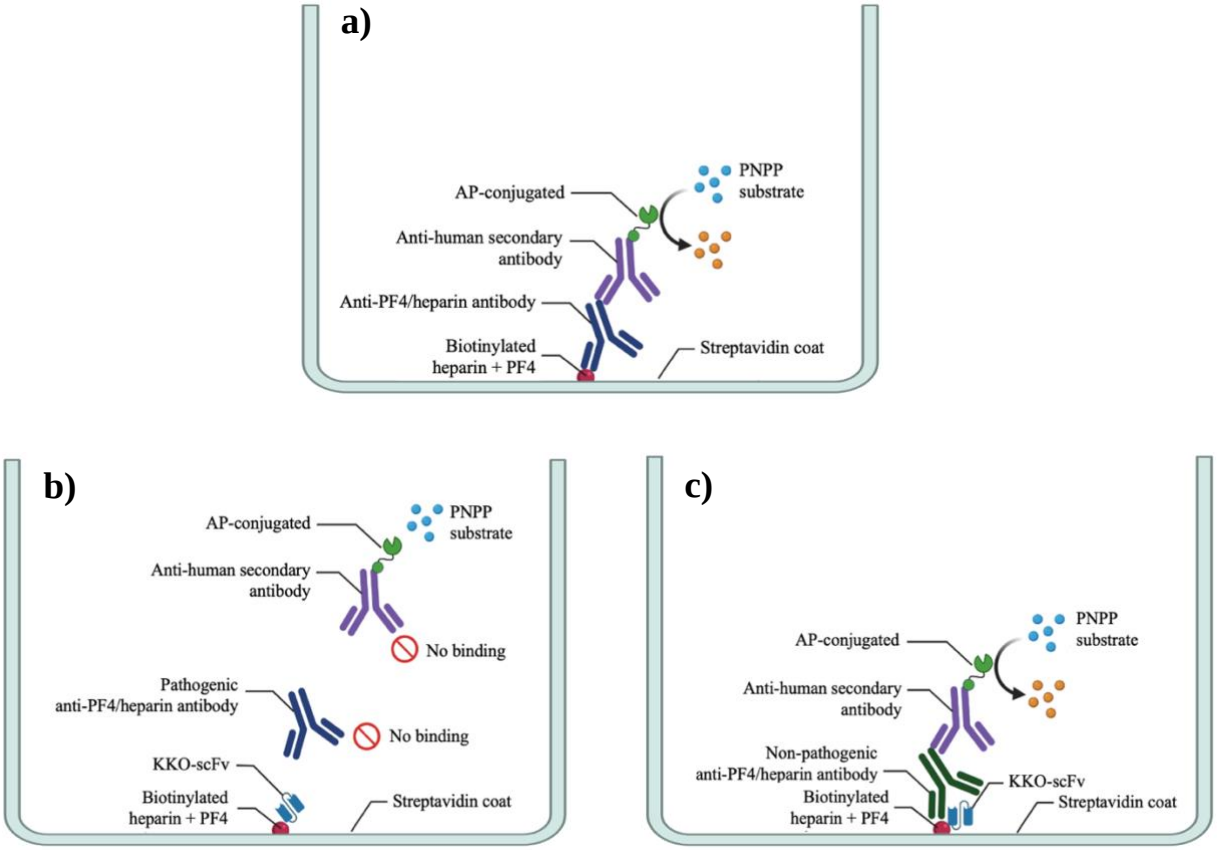

Figure 18. Schematic diagram of the IgG-specific streptavidin PF4/heparin EIA with and without KKO-scFv. Detection of anti-PF4/heparin antibodies is achieved using the streptavidin-biotin association. Biotinylated heparin complexed with PF4 is captured on streptavidin coated plates. Anti-PF4/heparin antibodies in patient sera bind to the PF4/heparin antigen and detected with an alkaline phosphatase (AP)-conjugated anti-human secondary antibody. Antibody binding is quantified by measuring the enzymatic activity of AP when substrate (p-nitrophenyl phosphate [PNPP]) is added. **a)** All anti-PF4/heparin antibodies present in patient sera are detected in this assay regardless of platelet-activating ability. When KKO-scFv is added **b)** pathogenic antibody binding to PF4/heparin is inhibited and the reporter enzyme reaction does not occur while **c)** non-pathogenic antibody binding to PF4/heparin is unaffected. This allows for differentiation between true-positive and false-positive signals in this assay (Figure generated using BioRender).

9.0. TABLES

Table 1: Current Development and Progress of Therapeutic Antibody Fragments.

Name	Type	Target	Status	Treatment
Brolucizumab	scFv	VEGF-A	Approved	Anti-VEGF intravitreal agent for treating AMD[91]
Efungumab	scFv	HSP 90	Phase III	Adjuvant anti-fungal agent for invasive candidiasis infection[178]
Gancotamab	scFv-drug conjugate	HER2	Phase II	HER2-positive advanced/ metastatic breast cancer[179]
Pexelizumab	scFv	C5	Phase III	C5 inhibitor to control inflammation during cardiac surgery[180]
Vicinium	scFv fusion (Pseudomonas exotoxin A)	EpCAM	Phase III	Induces tumor cell death by releasing exotoxin A upon binding to EpCAM antigen on bladder cancer cells.[93]
Flotetuzumab	Bi-specific scFv	CD123/ CD3	Phase I	T-cell re-targeting antibody for recurrent/refractory acute myeloid leukemia[181]
Caplacizumab	Nanobody	vWF	Approved	Prevent vWF/platelet interactions and thrombi formation in aTTP[172]
Vobarilizumab	Nanobody	IL-6R	Phase IIb	Inhibits IL-6 pro-inflammatory pathway in rheumatoid arthritis[182]
Belimumab*	IgG1λ	BLyS	Approved	Prevent BLyS interaction with B-lymphocytes for systemic lupus erythematous treatment[183]
COR-101*	IgG1 (FcγR-silenced Fc)	RBD	Phase 1b/II	Neutralizing antibody against SARS-CoV-2 RBD to inhibit ACE2 receptor interactions in COVID-19 patients.[171]

*****Isolated/developed as scFv using phage display and converted to IgG

Table 2: Phage library selection and enrichment process. Each round of bio-panning was performed using PF4 (30 μg/mL) and heparin (0.5 U/mL) complexes as the target antigen. Stringent washing steps were performed to remove unbound, non-specific, and weakly bound phage displaying KKO-scFv mutants. The number of input and out phage titers (phage/μL) were tracked throughout each cycle to monitor enrichment.

Panning Round	Antigen	Tween-20 (%)	No. of Washings	Input Phage (phage/μL)	Output Phage (phage/μL)
1	PF4 (30 μg/mL) Heparin (0.5 U/mL)	0.1	3 x 5 min	$6.8x10^{9}$	$6.0x10^{5}$
2	PF4 (30 μg/mL) Heparin (0.5 U/mL)	0.1	3 x 5 min	$2.0x10^{7}$	$5.0x10^{5}$
3	PF4 (30 μg/mL) Heparin (0.5 U/mL)	0.1	3 x 5 min	$3.5x10^{8}$	$4.6x10^{6}$
4	PF4 (30 μg/mL) Heparin (0.5 U/mL)	0.1	3 x 5 min	$2.0x10^{7}$	$9.6x10^{5}$
5	PF4 (30 μg/mL) Heparin (0.5 U/mL)	0.1	3 x 5 min	$2.4x10^{10}$	$3.7x10^{6}$

Table 3: Frequency of identical mutant sequences. Lead candidate KKO-scFv mutants were selected based on enrichment following five rounds of bio-panning.

Mutant ID	Grouped Mutations	Frequency (/Total Colonies)	Frequency (%)
B	R18K, N152K, D180N †	3/40	7.5
C	S50N, Y53H	3/40	7.5
D	Y156H*	6/40	15.0
E	Y156H*, D180G†, Q233P	5/40	12.5
F	E183V, E185K, G223R	2/48	4.0

***** Identical mutation

† Different mutation at overlapping residue

Table 4: Summary of experimental IC_{50} values for wildtype and mutant KKO-scFv constructs against full-length KKO with 95% confidence intervals (CI) and R^2 values.

Best-Fit Values	**Wildtype** KKO-scFv	**Mutant B** KKO-scFv	**Mutant C** KKO-scFv	**Mutant D** KKO-scFv	**Mutant E** KKO-scFv	**Mutant F** KKO-scFv
IC50 (µg/mL)	N/A	1.6	N/A	3.1	8.2	1.3
IC50 (nM)	4.9	57.3	7.7	111.1	292.8	46.8
95% CI	? to 112.1	27.2 to 119.4	? to 83.2	66.8 to 172.4	134.4 to 606.3	23.0 to 100.2
R^2	0.36	0.93	0.52	0.96	0.88	0.92

CI = Confidence Interval

Table 5: Mean absorbance (optical density [OD] @ 405nm) of anti-PF4/heparin antibodies from HIT-Positive (n=10) and HIT-negative (n=10) patient sera. Statistical significance (*p*-value) between anti-PF4/heparin antibody binding before (-) and after (+) the addition of 50 μg/mL wildtype or mutant KKO-scFv is shown.

KKO-scFv Construct	**HIT-Positive Sera** (Mean OD_{405nm}, n=10)		**Statistical Significance**
	- scFv	**+ scFv**	**(*p* value)**
Wildtype	1.657	0.931	0.018
Mutant B	1.565	0.275	0.001
Mutant C	1.684	0.799	0.010
Mutant D	1.840	0.283	0.001
Mutant E	1.682	0.319	0.001
Mutant F	1.723	0.281	0.002
KKO-scFv Construct	**HIT-Negative Sera** (Mean OD_{405nm}, n=10)		**Statistical Significance**
	- scFv	**+ scFv**	**(*p* value)**
Wildtype	1.083	1.407	0.303
Mutant B	0.893	1.102	0.438
Mutant C	0.932	1.235	0.285
Mutant D	0.910	1.002	0.700
Mutant E	0.876	1.080	0.430
Mutant F	0.841	1.189	0.195

Table 6: Wildtype and mutant KKO-scFv mean percent (%) inhibition of anti-PF4/heparin antibodies from HIT-Positive (n=10) and HIT-Negative (n=10) patient sera at 50 μg/mL.

KKO-scFv Construct	HIT-Positive Sera (% Inhibition) (Mean, n=10)	HIT-Negative Sera (% Inhibition) (Mean, n=10)	Statistical Significance (*p* value)
Wildtype	44.7%	-38.3%	0.0002
Mutant B	77.8%	-31.4%	<0.0001
Mutant C	50.6%	-42.5%	0.0004
Mutant D	78.3%	-17.3%	<0.0001
Mutant E	76.5%	-34.0%	0.0001
Mutant F	80.0%	-57.0%	0.0005

Table 7: Area under the curve (AUC) and positivity threshold for the streptavidin IgG-specific anti-PF4/heparin inhibitory enzyme immunoassay with KKO-scFv (KKO-scFv PF4/hep-EIA).

Assay Type	Area under curve (AUC) (95% CI)	Positivity Threshold (% Inhibition)
WT KKO-scFv PF4/hep-EIA	0.84 (0.71 to 0.97)	≥ 42.0%
Mutant B KKO-scFv PF4/hep-EIA	0.98 (0.95 to 1.00)	≥ 39.8%
Mutant F KKO-scFv PF4/hep-EIA	0.98 (0.94 to 1.00)	≥ 54.6%

CI = Confidence Interval

Table 8: Performance characteristics of a streptavidin IgG-specific anti-PF4/heparin inhibitory enzyme immunoassay with KKO-scFv (KKO-scFv PF4/hep-EIA).
CI = Confidence Interval

Assay Type	Sensitivity (95% CI)	Specificity (95% CI)	PPV (95% CI)	NPV (95% CI)
Wildtype KKO-scFv Streptavidin anti-PF4/hep EIA	70.0% (45.7-88.1%)	95.0% (75.1-99.9%)	93.3% (67.0-99.0%)	76.0% (61.7-86.2%)
Mutant B KKO-scFv Streptavidin anti-PF4/hep EIA	100.0% (83.2-100.0%)	90.0% (68.3-98.8%)	90.9% (72.9-97.4%)	100.0%
Mutant F KKO-scFv Streptavidin anti-PF4/hep EIA	95.0% (75.1-99.9%)	90.0% (68.3-98.8%)	90.5% (71.8-97.3%)	94.7% (79.6-98.4%)

10.0. SUPPLEMENTARY FIGURES

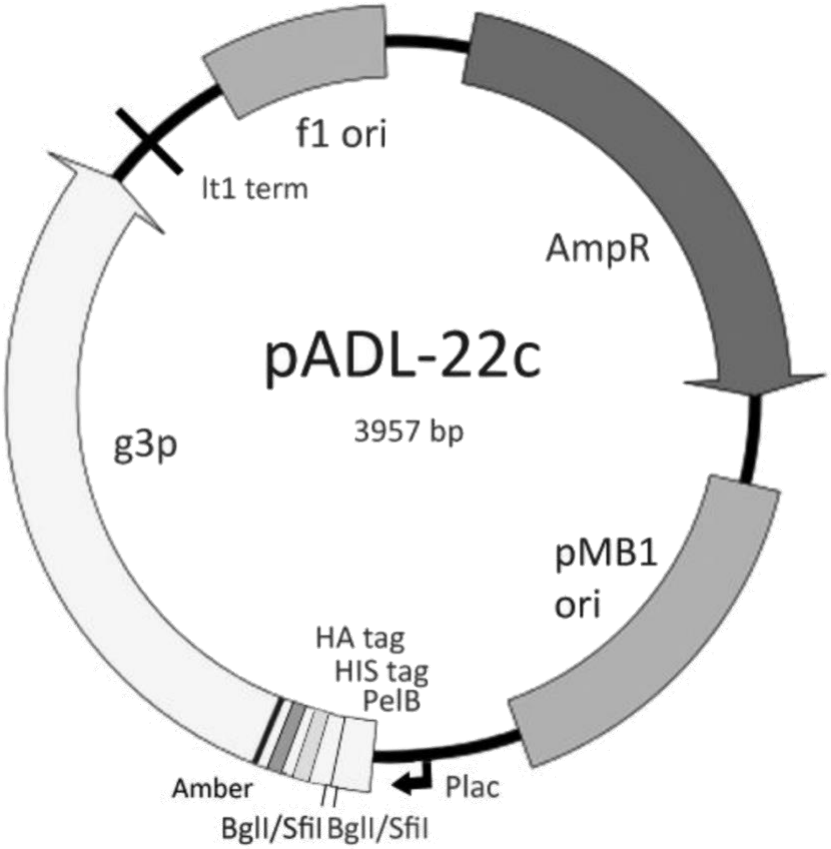

Supplementary Figure 1. Plasmid Map of pADL-22c Phagemid Vector. The KKO-scFv sequence was inserted between double *BglI/Sfi*I restriction enzyme sites. The full vector sequence is 3957 base pairs, expressing the full-length gene III protein (G3P), and an amber stop codon. An ampicillin resistance gene (*AmpR*) is expressed as a selective marker. Two affinity tags, hemagglutinin (HA) and histidine (HIS), are also expressed for detection and/or purification (Retrieved from Antibody Design Labs Inc., 2020).

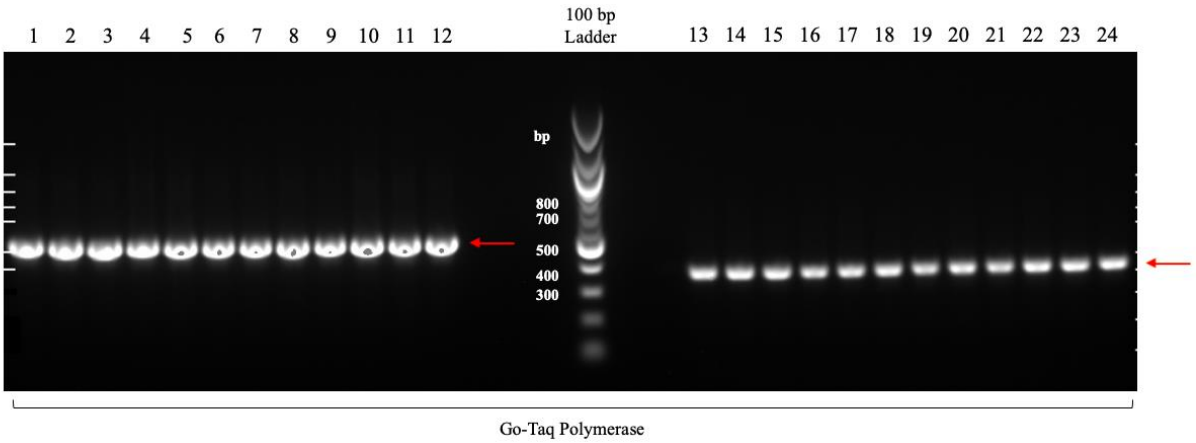

Supplementary Figure 2. Wildtype (WT) KKO-scFv phage colony screen polymerase chain reaction. Agarose gel electrophoresis analysis of WT KKO-scFv PCR products. After sub-cloning WT KKO-scFv into the phagemid pADL22-c, TG1 *E. coli* cells were electroporated and grown up overnight on LB + ampicillin agar plates. Following this, 12 random colonies were selected and used to assess correct WT KKO-scFv insertion. Two sets of gene-specific primers that overlap at each KKO-scFv DNA ligation site was used for each PCR reaction (Supplementary Table 1). PCR products were separated on a 1% agarose gel in 1X TAE buffer. Columns 1-24 represents GoTaq polymerase PCR products. The sizes of molecular weight standards are shown in the center lane (bp). The arrows indicate bands corresponding to the expected KKO-scFv DNA fragment size visualized at approximately 520 bp (Lanes 1-12) and 360 bp (Lanes 13-14), representing the complete sequence.

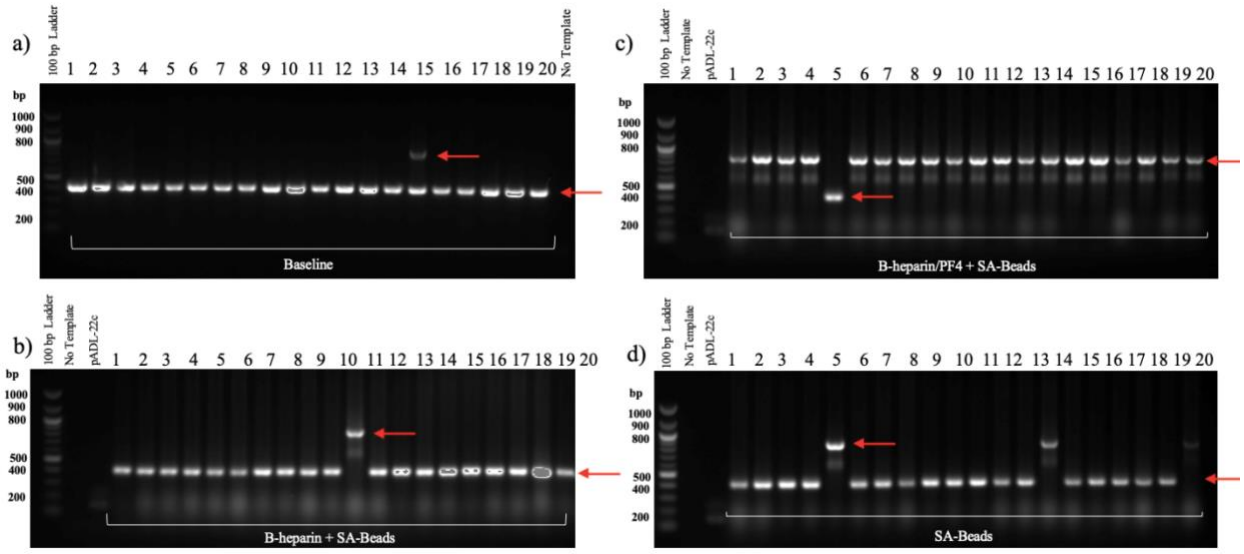

Supplementary Figure 3. Binding Characterization of KKO-scFv Phage Using von Willebrand Factor (vWF) D' Domain Phage on Streptavidin-Coated Magnetic Beads. Agarose gel electrophoresis analysis of vWF D' domain and WT KKO-scFv phage PCR products. **A)** K91 *E. coli* cells were infected with a 10:1 mixture of vWF D' and WT KKO-scFv phage and grown up overnight on LB + ampicillin agar plates to assess baseline infection ratios before selection. K91 *E. coli* cells were the infected with the same 10:1 phage mixture following selection on streptavidin magnetic beads coated with **B)** biotinylated-heparin/PF4, **C)** biotinylated-heparin and **D)** uncoated beads alone. Following this, 20 random colonies per selection condition were analyzed to assess WT KKO-scFv phage enrichment. Gene-specific primers for the pADL22c vector were used for each PCR reaction. PCR products were separated on a 1% agarose gel in 1X TAE buffer. Columns 1-20 represents GoTaq polymerase PCR products. The arrows indicate bands corresponding to the expected WT KKO-scFv and vWF D' domain fragment sizes, visualized at approximately 800 bp and 416 bp, respectively. The sizes of molecular weight standards are shown in the first lanes (bp) followed by no-template (ddH_2O) and an empty vector as negative controls.

```
Wildtype_KKO_scFv                          DIQMIQSQKFMSTSVGDRVTVTCKASQNVGTNVAWYQQKPGQSPNALIYSASYRYSGVPD 60
Mutant_B_KKO_scFv_(R18K,N152K,D180N)       DIQMIQSQKFMSTSVGDKVTVTCKASQNVGTNVAWYQQKPGQSPNALIYSASYRYSGVPD 60
Mutant_C_KKO_scFv_(S50N,Y53H)              DIQMIQSQKFMSTSVGDRVTVTCKASQNVGTNVAWYQQKPGQSPNALIYNASHRYSGVPD 60
Mutant_D_KKO_scFv_(Y156H)                  DIQMIQSQKFMSTSVGDRVTVTCKASQNVGTNVAWYQQKPGQSPNALIYSASYRYSGVPD 60
Mutant_E_KKO_scFv_(Y156H,D180G,Q233P)      DIQMIQSQKFMSTSVGDRVTVTCKASQNVGTNVAWYQQKPGQSPNALIYSASYRYSGVPD 60
Mutant_F_KKO_scFv_(E183V,E185K,G223R)      DIQMIQSQKFMSTSVGDRVTVTCKASQNVGTNVAWYQQKPGQSPNALIYSASYRYSGVPD 60
                                           *****************:*******************************.**:*******

Wildtype_KKO_scFv                          RFTGSGSGTDFTLTITNVQSEDLADYFCQQYNSYPLTFGTGTKLDLKGGGGSGGGGSGGG 120
Mutant_B_KKO_scFv_(R18K,N152K,D180N)       RFTGSGSGTDFTLTITNVQSEDLADYFCQQYNSYPLTFGTGTKLDLKGGGGSGGGGSGGG 120
Mutant_C_KKO_scFv_(S50N,Y53H)              RFTGSGSGTDFTLTITNVQSEDLADYFCQQYNSYPLTFGTGTKLDLKGGGGSGGGGSGGG 120
Mutant_D_KKO_scFv_(Y156H)                  RFTGSGSGTDFTLTITNVQSEDLADYFCQQYNSYPLTFGTGTKLDLKGGGGSGGGGSGGG 120
Mutant_E_KKO_scFv_(Y156H,D180G,Q233P)      RFTGSGSGTDFTLTITNVQSEDLADYFCQQYNSYPLTFGTGTKLDLKGGGGSGGGGSGGG 120
Mutant_F_KKO_scFv_(E183V,E185K,G223R)      RFTGSGSGTDFTLTITNVQSEDLADYFCQQYNSYPLTFGTGTKLDLKGGGGSGGGGSGGG 120
                                           ************************************************************

Wildtype_KKO_scFv                          GSVQLQQSGAELVKPGASVKLSCKASGYTFTNYFIYWVKQRPGQGLEWIGEINPRNGDTD 180
Mutant_B_KKO_scFv_(R18K,N152K,D180N)       GSVQLQQSGAELVKPGASVKLSCKASGYTFTKYFIYWVKQRPGQGLEWIGEINPRNGDTN 180
Mutant_C_KKO_scFv_(S50N,Y53H)              GSVQLQQSGAELVKPGASVKLSCKASGYTFTNYFIYWVKQRPGQGLEWIGEINPRNGDTD 180
Mutant_D_KKO_scFv_(Y156H)                  GSVQLQQSGAELVKPGASVKLSCKASGYTFTNYFIHWVKQRPGQGLEWIGEINPRNGDTD 180
Mutant_E_KKO_scFv_(Y156H,D180G,Q233P)      GSVQLQQSGAELVKPGASVKLSCKASGYTFTNYFIHWVKQRPGQGLEWIGEINPRNGDTG 180
Mutant_F_KKO_scFv_(E183V,E185K,G223R)      GSVQLQQSGAELVKPGASVKLSCKASGYTFTNYFIYWIKQRPGQGLEWIGEINPRNGDTD 180
                                           *******************************:***:*:*********************.

Wildtype_KKO_scFv                          FNEKFESRATLTVDKSSSTAYMQLSSLTSEDSAIYYCTRSPYGNNYGFTYWGQGTLVTVS 240
Mutant_B_KKO_scFv_(R18K,N152K,D180N)       FNEKFESRATLTVDKSSSTAYMQLSSLTSEDSAIYYCTRSPYGNNYGFTYWGQGTLVTVS 240
Mutant_C_KKO_scFv_(S50N,Y53H)              FNEKFESRATLTVDKSSSTAYMQLSSLTSEDSAIYYCTRSPYGNNYGFTYWGQGTLVTVS 240
Mutant_D_KKO_scFv_(Y156H)                  FNEKFESRATLTVDKSSSTAYMQLSSLTSEDSAIYYCTRSPYGNNYGFTYWGQGTLVTVS 240
Mutant_E_KKO_scFv_(Y156H,D180G,Q233P)      FNEKFESRATLTVDKSSSTAYMQLSSLTSEDSAIYYCTRSPYGNNYGFTYWGPGTLVTVS 240
Mutant_F_KKO_scFv_(E183V,E185K,G223R)      FNVKFKSRATLTVDKSSSTAYMQLSSLTSEDSAIYYCTRSPYRNNYGFTYWGQGTLVTVS 240
                                           ** **:************************************ ********* *******

Wildtype_KKO_scFv                          A    241
Mutant_B_KKO_scFv_(R18K,N152K,D180N)       A    241
Mutant_C_KKO_scFv_(S50N,Y53H)              A    241
Mutant_D_KKO_scFv_(Y156H)                  A    241
Mutant_E_KKO_scFv_(Y156H,D180G,Q233P)      A    241
Mutant_F_KKO_scFv_(E183V,E185K,G223R)      A    241
                                           *
```

Supplementary Figure 4. Aligned sequences of wildtype and mutant KKO-scFv. Lead mutant candidates were selected after five rounds of phage display bio-panning based on enrichment. Individual amino acids are colored corresponding to physiochemical properties. Asterisks (*) indicate conserved residues, colons (:) indicate residues with strongly similar properties, and periods (.) indicate residues with weakly similar properties. Red represents small hydrophobic residues (including aromatic side chains), blue represents acidic residues, purple represents basic residues, and green represents residues with hydroxyl/sulfhydryl/amine side chains. Sequence alignment, analysis, and figure was generated using Clustal Omega version 1.2.4.

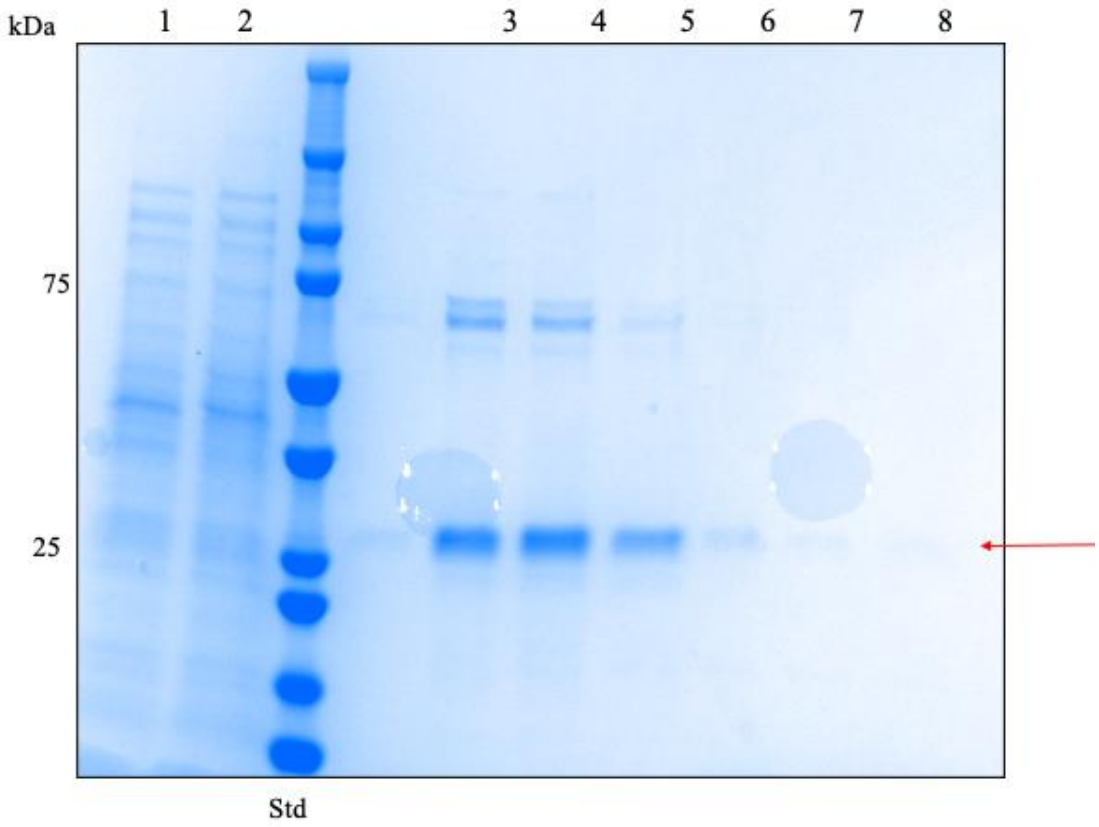

Supplementary Figure 5. Purification of Wild-Type KKO-scFv from BL21 cells using affinity chromatography. SDS-PAGE and Coomassie SimplyBlue™ SafeStain analysis analysis of NI-NTA column purification of wildtype KKO-scFv. Std represents protein ladder standards (kDa). Lanes 1 and 2 show bacterial lysate after sonication and flow through of proteins that do not bind the NI-NTA column, respectively. Lanes 3-8 shows protein eluates containing KKO-scFv displaced from the column at 500 mM imidazole buffer. The red arrow indicates protein band corresponding to purified KKO-scFv at approximately 28 kDa. All samples were separated on a denaturing 4-20% SDS polyacrylamide gradient gel followed by staining.

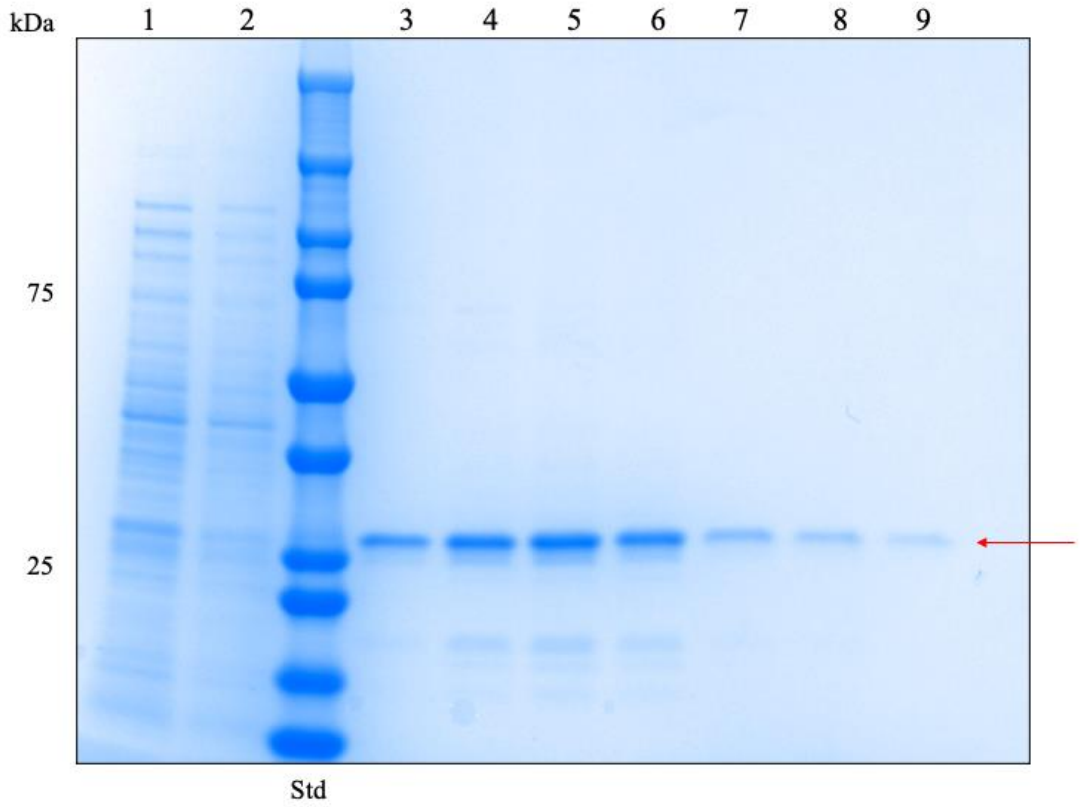

Supplementary Figure 6. Purification of Mutant B KKO-scFv from BL21 cells using affinity chromatography. SDS-PAGE and Coomassie SimplyBlue™ SafeStain analysis analysis of NI-NTA column purification of KKO-scFv mutant B. Std represents protein ladder standards (kDa). Lanes 1 and 2 show bacterial lysate after sonication and flow through of proteins that do not bind the NI-NTA column, respectively. Lanes 3-9 shows protein eluates containing KKO-scFv displaced from the column at 500 mM imidazole buffer. The red arrow indicates protein band corresponding to purified KKO-scFv at approximately 28 kDa. All samples were separated on a denaturing 4-20% SDS polyacrylamide gradient gel followed by staining.

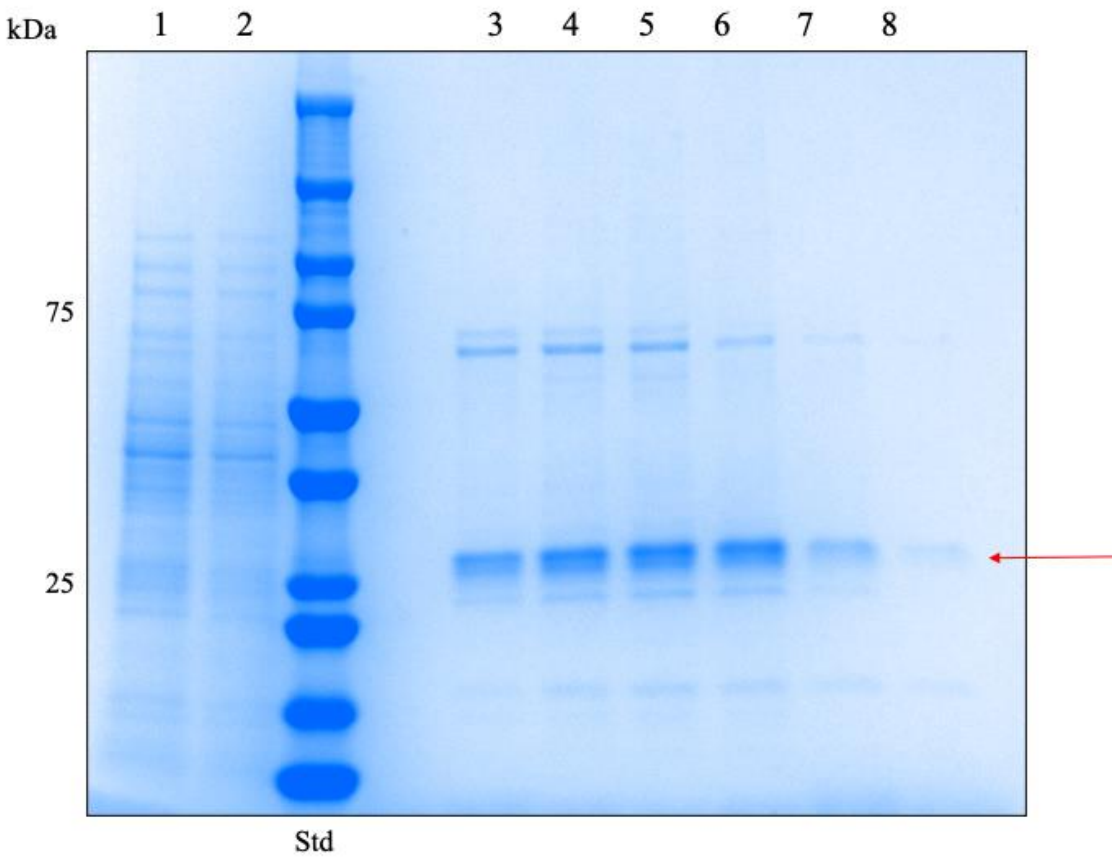

Supplementary Figure 7. Purification of Mutant C KKO-scFv from BL21 cells using affinity chromatography. SDS-PAGE and Coomassie SimplyBlue™ SafeStain analysis analysis of NI-NTA column purification of KKO-scFv mutant C. Std represents protein ladder standards (kDa). Lanes 1 and 2 show bacterial lysate after sonication and flow through of proteins that do not bind the NI-NTA column, respectively. Lanes 3-8 shows protein eluates containing KKO-scFv displaced from the column at 500 mM imidazole buffer. The red arrow indicates protein band corresponding to purified KKO-scFv at approximately 28 kDa. All samples were separated on a denaturing 4-20% SDS polyacrylamide gradient gel followed by staining.

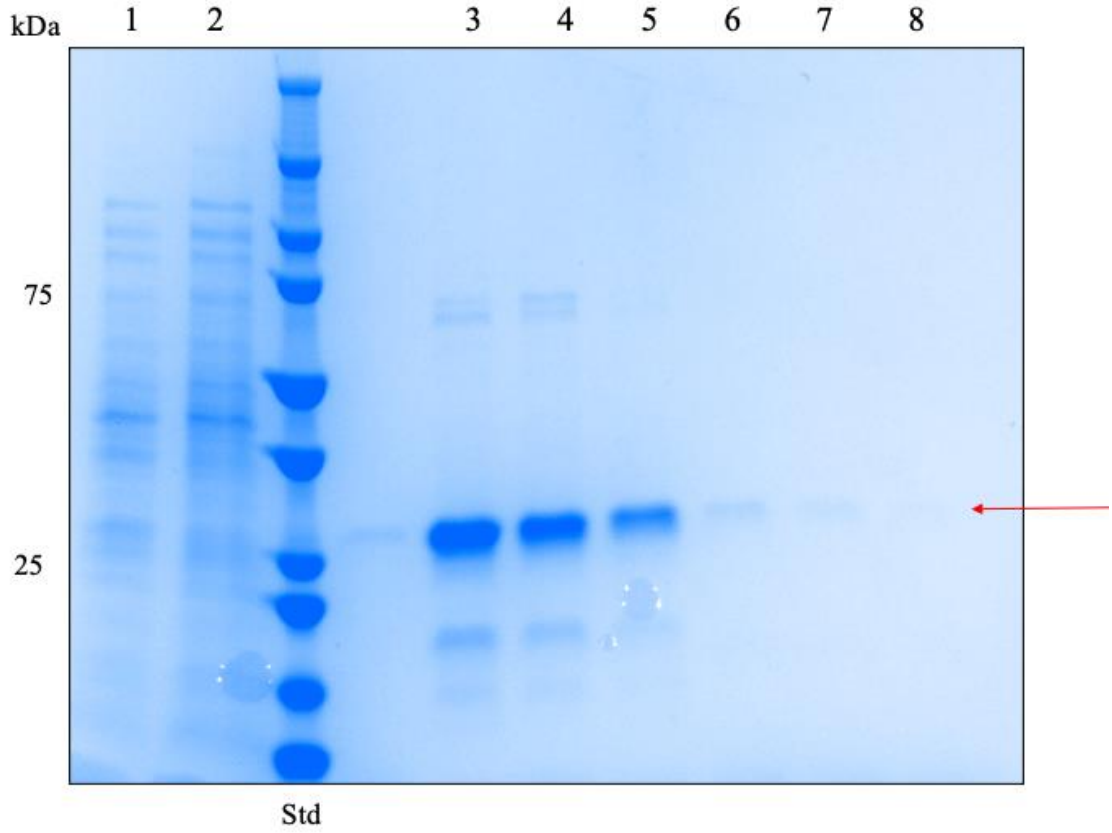

Supplementary Figure 8. Purification of Mutant D KKO-scFv from BL21 cells using affinity chromatography. SDS-PAGE and Coomassie SimplyBlue™ SafeStain analysis analysis of NI-NTA column purification of KKO-scFv mutant D. Std represents protein ladder standards (kDa). Lanes 1 and 2 show bacterial lysate after sonication and flow through of proteins that do not bind the NI-NTA column, respectively. Lanes 3-8 shows protein eluates containing KKO-scFv displaced from the column at 500 mM imidazole buffer. The red arrow indicates protein band corresponding to purified KKO-scFv at approximately 28 kDa. All samples were separated on a denaturing 4-20% SDS polyacrylamide gradient gel followed by staining.

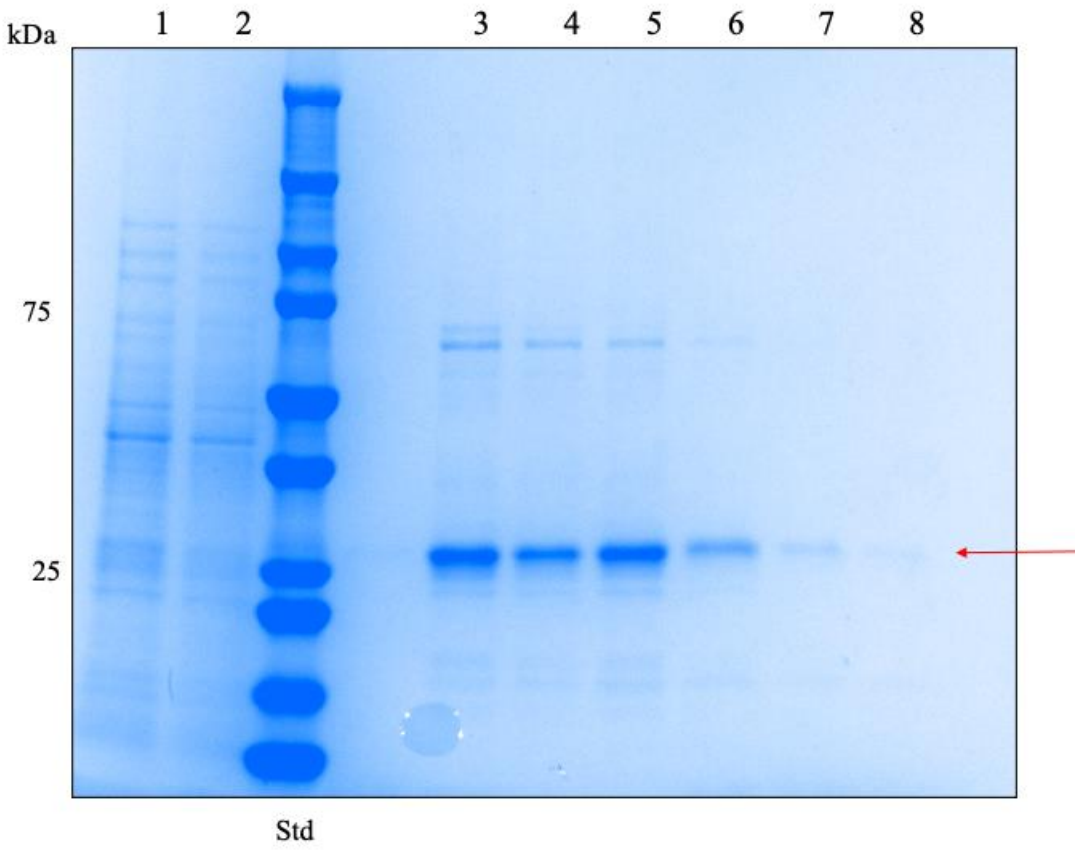

Supplementary Figure 9. Purification of Mutant E KKO-scFv from BL21 cells using affinity chromatography. SDS-PAGE and Coomassie SimplyBlue™ SafeStain analysis analysis of NI-NTA column purification of KKO-scFv mutant E. Std represents protein ladder standards (kDa). Lanes 1 and 2 show bacterial lysate after sonication and flow through of proteins that do not bind the NI-NTA column, respectively. Lanes 3-8 shows protein eluates containing KKO-scFv displaced from the column at 500 mM imidazole buffer. The red arrow indicates protein band corresponding to purified KKO-scFv at approximately 28 kDa. All samples were separated on a denaturing 4-20% SDS polyacrylamide gradient gel followed by staining.

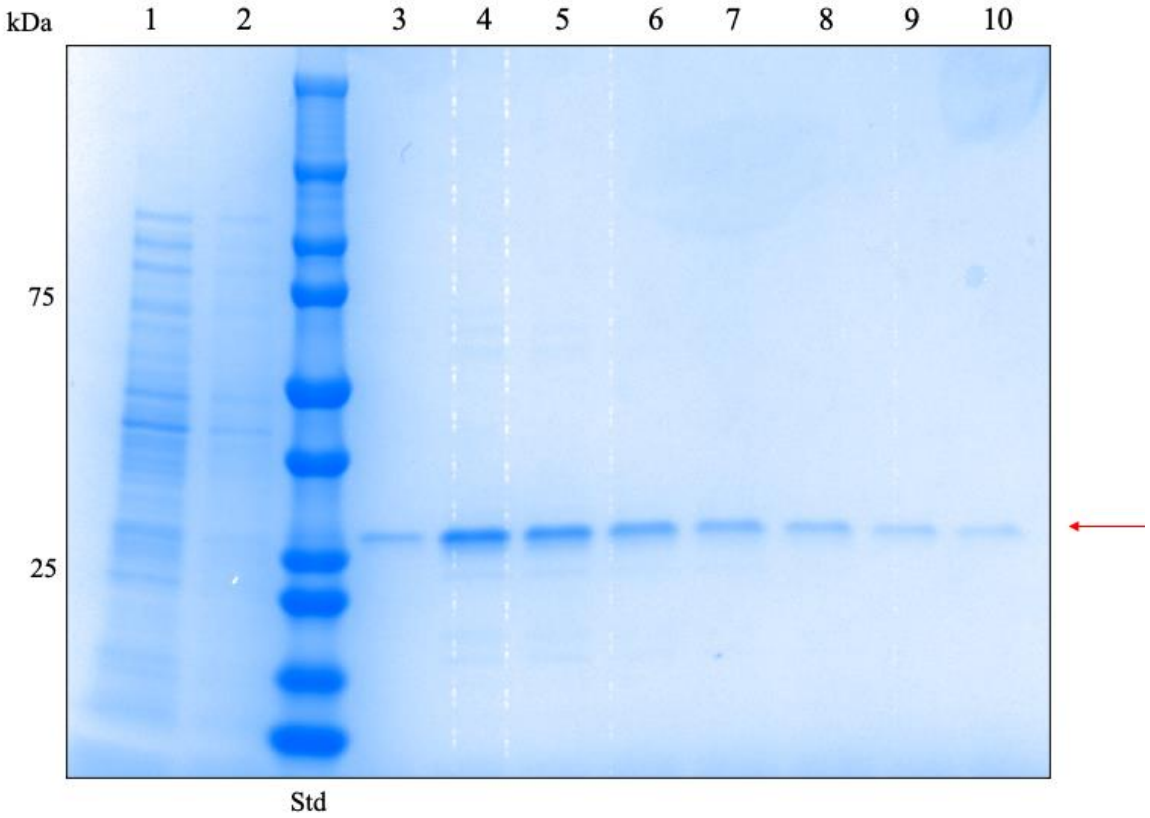

Supplementary Figure 10. Purification of Mutant F KKO-scFv from BL21 cells using affinity chromatography. SDS-PAGE and Coomassie SimplyBlue™ SafeStain analysis analysis of NI-NTA column purification of KKO-scFv mutant F. Std represents protein ladder standards (kDa). Lanes 1 and 2 show bacterial lysate after sonication and flow through of proteins that do not bind the NI-NTA column, respectively. Lanes 3-10 shows protein eluates containing KKO-scFv displaced from the column at 500 mM imidazole buffer. The red arrow indicates protein band corresponding to purified KKO-scFv at approximately 28 kDa. All samples were separated on a denaturing 4-20% SDS polyacrylamide gradient gel followed by staining.

a)

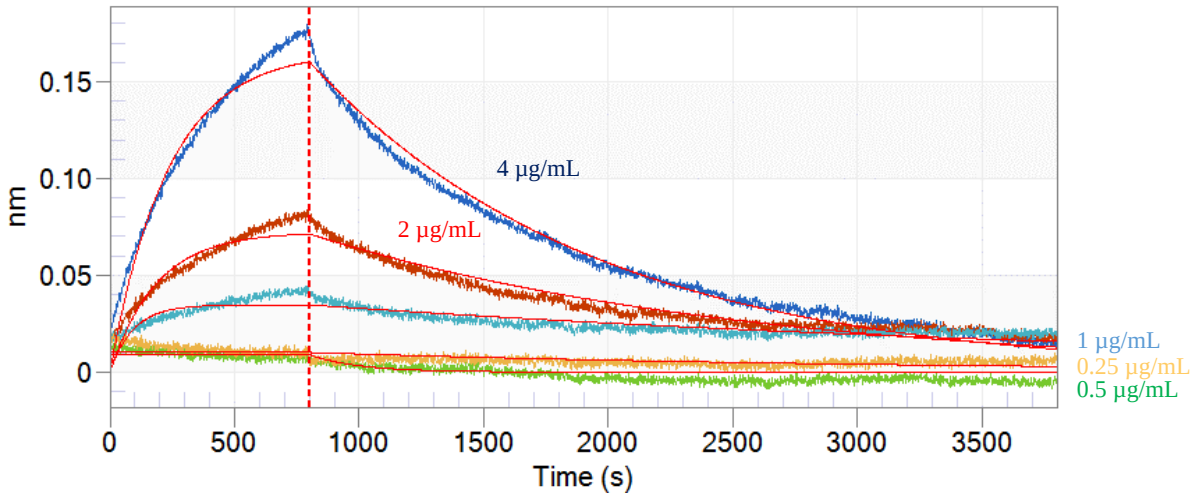

b)

Conc. (µg/mL)	Response (nm)	K_D (M)	k_{on} ($M^{-1}s^{-1}$)	k_{off} (s^{-1})
4.0	0.1223	$3.93x10^{-8}$	$2.22x10^{4}$	$8.71x10^{-4}$
2.0	0.0579	$9.18x10^{-9}$	$6.21x10^{4}$	$5.71x10^{-4}$
1.0	0.0327	$9.61x10^{-10}$	$2.74x10^{5}$	$2.64x10^{-4}$
0.5	0.0092	$<1.0x10^{-12}$	$4.21x10^{127}$	$5.04x10^{-3}$
0.25	0.0122	$<1.0x10^{-12}$	$1.41x10^{108}$	$4.20x10^{-4}$

Supplementary Figure 11. Binding kinetics of wildtype KKO-scFv against biotinylated PF4 and heparin complexes immobilized on streptavidin sensors. a) Spectrogram showing the binding response of wildtype KKO-scFv with lines of best fit (n=1). Binding was measured at six different concentrations: 4 µg/mL (dark blue), 2 µg/mL (red), 1 µg/mL (light blue), 0.5 µg/mL (green), and 0.25 µg/mL (yellow). **b)** Table showing BLI binding responses (nm) and kinetic data, including affinity constants (K_D) as well as association (k_{on}) and dissociation (k_{off}) rates. All data was analyzed based on a 1:1 homogenous ligand binding model using Octet® User Software version 3.1.

a)

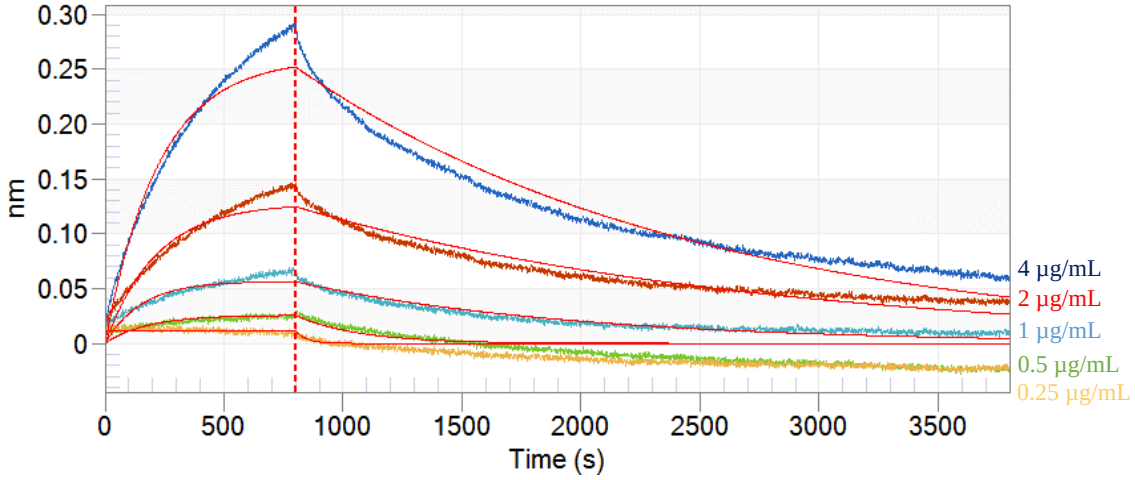

b)

Conc. (µg/mL)	Response (nm)	K_D (M)	k_{on} ($M^{-1}s^{-1}$)	k_{off} (s^{-1})
4.0	0.1958	$2.41x10^{-8}$	$2.48x10^{4}$	$5.96x10^{-4}$
2.0	0.0986	$9.59x10^{-9}$	$5.38x10^{4}$	$5.15x10^{-4}$
1.0	0.0481	$5.71x10^{-9}$	$1.49x10^{5}$	$8.53x10^{-4}$
0.5	0.0199	$3.45x10^{-8}$	$1.07x10^{5}$	$3.70x10^{-3}$
0.25	0.0120	$<1.0x10^{-12}$	$1.42x10^{135}$	$2.10x10^{-2}$

Supplementary Figure 12. Binding kinetics of wildtype KKO-scFv against biotinylated PF4 complexes immobilized on streptavidin sensors. a) Spectrogram representing the binding response of wildtype KKO-scFv with lines of best fit (n=1). Binding was measured at six different concentrations: 4 µg/mL (dark blue), 2 µg/mL (red), 1 µg/mL (light blue), 0.5 µg/mL (green), and 0.25 µg/mL (yellow). **b)** Table showing BLI binding responses (nm) and kinetic data, including affinity constants (K_D) as well as association (k_{on}) and dissociation (k_{off}) rates. All data was analyzed based on a 1:1 homogenous ligand binding model using Octet® User Software version 3.1.

a)

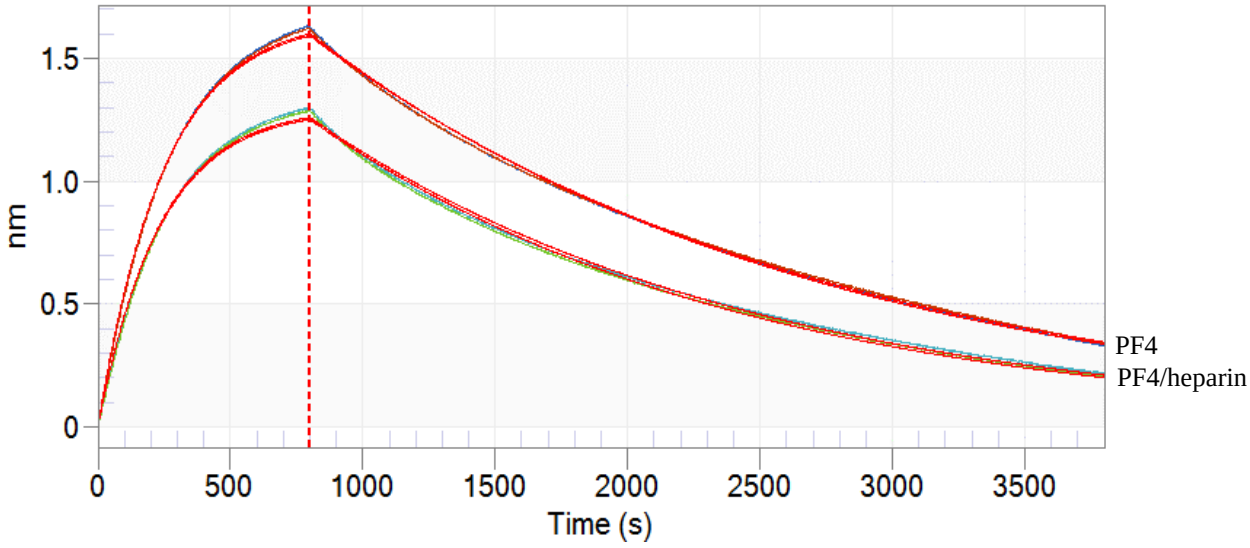

b)

Biotinylated Antigen	Response (nm) ± s.d.	K_D (M) ± s.d.	K_{on}($M^{-1}s^{-1}$) ± s.d.	K_{off}(s^{-1}) ± s.d.
PF4	1.626 ± 0.01	$1.97x10^{-9} \pm 3.54x10^{-11}$	$2.61x10^{5} \pm 1.13x10^{3}$	$5.15x10^{-4} \pm 7.00x10^{-6}$
PF4/heparin	1.290 ± 0.01	$2.19x10^{-9} \pm 5.59x10^{-11}$	$2.75x10^{5} \pm 2.19x10^{3}$	$6.04x10^{-4} \pm 1.06x10^{-5}$

Supplementary Figure 13. Binding kinetics of full-length KKO against biotinylated PF4 and PF4/heparin complexes immobilized on streptavidin sensors. a) Spectrogram representing the binding response of KKO with lines of best fit (n=2). Binding was measured against PF4 (blue) and PF4/heparin (green) at 2 µg/mL. **b)** Table showing BLI binding responses (nm) and kinetic data, including affinity constants (K_D) as well as association (k_{on}) and dissociation (k_{off}) rates. All data was analyzed based on a 1:1 homogenous ligand binding model using Octet® User Software version 3.1.

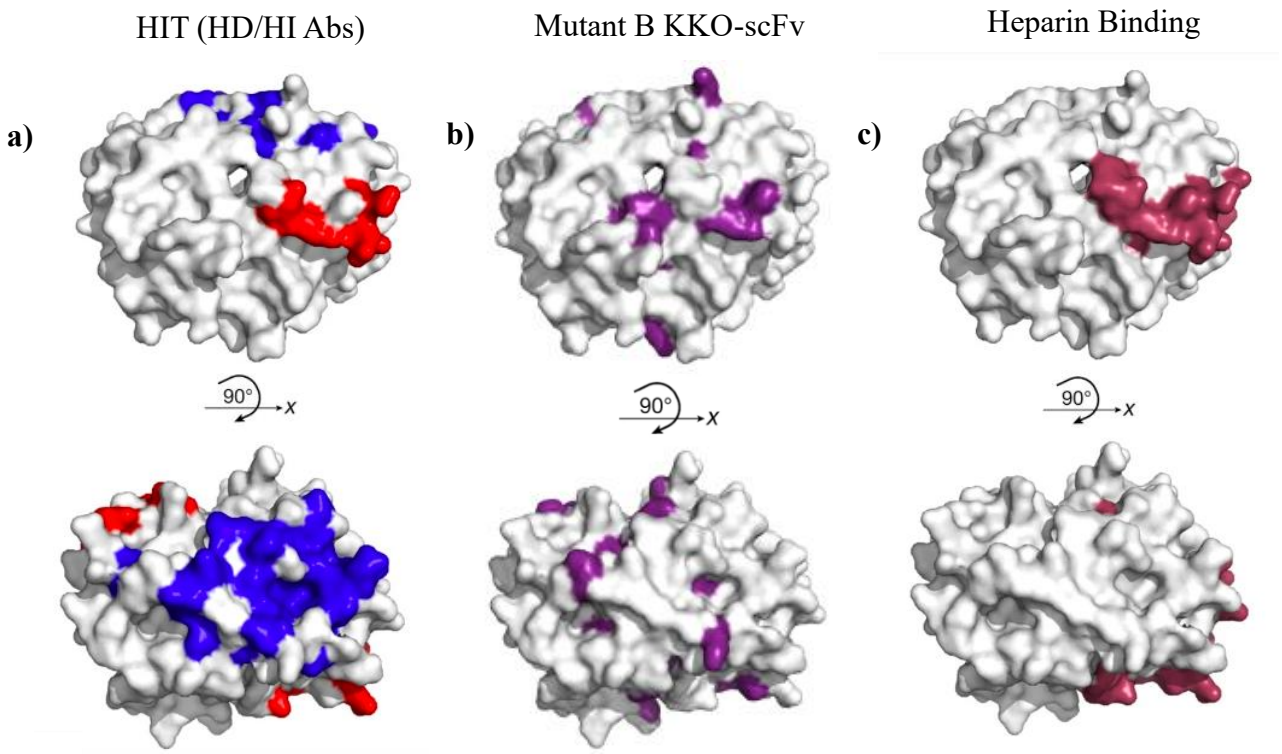

Supplementary Figure 14. Heparin-dependent and -independent pathogenic antibody binding sites on PF4. Amino acids highlighted on the surface of PF4 tetramers that make up the epitope for **a)** HIT patients with heparin-dependent (HD, blue) and heparin-independent (HI, red) antibodies (abs) and **b)** Mutant B KKO-scFv (purple) compared to the **c)** heparin-binding site (brown). Figure adapted from: Huynh, A., Kelton, J.G., Arnold, D.M. *et al.* Antibody epitopes in vaccine-induced immune thrombotic thrombocytopaenia. *Nature* **596,** 565–569 (2021).

11.0. SUPPLEMENTARY TABLES

Supplementary Table 1: Initial primer sets used for verifying correct wildtype and mutant KKO-scFv insertion into the pADL-22c phagemid vector that overlap with the ligation sites at both ends.

Primer"	Sequence
S2A…Sense Primer A	5' – TCAAGGAGACAGTCATAATGAAA – 3'
AS2A…Anti-Sense Primer A	5' – GGTAGCTGTTGTACTGCT – 3'
S2B…Sense Primer B	5' – CAGCAGTACAACAGCTACC – 3'
AS2B…Anti-Sense Primer B	5' – GGCACATCATACGGATATGC – 3'

12.0. BIBLIOGRAPHY

1. Warkentin TE, Kelton JG. A 14-year study of heparin-induced thrombocytopenia. *Am J Med* 1996; **101**(5): 502-7.
2. Warkentin TE, Sheppard JA, Horsewood P, Simpson PJ, Moore JC, Kelton JG. Impact of the patient population on the risk for heparin-induced thrombocytopenia. *Blood* 2000; **96**(5): 1703-8.
3. Greinacher A, Gopinadhan M, Gunther JU, et al. Close approximation of two platelet factor 4 tetramers by charge neutralization forms the antigens recognized by HIT antibodies. *Arterioscler Thromb Vasc Biol* 2006; **26**(10): 2386-93.
4. Rauova L, Poncz M, McKenzie SE, et al. Ultralarge complexes of PF4 and heparin are central to the pathogenesis of heparin-induced thrombocytopenia. *Blood* 2005; **105**(1): 131-8.
5. Warkentin TE, Sheppard JI. Generation of platelet-derived microparticles and procoagulant activity by heparin-induced thrombocytopenia IgG/serum and other IgG platelet agonists: a comparison with standard platelet agonists. *Platelets* 1999; **10**(5): 319-26.
6. Warkentin TE, Hayward CP, Boshkov LK, et al. Sera from patients with heparin-induced thrombocytopenia generate platelet-derived microparticles with procoagulant activity: an explanation for the thrombotic complications of heparin-induced thrombocytopenia. *Blood* 1994; **84**(11): 3691-9.
7. Amiral J, Bridey F, Wolf M, et al. Antibodies to macromolecular platelet factor 4-heparin complexes in heparin-induced thrombocytopenia: a study of 44 cases. *Thromb Haemost* 1995; **73**(1): 21-8.
8. Visentin GP, Malik M, Cyganiak KA, Aster RH. Patients treated with unfractionated heparin during open heart surgery are at high risk to form antibodies reactive with heparin:platelet factor 4 complexes. *J Lab Clin Med* 1996; **128**(4): 376-83.
9. Warkentin TE, Sheppard JI, Sun JC, Jung H, Eikelboom JW. Anti-PF4/heparin antibodies and venous graft occlusion in postcoronary artery bypass surgery patients randomized to postoperative unfractionated heparin or fondaparinux thromboprophylaxis. *J Thromb Haemost* 2013; **11**(2): 253-60.
10. Nazi I, Arnold DM, Moore JC, et al. Pitfalls in the diagnosis of heparin-Induced thrombocytopenia: A 6-year experience from a reference laboratory. *Am J Hematol* 2015; **90**(7): 629-33.
11. Nazi I, Arnold DM, Warkentin TE, Smith JW, Staibano P, Kelton JG. Distinguishing between anti-platelet factor 4/heparin antibodies that can and cannot cause heparin-induced thrombocytopenia. *J Thromb Haemost* 2015; **13**(10): 1900-7.
12. Nguyen TH, Greinacher A. Distinct Binding Characteristics of Pathogenic Anti-Platelet Factor-4/Polyanion Antibodies to Antigens Coated on Different Substrates: A Perspective on Clinical Application. *ACS Nano* 2018; **12**(12): 12030-41.
13. Huynh A, Arnold DM, Kelton JG, et al. Characterization of platelet factor 4 amino acids that bind pathogenic antibodies in heparin-induced thrombocytopenia. *J Thromb Haemost* 2019; **17**(2): 389-99.
14. Lo GK, Sigouin CS, Warkentin TE. What is the potential for overdiagnosis of heparin-induced thrombocytopenia? *Am J Hematol* 2007; **82**(12): 1037-43.
15. Warkentin TE. Laboratory diagnosis of heparin-induced thrombocytopenia. *Int J Lab Hematol* 2019; **41 Suppl 1**: 15-25.

16. Arepally GM, Kamei S, Park KS, et al. Characterization of a murine monoclonal antibody that mimics heparin-induced thrombocytopenia antibodies. *Blood* 2000; **95**(5): 1533-40.
17. Thomas GS. The Structure of Resting and Activated Platelets. In: Michelson AD, Frelinger, A., Cattaneo, M., Newman., P., ed. Platelets. 4th ed. United Kingdom: Academic Press; 2019.
18. van der Meijden PEJ, Heemskerk JWM. Platelet biology and functions: new concepts and clinical perspectives. *Nat Rev Cardiol* 2019; **16**(3): 166-79.
19. Giannini S, Falet, H., & Hoffmeister, K. Platelet Glycobiology and the Control of Platelet Function and Lifespan. In: Michelson AD, Frelinger, A., Cattaneo, M., Newman., P., ed. Platelets. 4th ed. United Kingdom: Academic Press; 2019: 79-97.
20. O'Donnell JS OSJ, Preston RJS. Advances in understanding the molecular mechanisms that maintain normal haemostasis. *Br J Haematol* 2019; **182**(1): 24-36.
21. Estevez B, Du X. New Concepts and Mechanisms of Platelet Activation Signaling. *Physiology (Bethesda)* 2017; **32**(2): 162-77.
22. Jurk K, and Kehrel, E. B. Platelets: Physiology and Biochemistry. *SEMINARS IN THROMBOSIS AND HEMOSTASIS* 2005; **31**(4): 12.
23. Li Z, Delaney MK, O'Brien KA, Du X. Signaling during platelet adhesion and activation. *Arterioscler Thromb Vasc Biol* 2010; **30**(12): 2341-9.
24. Ho KH, van Hove M, Leng G. Trends in anticoagulant prescribing: a review of local policies in English primary care. *BMC Health Serv Res* 2020; **20**(1): 279.
25. Crowther MA, Warkentin TE. Bleeding risk and the management of bleeding complications in patients undergoing anticoagulant therapy: focus on new anticoagulant agents. *Blood* 2008; **111**(10): 4871-9.
26. Ahmed I, Majeed A, Powell R. Heparin induced thrombocytopenia: diagnosis and management update. *Postgrad Med J* 2007; **83**(983): 575-82.
27. Hirsh J, Anand SS, Halperin JL, Fuster V, American Heart A. Guide to anticoagulant therapy: Heparin : a statement for healthcare professionals from the American Heart Association. *Circulation* 2001; **103**(24): 2994-3018.
28. Weitz JI. Low-molecular-weight heparins. *N Engl J Med* 1997; **337**(10): 688-98.
29. Noti C, Seeberger PH. Chemical approaches to define the structure-activity relationship of heparin-like glycosaminoglycans. *Chem Biol* 2005; **12**(7): 731-56.
30. Hirsh J, Warkentin TE, Shaughnessy SG, et al. Heparin and low-molecular-weight heparin: mechanisms of action, pharmacokinetics, dosing, monitoring, efficacy, and safety. *Chest* 2001; **119**(1 Suppl): 64S-94S.
31. Gettins PG, Fan B, Crews BC, Turko IV, Olson ST, Streusand VJ. Transmission of conformational change from the heparin binding site to the reactive center of antithrombin. *Biochemistry* 1993; **32**(33): 8385-9.
32. Jin L, Abrahams JP, Skinner R, Petitou M, Pike RN, Carrell RW. The anticoagulant activation of antithrombin by heparin. *Proc Natl Acad Sci U S A* 1997; **94**(26): 14683-8.
33. Warkentin TE, Levine MN, Hirsh J, et al. Heparin-induced thrombocytopenia in patients treated with low-molecular-weight heparin or unfractionated heparin. *N Engl J Med* 1995; **332**(20): 1330-5.
34. Lee DHW, A. E. Frequency of heparin-induced thrombocytopenia. In: Warkentin AEG, A., ed. Heparin-induced thrombocytopenia. 3th ed; 2004: 107-48.
35. Cuker A, Cines DB. How I treat heparin-induced thrombocytopenia. *Blood* 2012; **119**(10): 2209-18.

36. Warkentin TE. Heparin-induced thrombocytopenia: pathogenesis and management. *Br J Haematol* 2003; **121**(4): 535-55.
37. Warkentin TE, Kelton JG. Temporal aspects of heparin-induced thrombocytopenia. *N Engl J Med* 2001; **344**(17): 1286-92.
38. Arepally GM, Padmanabhan A. Heparin-Induced Thrombocytopenia: A Focus on Thrombosis. *Arterioscler Thromb Vasc Biol* 2021; **41**(1): 141-52.
39. Amiral J, Bridey F, Dreyfus M, et al. Platelet factor 4 complexed to heparin is the target for antibodies generated in heparin-induced thrombocytopenia. *Thromb Haemost* 1992; **68**(1): 95-6.
40. Reilly MP, Taylor SM, Hartman NK, et al. Heparin-induced thrombocytopenia/thrombosis in a transgenic mouse model requires human platelet factor 4 and platelet activation through FcgammaRIIA. *Blood* 2001; **98**(8): 2442-7.
41. Shuster TA, Silliman WR, Coats RD, Mureebe L, Silver D. Heparin-induced thrombocytopenia: twenty-nine years later. *J Vasc Surg* 2003; **38**(6): 1316-22.
42. Nand S, Wong W, Yuen B, Yetter A, Schmulbach E, Gross Fisher S. Heparin-induced thrombocytopenia with thrombosis: incidence, analysis of risk factors, and clinical outcomes in 108 consecutive patients treated at a single institution. *Am J Hematol* 1997; **56**(1): 12-6.
43. Girolami B, Prandoni P, Stefani PM, et al. The incidence of heparin-induced thrombocytopenia in hospitalized medical patients treated with subcutaneous unfractionated heparin: a prospective cohort study. *Blood* 2003; **101**(8): 2955-9.
44. Gruel Y, De Maistre E, Pouplard C, et al. Diagnosis and management of heparin-induced thrombocytopenia. *Anaesth Crit Care Pain Med* 2020; **39**(2): 291-310.
45. Hogan M, Berger JS. Heparin-induced thrombocytopenia (HIT): Review of incidence, diagnosis, and management. *Vasc Med* 2020; **25**(2): 160-73.
46. Warkentin TE, Sheppard JA, Moore JC, Cook RJ, Kelton JG. Studies of the immune response in heparin-induced thrombocytopenia. *Blood* 2009; **113**(20): 4963-9.
47. Cai Z, Yarovoi SV, Zhu Z, et al. Atomic description of the immune complex involved in heparin-induced thrombocytopenia. *Nat Commun* 2015; **6**: 8277.
48. Brandt S, Krauel K, Gottschalk KE, et al. Characterisation of the conformational changes in platelet factor 4 induced by polyanions: towards in vitro prediction of antigenicity. *Thromb Haemost* 2014; **112**(1): 53-64.
49. Staibano P, Arnold DM, Bowdish DM, Nazy I. The unique immunological features of heparin-induced thrombocytopenia. *Br J Haematol* 2017; **177**(2): 198-207.
50. Tutwiler V, Madeeva D, Ahn HS, et al. Platelet transactivation by monocytes promotes thrombosis in heparin-induced thrombocytopenia. *Blood* 2016; **127**(4): 464-72.
51. Kelton JG, Sheridan D, Santos A, et al. Heparin-induced thrombocytopenia: laboratory studies. *Blood* 1988; **72**(3): 925-30.
52. Denomme GA. The platelet Fc receptor in heparin-induced thrombocytopenia. 6 ed: CRC Press; 2001.
53. Arman M, Krauel K. Human platelet IgG Fc receptor FcgammaRIIA in immunity and thrombosis. *J Thromb Haemost* 2015; **13**(6): 893-908.
54. Vogelpoel LT, Baeten DL, de Jong EC, den Dunnen J. Control of cytokine production by human fc gamma receptors: implications for pathogen defense and autoimmunity. *Front Immunol* 2015; **6**: 79.
55. Haile LA, Rao R, Polumuri SK, et al. PF4-HIT antibody (KKO) complexes activate broad innate immune and inflammatory responses. *Thromb Res* 2017; **159**: 39-47.

56. Radziwon P, Boczkowska-Radziwon B, Schenk JF, et al. Platelet activation and its role in thrombin generation in platelet-induced thrombin generation time. *Thromb Res* 2000; **100**(5): 419-26.
57. Nevzorova TA, Mordakhanova ER, Daminova AG, et al. Platelet factor 4-containing immune complexes induce platelet activation followed by calpain-dependent platelet death. *Cell Death Discov* 2019; **5**: 106.
58. Arepally G, Poncz, M., & Cines, D. Autoantibodies in heparin-induced thrombocytopenia In: Shoenfeld Y, Gershwin, E., & Meroni, P., ed. Autoantibodies. 2nd ed: Elsevier; 2007: 511-9.
59. Files JC, Malpass TW, Yee EK, Ritchie JL, Harker LA. Studies of human plate alpha-granule release in vivo. *Blood* 1981; **58**(3): 607-18.
60. Zucker MB, Katz IR. Platelet factor 4: production, structure, and physiologic and immunologic action. *Proc Soc Exp Biol Med* 1991; **198**(2): 693-702.
61. Greinacher A, Selleng K, Warkentin TE. Autoimmune heparin-induced thrombocytopenia. *J Thromb Haemost* 2017; **15**(11): 2099-114.
62. Schultz NH, Sorvoll IH, Michelsen AE, et al. Thrombosis and Thrombocytopenia after ChAdOx1 nCoV-19 Vaccination. *N Engl J Med* 2021; **384**(22): 2124-30.
63. Huynh A, Kelton JG, Arnold DM, Daka M, Nazy I. Antibody epitopes in vaccine-induced immune thrombotic thrombocytopaenia. *Nature* 2021; **596**(7873): 565-9.
64. Nguyen TH, Medvedev N, Delcea M, Greinacher A. Anti-platelet factor 4/polyanion antibodies mediate a new mechanism of autoimmunity. *Nat Commun* 2017; **8**: 14945.
65. Kreimann M, Brandt S, Krauel K, et al. Binding of anti-platelet factor 4/heparin antibodies depends on the thermodynamics of conformational changes in platelet factor 4. *Blood* 2014; **124**(15): 2442-9.
66. Cuker A, Gimotty PA, Crowther MA, Warkentin TE. Predictive value of the 4Ts scoring system for heparin-induced thrombocytopenia: a systematic review and meta-analysis. *Blood* 2012; **120**(20): 4160-7.
67. Warkentin TE, Sheppard JI, Moore JC, Sigouin CS, Kelton JG. Quantitative interpretation of optical density measurements using PF4-dependent enzyme-immunoassays. *J Thromb Haemost* 2008; **6**(8): 1304-12.
68. Warkentin TE, Sheppard JI, Smith JW, et al. Combination of two complementary automated rapid assays for diagnosis of heparin-induced thrombocytopenia (HIT). *J Thromb Haemost* 2020; **18**(6): 1435-46.
69. Meyer O, Salama A, Pittet N, Schwind P. Rapid detection of heparin-induced platelet antibodies with particle gel immunoassay (ID-HPF4). *Lancet* 1999; **354**(9189): 1525-6.
70. Refaai MA, Conley G, Ortel TL, Francis JL. Evaluation of a rapid and automated heparin-induced thrombocytopenia immunoassay. *Int J Lab Hematol* 2019; **41**(4): 478-84.
71. Sachs UJ, von Hesberg J, Santoso S, Bein G, Bakchoul T. Evaluation of a new nanoparticle-based lateral-flow immunoassay for the exclusion of heparin-induced thrombocytopenia (HIT). *Thromb Haemost* 2011; **106**(6): 1197-202.
72. Althaus K, Hron G, Strobel U, et al. Evaluation of automated immunoassays in the diagnosis of heparin induced thrombocytopenia. *Thromb Res* 2013; **131**(3): e85-90.
73. Warkentin TE, Sheppard JI, Linkins LA, Arnold DM, Nazy I. Performance characteristics of an automated latex immunoturbidimetric assay [HemosIL((R)) HIT-Ab(PF4-H)] for the diagnosis of immune heparin-induced thrombocytopenia. *Thromb Res* 2017; **153**: 108-17.

74. Althaus K, Strobel U, Warkentin TE, Greinacher A. Combined use of the high heparin step and optical density to optimize diagnostic sensitivity and specificity of an anti-PF4/heparin enzyme-immunoassay. *Thromb Res* 2011; **128**(3): 256-60.
75. Warkentin TE, Arnold DM, Nazi I, Kelton JG. The platelet serotonin-release assay. *Am J Hematol* 2015; **90**(6): 564-72.
76. Gerotziafas GT, Elalamy I, Lecrubier C, et al. The role of platelet factor 4 in platelet aggregation induced by the antibodies implicated in heparin-induced thrombocytopenia. *Blood Coagul Fibrinolysis* 2001; **12**(7): 511-20.
77. Cines DB, Rauova L, Arepally G, et al. Heparin-induced thrombocytopenia: an autoimmune disorder regulated through dynamic autoantigen assembly/disassembly. *J Clin Apher* 2007; **22**(1): 31-6.
78. Trossaert M, Gaillard A, Commin PL, Amiral J, Vissac AM, Fressinaud E. High incidence of anti-heparin/platelet factor 4 antibodies after cardiopulmonary bypass surgery. *Br J Haematol* 1998; **101**(4): 653-5.
79. Selleng S, Selleng K, Wollert HG, et al. Heparin-induced thrombocytopenia in patients requiring prolonged intensive care unit treatment after cardiopulmonary bypass. *J Thromb Haemost* 2008; **6**(3): 428-35.
80. Caton S, O'Brien E, Pannelay AJ, Cook RG. Assessing the clinical and cost impact of on-demand immunoassay testing for the diagnosis of heparin induced thrombocytopenia. *Thromb Res* 2016; **140**: 155-62.
81. Wilke T, Tesch S, Scholz A, Kohlmann T, Greinacher A. The costs of heparin-induced thrombocytopenia: a patient-based cost of illness analysis. *J Thromb Haemost* 2009; **7**(5): 766-73.
82. Lee GM, Arepally GM. Diagnosis and management of heparin-induced thrombocytopenia. *Hematol Oncol Clin North Am* 2013; **27**(3): 541-63.
83. Litvinov RI, Yarovoi SV, Rauova L, et al. Distinct specificity and single-molecule kinetics characterize the interaction of pathogenic and non-pathogenic antibodies against platelet factor 4-heparin complexes with platelet factor 4. *J Biol Chem* 2013; **288**(46): 33060-70.
84. Suh JS, Aster RH, Visentin GP. Antibodies from patients with heparin-induced thrombocytopenia/thrombosis recognize different epitopes on heparin: platelet factor 4. *Blood* 1998; **91**(3): 916-22.
85. Li ZQ, Liu W, Park KS, et al. Defining a second epitope for heparin-induced thrombocytopenia/thrombosis antibodies using KKO, a murine HIT-like monoclonal antibody. *Blood* 2002; **99**(4): 1230-6.
86. Kizlik-Masson C, Vayne C, McKenzie SE, et al. 5B9, a monoclonal antiplatelet factor 4/heparin IgG with a human Fc fragment that mimics heparin-induced thrombocytopenia antibodies. *J Thromb Haemost* 2017; **15**(10): 2065-75.
87. Sachais BS, Litvinov RI, Yarovoi SV, et al. Dynamic antibody-binding properties in the pathogenesis of HIT. *Blood* 2012; **120**(5): 1137-42.
88. Vayne C, Nguyen TH, Rollin J, et al. Characterization of New Monoclonal PF4-Specific Antibodies as Useful Tools for Studies on Typical and Autoimmune Heparin-Induced Thrombocytopenia. *Thromb Haemost* 2021; **121**(3): 322-31.
89. Huber R. Spatial structure of immunoglobulin molecules. *Klin Wochenschr* 1980; **58**(22): 1217-31.
90. Griffiths AD, Duncan AR. Strategies for selection of antibodies by phage display. *Curr Opin Biotechnol* 1998; **9**(1): 102-8.

91. Yannuzzi NA, Freund KB. Brolucizumab: evidence to date in the treatment of neovascular age-related macular degeneration. *Clin Ophthalmol* 2019; **13**: 1323-9.
92. Biggers K, Scheinfeld N. VB4-845, a conjugated recombinant antibody and immunotoxin for head and neck cancer and bladder cancer. *Curr Opin Mol Ther* 2008; **10**(2): 176-86.
93. Jin S, Sun Y, Liang X, et al. Emerging new therapeutic antibody derivatives for cancer treatment. *Signal Transduct Target Ther* 2022; **7**(1): 39.
94. Minenkova O, Santapaola D, Milazzo FM, et al. Human inhalable antibody fragments neutralizing SARS-CoV-2 variants for COVID-19 therapy. *Mol Ther* 2022; **30**(5): 1979-93.
95. Zhou J, He L, Pang Z, et al. Identification and validation of FGFR2 peptide for detection of early Barrett's neoplasia. *Oncotarget* 2017; **8**(50): 87095-106.
96. Zhang D, Jia H, Wang Y, et al. A CD44 specific peptide developed by phage display for targeting gastric cancer. *Biotechnol Lett* 2015; **37**(11): 2311-20.
97. Peng L, Shang W, Guo P, et al. Phage Display-Derived Peptide-Based Dual-Modality Imaging Probe for Bladder Cancer Diagnosis and Resection Postinstillation: A Preclinical Study. *Mol Cancer Ther* 2018; **17**(10): 2100-11.
98. Wu FL, Lai DY, Ding HH, et al. Identification of Serum Biomarkers for Systemic Lupus Erythematosus Using a Library of Phage Displayed Random Peptides and Deep Sequencing. *Mol Cell Proteomics* 2019; **18**(9): 1851-63.
99. Li TW, Cheng SF, Tseng YT, et al. Development of single-chain variable fragments (scFv) against influenza virus targeting hemagglutinin subunit 2 (HA2). *Arch Virol* 2016; **161**(1): 19-31.
100. Wu J, Zeng XQ, Zhang HB, et al. Novel phage display-derived H5N1-specific scFvs with potential use in rapid avian flu diagnosis. *J Microbiol Biotechnol* 2014; **24**(5): 704-13.
101. Parray HA, Chiranjivi AK, Asthana S, et al. Identification of an anti-SARS-CoV-2 receptor-binding domain-directed human monoclonal antibody from a naive semisynthetic library. *J Biol Chem* 2020; **295**(36): 12814-21.
102. Bertoglio F, Meier D, Langreder N, et al. SARS-CoV-2 neutralizing human recombinant antibodies selected from pre-pandemic healthy donors binding at RBD-ACE2 interface. *Nat Commun* 2021; **12**(1): 1577.
103. Kim HY, Lee JH, Kim MJ, et al. Development of a SARS-CoV-2-specific biosensor for antigen detection using scFv-Fc fusion proteins. *Biosens Bioelectron* 2021; **175**: 112868.
104. Antoine D, Mohammadi M, Vitt M, et al. Rapid, Point-of-Care scFv-SERS Assay for Femtogram Level Detection of SARS-CoV-2. *ACS Sens* 2022; **7**(3): 866-73.
105. Duranti C, Carraresi L, Sette A, et al. Generation and characterization of novel recombinant anti-hERG1 scFv antibodies for cancer molecular imaging. *Oncotarget* 2018; **9**(79): 34972-89.
106. Sachais BS, Rux AH, Cines DB, et al. Rational design and characterization of platelet factor 4 antagonists for the study of heparin-induced thrombocytopenia. *Blood* 2012; **119**(25): 5955-62.
107. Thie H. Affinity Maturation by Random Mutagenesis and Phage Display. Berlin, Heidelberg: Springer 2010.
108. Dufner P, Jermutus L, Minter RR. Harnessing phage and ribosome display for antibody optimisation. *Trends Biotechnol* 2006; **24**(11): 523-9.
109. Frei JC, Lai JR. Protein and Antibody Engineering by Phage Display. *Methods Enzymol* 2016; **580**: 45-87.
110. Daugherty PS, Chen G, Iverson BL, Georgiou G. Quantitative analysis of the effect of the mutation frequency on the affinity maturation of single chain Fv antibodies. *Proc Natl Acad Sci U S A* 2000; **97**(5): 2029-34.

111. Krumpe LR, Atkinson AJ, Smythers GW, et al. T7 lytic phage-displayed peptide libraries exhibit less sequence bias than M13 filamentous phage-displayed peptide libraries. *Proteomics* 2006; **6**(15): 4210-22.
112. Hagay Y, Lahav J, Levanon A, Panet A. Function-modulating human monoclonal antibodies against platelet-membrane receptors isolated from a phage-display library. *J Thromb Haemost* 2003; **1**(8): 1829-36.
113. Mimmi S, Maisano D, Quinto I, Iaccino E. Phage Display: An Overview in Context to Drug Discovery. *Trends Pharmacol Sci* 2019; **40**(2): 87-91.
114. Qi H, Lu H, Qiu HJ, Petrenko V, Liu A. Phagemid vectors for phage display: properties, characteristics and construction. *J Mol Biol* 2012; **417**(3): 129-43.
115. Hoogenboom HR. Selecting and screening recombinant antibody libraries. *Nat Biotechnol* 2005; **23**(9): 1105-16.
116. Sheets MD, Amersdorfer P, Finnern R, et al. Efficient construction of a large nonimmune phage antibody library: the production of high-affinity human single-chain antibodies to protein antigens. *Proc Natl Acad Sci U S A* 1998; **95**(11): 6157-62.
117. Rajpal A, Beyaz N, Haber L, et al. A general method for greatly improving the affinity of antibodies by using combinatorial libraries. *Proc Natl Acad Sci U S A* 2005; **102**(24): 8466-71.
118. Barbas CF, Burton, D.R., Scott, J. K. & Silverman, G. J. Phage Display: A Laboratory Manual: Cold Springs Harbor Laboratory Press; 2001.
119. Kretz CA. Mapping the Substrate Recognition Landscapes of Metalloproteases Using Comprehensive Mutagenesis. *Methods Mol Biol* 2017; **1579**: 209-28.
120. Huynh A, Arnold DM, Moore JC, Smith JW, Kelton JG, Nazy I. Development of a high-yield expression and purification system for platelet factor 4. *Platelets* 2018; **29**(3): 249-56.
121. Huynh A, Arnold DM, Smith JW, et al. The role of fluid-phase immune complexes in the pathogenesis of heparin-induced thrombocytopenia. *Thromb Res* 2020; **194**: 135-41.
122. Dong X, Leksa NC, Chhabra ES, et al. The von Willebrand factor D'D3 assembly and structural principles for factor VIII binding and concatemer biogenesis. *Blood* 2019; **133**(14): 1523-33.
123. Krauel K, Weber C, Brandt S, et al. Platelet factor 4 binding to lipid A of Gram-negative bacteria exposes PF4/heparin-like epitopes. *Blood* 2012; **120**(16): 3345-52.
124. Mandrekar JN. Receiver operating characteristic curve in diagnostic test assessment. *J Thorac Oncol* 2010; **5**(9): 1315-6.
125. Butler JE, Navarro P, Sun J. Adsorption-induced antigenic changes and their significance in ELISA and immunological disorders. *Immunol Invest* 1997; **26**(1-2): 39-54.
126. Vodnik M, Strukelj B, Lunder M. HWGMWSY, an unanticipated polystyrene binding peptide from random phage display libraries. *Anal Biochem* 2012; **424**(2): 83-6.
127. Menendez A, Scott JK. The nature of target-unrelated peptides recovered in the screening of phage-displayed random peptide libraries with antibodies. *Anal Biochem* 2005; **336**(2): 145-57.
128. Adey NB, Mataragnon AH, Rider JE, Carter JM, Kay BK. Characterization of phage that bind plastic from phage-displayed random peptide libraries. *Gene* 1995; **156**(1): 27-31.
129. Raghunathan G, Smart J, Williams J, Almagro JC. Antigen-binding site anatomy and somatic mutations in antibodies that recognize different types of antigens. *J Mol Recognit* 2012; **25**(3): 103-13.
130. Clark LA, Ganesan S, Papp S, van Vlijmen HW. Trends in antibody sequence changes during the somatic hypermutation process. *J Immunol* 2006; **177**(1): 333-40.

131. Basak S, Nobrega RP, Tavella D, et al. Networks of electrostatic and hydrophobic interactions modulate the complex folding free energy surface of a designed betaalpha protein. *Proc Natl Acad Sci U S A* 2019; **116**(14): 6806-11.
132. Neuberger MS, Milstein C. Somatic hypermutation. *Curr Opin Immunol* 1995; **7**(2): 248-54.
133. Ho M, Kreitman RJ, Onda M, Pastan I. In vitro antibody evolution targeting germline hot spots to increase activity of an anti-CD22 immunotoxin. *J Biol Chem* 2005; **280**(1): 607-17.
134. Salvatore G, Beers R, Margulies I, Kreitman RJ, Pastan I. Improved cytotoxic activity toward cell lines and fresh leukemia cells of a mutant anti-CD22 immunotoxin obtained by antibody phage display. *Clin Cancer Res* 2002; **8**(4): 995-1002.
135. Ting JP, Tung F, Antonysamy S, et al. Utilization of peptide phage display to investigate hotspots on IL-17A and what it means for drug discovery. *PLoS One* 2018; **13**(1): e0190850.
136. Oyama H, Kiguchi Y, Morita I, et al. Seeking high-priority mutations enabling successful antibody-breeding: systematic analysis of a mutant that gained over 100-fold enhanced affinity. *Sci Rep* 2020; **10**(1): 4807.
137. Kiguchi Y, Oyama H, Morita I, Nagata Y, Umezawa N, Kobayashi N. The VH framework region 1 as a target of efficient mutagenesis for generating a variety of affinity-matured scFv mutants. *Sci Rep* 2021; **11**(1): 8201.
138. Lowe DC, Gerhardt S, Ward A, et al. Engineering a high-affinity anti-IL-15 antibody: crystal structure reveals an alpha-helix in VH CDR3 as key component of paratope. *J Mol Biol* 2011; **406**(1): 160-75.
139. Furukawa K, Shirai H, Azuma T, Nakamura H. A role of the third complementarity-determining region in the affinity maturation of an antibody. *J Biol Chem* 2001; **276**(29): 27622-8.
140. Verma R, Boleti E, George AJ. Antibody engineering: comparison of bacterial, yeast, insect and mammalian expression systems. *J Immunol Methods* 1998; **216**(1-2): 165-81.
141. Rosano GL, Ceccarelli EA. Recombinant protein expression in Escherichia coli: advances and challenges. *Front Microbiol* 2014; **5**: 172.
142. Ahmad ZA, Yeap SK, Ali AM, Ho WY, Alitheen NB, Hamid M. scFv antibody: principles and clinical application. *Clin Dev Immunol* 2012; **2012**: 980250.
143. Sarker A, Rathore AS, Gupta RD. Evaluation of scFv protein recovery from E. coli by in vitro refolding and mild solubilization process. *Microb Cell Fact* 2019; **18**(1): 5.
144. de Aguiar RB, da Silva TA, Costa BA, et al. Generation and functional characterization of a single-chain variable fragment (scFv) of the anti-FGF2 3F12E7 monoclonal antibody. *Sci Rep* 2021; **11**(1): 1432.
145. Song YH, Sun XW, Jiang B, Liu JE, Su XH. Purification optimization for a recombinant single-chain variable fragment against type 1 insulin-like growth factor receptor (IGF-1R) by using design of experiment (DoE). *Protein Expr Purif* 2015; **116**: 98-104.
146. Wang R, Xiang S, Feng Y, et al. Engineering production of functional scFv antibody in E. coli by co-expressing the molecule chaperone Skp. *Front Cell Infect Microbiol* 2013; **3**: 72.
147. Zhang J, Valianou M, Simmons H, et al. Identification of inhibitory scFv antibodies targeting fibroblast activation protein utilizing phage display functional screens. *FASEB J* 2013; **27**(2): 581-9.
148. Cuker A, Rux AH, Hinds JL, et al. Novel diagnostic assays for heparin-induced thrombocytopenia. *Blood* 2013; **121**(18): 3727-32.

149. Weisser NE, Hall JC. Applications of single-chain variable fragment antibodies in therapeutics and diagnostics. *Biotechnol Adv* 2009; **27**(4): 502-20.
150. Gutierrez-Gonzalez M, Farias C, Tello S, et al. Optimization of culture conditions for the expression of three different insoluble proteins in Escherichia coli. *Sci Rep* 2019; **9**(1): 16850.
151. Berkmen M. Production of disulfide-bonded proteins in Escherichia coli. *Protein Expr Purif* 2012; **82**(1): 240-51.
152. Dewi KS, Retnoningrum DS, Riani C, Fuad AM. Construction and Periplasmic Expression of the Anti-EGFRvIII ScFv Antibody Gene in Escherichia coli. *Sci Pharm* 2016; **84**(1): 141-52.
153. Bach H, Mazor Y, Shaky S, et al. Escherichia coli maltose-binding protein as a molecular chaperone for recombinant intracellular cytoplasmic single-chain antibodies. *J Mol Biol* 2001; **312**(1): 79-93.
154. Barderas R, Shochat S, Martinez-Torrecuadrada J, Altschuh D, Meloen R, Ignacio Casal J. A fast mutagenesis procedure to recover soluble and functional scFvs containing amber stop codons from synthetic and semisynthetic antibody libraries. *J Immunol Methods* 2006; **312**(1-2): 182-9.
155. Lebendiker M, Danieli T. Production of prone-to-aggregate proteins. *FEBS Lett* 2014; **588**(2): 236-46.
156. Terpe K. Overview of bacterial expression systems for heterologous protein production: from molecular and biochemical fundamentals to commercial systems. *Appl Microbiol Biotechnol* 2006; **72**(2): 211-22.
157. Bessette PH, Aslund F, Beckwith J, Georgiou G. Efficient folding of proteins with multiple disulfide bonds in the Escherichia coli cytoplasm. *Proc Natl Acad Sci U S A* 1999; **96**(24): 13703-8.
158. Ramm K, Gehrig P, Pluckthun A. Removal of the conserved disulfide bridges from the scFv fragment of an antibody: effects on folding kinetics and aggregation. *J Mol Biol* 1999; **290**(2): 535-46.
159. Gaciarz A, Ruddock LW. Complementarity determining regions and frameworks contribute to the disulfide bond independent folding of intrinsically stable scFv. *PLoS One* 2017; **12**(12): e0189964.
160. Glockshuber R, Schmidt T, Pluckthun A. The disulfide bonds in antibody variable domains: effects on stability, folding in vitro, and functional expression in Escherichia coli. *Biochemistry* 1992; **31**(5): 1270-9.
161. Dabrowski M, Bukowy-Bieryllo Z, Zietkiewicz E. Translational readthrough potential of natural termination codons in eucaryotes--The impact of RNA sequence. *RNA Biol* 2015; **12**(9): 950-8.
162. Fan Y, Evans CR, Barber KW, et al. Heterogeneity of Stop Codon Readthrough in Single Bacterial Cells and Implications for Population Fitness. *Mol Cell* 2017; **67**(5): 826-36 e5.
163. Pina AS, Batalha IL, Dias A, Roque ACA. Affinity Tags in Protein Purification and Peptide Enrichment: An Overview. *Methods Mol Biol* 2021; **2178**: 107-32.
164. Greinacher A, Thiele T, Warkentin TE, Weisser K, Kyrle PA, Eichinger S. Thrombotic Thrombocytopenia after ChAdOx1 nCov-19 Vaccination. *N Engl J Med* 2021; **384**(22): 2092-101.
165. Scully M, Singh D, Lown R, et al. Pathologic Antibodies to Platelet Factor 4 after ChAdOx1 nCoV-19 Vaccination. *N Engl J Med* 2021; **384**(23): 2202-11.
166. Bissola AL, Daka M, Arnold DM, et al. The clinical and laboratory diagnosis of vaccine-induced immune thrombotic thrombocytopenia. *Blood Adv* 2022.

167. Favaloro EJ, Pasalic L, Henry B, Lippi G. Laboratory testing for platelet factor 4 antibodies: differential utility for diagnosis/exclusion of heparin induced thrombocytopenia versus suspected vaccine induced thrombotic thrombocytopenia. *Pathology* 2022.
168. Tiller KE, Li L, Kumar S, Julian MC, Garde S, Tessier PM. Arginine mutations in antibody complementarity-determining regions display context-dependent affinity/specificity trade-offs. *J Biol Chem* 2017; **292**(40): 16638-52.
169. Lim CC, Woo PCY, Lim TS. Development of a Phage Display Panning Strategy Utilizing Crude Antigens: Isolation of MERS-CoV Nucleoprotein human antibodies. *Sci Rep* 2019; **9**(1): 6088.
170. Borras L, Gunde T, Tietz J, et al. Generic approach for the generation of stable humanized single-chain Fv fragments from rabbit monoclonal antibodies. *J Biol Chem* 2010; **285**(12): 9054-66.
171. Bertoglio F, Fuhner V, Ruschig M, et al. A SARS-CoV-2 neutralizing antibody selected from COVID-19 patients binds to the ACE2-RBD interface and is tolerant to most known RBD mutations. *Cell Rep* 2021; **36**(4): 109433.
172. Knoebl P, Cataland S, Peyvandi F, et al. Efficacy and safety of open-label caplacizumab in patients with exacerbations of acquired thrombotic thrombocytopenic purpura in the HERCULES study. *J Thromb Haemost* 2020; **18**(2): 479-84.
173. Scully M, Cataland SR, Peyvandi F, et al. Caplacizumab Treatment for Acquired Thrombotic Thrombocytopenic Purpura. *N Engl J Med* 2019; **380**(4): 335-46.
174. Callewaert F, Roodt J, Ulrichts H, et al. Evaluation of efficacy and safety of the anti-VWF Nanobody ALX-0681 in a preclinical baboon model of acquired thrombotic thrombocytopenic purpura. *Blood* 2012; **120**(17): 3603-10.
175. Srinivasan AF, Rice L, Bartholomew JR, et al. Warfarin-induced skin necrosis and venous limb gangrene in the setting of heparin-induced thrombocytopenia. *Arch Intern Med* 2004; **164**(1): 66-70.
176. Messmore H, Jeske W, Wehrmacher W, Walenga J. Benefit-risk assessment of treatments for heparin-induced thrombocytopenia. *Drug Saf* 2003; **26**(9): 625-41.
177. Pathak R, Bhatt VR, Karmacharya P, Aryal MR, Donato AA. Medical and Economic Burden of Heparin-Induced Thrombocytopenia: A Retrospective Nationwide Inpatient Sample (NIS) Study. *J Hosp Med* 2017; **12**(2): 94-7.
178. Pachl J, Svoboda P, Jacobs F, et al. A randomized, blinded, multicenter trial of lipid-associated amphotericin B alone versus in combination with an antibody-based inhibitor of heat shock protein 90 in patients with invasive candidiasis. *Clin Infect Dis* 2006; **42**(10): 1404-13.
179. Miller K, Cortes J, Hurvitz SA, et al. HERMIONE: a randomized Phase 2 trial of MM-302 plus trastuzumab versus chemotherapy of physician's choice plus trastuzumab in patients with previously treated, anthracycline-naive, HER2-positive, locally advanced/metastatic breast cancer. *BMC Cancer* 2016; **16**: 352.
180. Fleisig AJ, Verrier ED. Pexelizumab -- a C5 complement inhibitor for use in both acute myocardial infarction and cardiac surgery with cardiopulmonary bypass. *Expert Opin Biol Ther* 2005; **5**(6): 833-9.
181. Winer ES, Stone RM. Novel therapy in Acute myeloid leukemia (AML): moving toward targeted approaches. *Ther Adv Hematol* 2019; **10**: 2040620719860645.
182. Van Roy M, Ververken C, Beirnaert E, et al. The preclinical pharmacology of the high affinity anti-IL-6R Nanobody(R) ALX-0061 supports its clinical development in rheumatoid arthritis. *Arthritis Res Ther* 2015; **17**: 135.

183. Baker KP, Edwards BM, Main SH, et al. Generation and characterization of LymphoStat-B, a human monoclonal antibody that antagonizes the bioactivities of B lymphocyte stimulator. *Arthritis Rheum* 2003; **48**(11): 3253-65.